



**APPLICATION OF STEMMING PLUGS FOR THE REDUCTION
OF AIR BLAST INDUCED DURING SURFACE MINE
BLASTING**

by

Talent Mushwana (14758830)

submitted in accordance with the requirements for the degree of

MASTER OF ENGINEERING

in the subject

MINING ENGINEERING

at the

UNIVERSITY OF SOUTH AFRICA

Supervisor: Prof Francois Mulenga

November 2024

Declaration

Name: **Talent Mushwana**

Student number: 14758830

Degree: **Master of Engineering in Mining Engineering**

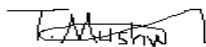
Exact wording of the title of the dissertation as appearing on the electronic copy submitted for examination:

APPLICATION OF STEMMING PLUGS FOR THE REDUCTION OF AIR BLAST INDUCED DURING SURFACE MINE BLASTING

I declare that the above dissertation is my own work and that all the sources that I have used or quoted have been indicated and acknowledged by means of complete references.

I further declare that I submitted the dissertation to originality checking software and that it falls within the accepted requirements for originality.

I further declare that I have not previously submitted this work, or part of it, for examination at Unisa for another qualification or at any other higher education institution.



11/11/2024

.....

.....

Signature

Date

Dedication

This dissertation is dedicated to my parents **Maureen Nkhensani Rikhotso** and **Friday Professor Mushwana**, who have always motivated me to excel. Thank you for giving me all the support to reach my goals.

Acknowledgements

Firstly, I would like to sincerely thank the Almighty God for always being there when I am in need. Thank you for working through me and giving me strength throughout my study.

I would also like to express my heartfelt gratitude to my supervisor, Professor Francois Mulenga. Your enormous contribution and guidance throughout my research study made my completion of this degree possible.

I am sincerely grateful to Professor Elvis Fosso-Kankeu and Dr Monique Chiloane for their invaluable advice and guidance during the inception of my research.

Moreover, I would also like to give my special thanks to my family as a whole. Your prayers and continuous support carried me through this journey. I will forever be grateful to you.

Lastly, I am also grateful to the quarry company and their wonderful staff for allowing me the opportunity to collect data for my research study. Your patience and guidance are highly appreciated.

Abstract

The use of stemming plugs with the intention of optimizing blast performance is gaining popularity in surface mining. This is because stemming plugs are purported to enhance energy retention and reduce the environmental impacts of blasting. The main objective of this study was to assess the potential of stemming plugs in reducing air blast at a quarry.

The stemming plugs commercially known as Varistem® of diameter 102 mm were used for onsite testing. A total of 27 blasts were carried out under similar blast design conditions except for the stemming length that was varied between 1.9 and 3 m. The resultant air blast levels were recorded from two different monitoring stations around the pit. From the test programme, 15 blasts incorporated the Varistem® stemming plugs while the remaining 12 were conducted using standard stemming with aggregates only. The first monitoring station (i.e., Station A) was approximately 100 m away from the blast block while the second (i.e., Station B) was 700 m away. Data was collected from these two stations simultaneously for each of the 27 blasts. Using this arrangement, the data was modelled to correlated air blast and scaled distance. Finally, a comparison by statistical analysis was then carried out between the Varistem® blasts and the standard blasts.

Results from Station A showed that 33% of the Varistem® blasts in contrast to 67% of the standard tests exceeded the regulatory threshold limit of 134 dB set by the United States Bureau of Mines (USBM). From Station B, all the Varistem® blasts were below the threshold while about 25% of the standard blasts were above the limit. The scaled depth of burial was also determined to estimate the level of blast energy containment. It was subsequently found that all Varistem® blasts were within the controlled energy range explaining why acceptable air blast levels were produced. Lastly, the empirical model by the USBM was found to describe the air blast of the quarry better than McKenzie's model. In essence, the results produced from this study showed that the Varistem® stemming plugs are doing some work in reducing blast induced air blast compared to standard stemming methods. Nevertheless,

on the body of knowledge, there exists no model specifically applicable to the Varistem® stemming plugs. There are also currently no guidelines available for the design of a blast involving Varistem® plugs in compliance with regulatory standards on air blast. Understanding the contribution of Varistem® stemming plugs to blasting operations is expected to add value to the body of knowledge by making available data for use by the scientific community.

Keywords: Varistem®, air blast, stemming plugs, blasting, USBM model, McKenzie's model

Table of contents

Declaration	i
Dedication.....	ii
Acknowledgements.....	iii
Abstract	iv
List of Figures	ix
List of Tables	xiii
List of Symbols	xiv
List of abbreviations and acronyms	xvii
Chapter 1 Introduction	1
1.1 Background	1
1.2 Problem statement	4
1.3 Aim and objectives of the study	5
1.4 Significance of the study.....	6
1.5 Structure of the dissertation.....	6
Chapter 2 Literature review	8
2.1 Introduction.....	8
2.2 Background on air blast.....	9
2.2.1 Sources of air blast.....	11
2.2.2 Measurement of air blast.....	13
2.2.3 Human and structural response to air blast.....	15
2.3 Factors influencing the level of air blast in surface mining	16
2.3.1 Effects of controllable blast design parameters on air blast .	16
2.3.2 Influence of weather on air blast	20
2.3.3 Influence of topography on air blast	24
2.4 Review of stemming techniques available in the mining industry	25

2.4.1	Conventional stemming material	26
2.4.2	Deck-charge blasting.....	30
2.4.3	Varistem® plugs.....	32
2.4.4	SPARSH	35
2.5	Significance of energy containment during a blast	37
2.6	Previous studies on air blast reduction	40
2.7	Concluding remarks	49
Chapter 3 Experimental work and data collection.....		52
3.1	Introduction	52
3.2	Overview	52
3.2.1	Overview of the quarry	53
3.2.2	Site description.....	56
3.3	Experimental work and equipment used for collecting data.....	57
3.3.1	Data acquisition and experimental setup.....	57
3.3.2	Equipment and tools used for the collection of data	61
3.4	Data analysis used for the study	84
3.5	Challenges encountered during the research study	85
Chapter 4: Estimation of the contribution of stemming plugs to air blast reduction.....		87
4.1	Introduction.....	87
4.2	Air blast profile from Station A and Station B.....	87
4.2.1	Air blast profile from Station A.....	87
4.2.2	Air blast profile from Station B.....	91
4.2.3	Calculated scaled depth of burial – Observations	94
4.3	Modelling air overpressure as a function of scaled distance	98
4.3.1	USBM predictor model	98
4.3.2	Mckenzie’s predictor model.....	98

4.3.3	Comparison of the two predictor models	99
4.4	Comparing air blasts with and without stemming plugs	107
4.5	Summary of findings.....	110
Chapter 5 Understanding the effects of stemming plugs on the reduction of air blast		112
5.1	Introduction.....	112
5.2	Effect of stemming plugs on air blast at Station A	112
5.3	Effect of stemming plugs on air blast at Station B	119
5.4	Linking air blast reduction to blast energy confinement.....	123
5.5	Air overpressure as a function of scaled distance	125
5.6	Testing the contribution of stemming plugs to air blast.....	128
5.7	Summary of findings.....	129
Chapter 6 Conclusion and recommendations.....		130
6.1	Introduction.....	130
6.2	Varistem® stemming plugs on air blast reduction	130
6.3	Recommendations for future work.....	132
References		133
Appendices.....		145

List of Figures

Figure 1.1: Schematic of design parameters for bench blasting (Siamaki, 2022)	2
Figure 2.1: A bench showing how blastholes are drilled and connected with initiation systems (adapted from Segarra et al., 2010).....	10
Figure 2.2: Vibration analysis report showing the RPP and APP on the waveform analysis plot (Docrat, 2023).....	12
Figure 2.3: Parts of the seismograph units illustrating (A) Geophone sensor and (B) Microphone (Kabwe and Wang, 2016).....	14
Figure 2.4: A section of the blasthole showing the crushing zone (After Silva, 2019)	17
Figure 2.5: Illustration of cratering around a blasthole on a bench (Kuzu et al., 2009).....	17
Figure 2.6: Typical layout of a bench blast (Adapted from Szendrei and Tose, 2024)	18
Figure 2.7: An illustration of timing sequence of blastholes in a bench (Choudhary et al., 2021)	19
Figure 2.8: Effect of wind speed on sound diffraction (Hannah, 2007)	21
Figure 2.9: Effect of temperature inversion on sound transmission (After Ratcliff et al., 2011).....	23
Figure 2.10: Typical illustration of topographic shielding in blasting (Richards, 2013)	24
Figure 2.11: (a) Crushed aggregates; (b) Blasthole filled with crushed aggregates (Own picture taken by the author at Quarry TM).....	28
Figure 2.12: (a) Application of plaster paste into the blasthole collar; (b) Blasthole filled with hardened plaster (Cevizci, 2013).....	29
Figure 2.13: Deck-charge arrangement for a quarry blast (Balamadeswaran et al., 2018).....	30
Figure 2.14: Different sizes of Varistem® plugs available for use in blasting (ERG Industrial, 2023)	32
Figure 2.15: Schematic showing the installation of a Varistem® stemming plug into a blasthole (ERG Industrial, 2020)	33

Figure 2.16: Performance of the standard versus Varistem® blast at Rooikraal quarry (ERG Industrial, 2021).....	34
Figure 2.17: Arrangement of the SPARSH (Sazid, 2014)	36
Figure 2.18: A comparison between standard stemming arrangement versus SPARSH (Saharan et al., 2017)	36
Figure 2.19: Schematic illustrating the scaled depth of burial concept (Chiappetta, 2010)	39
Figure 2.20: Pictorial definition of the scaled depth of burial (Chiappetta, 2010)	40
Figure 2.21: (A) Wavefront propagation from a blasthole; (B) wavefronts from two blastholes with time delay between initiations; (C) reinforcing wavefronts from two blastholes with time delay between initiations (Richards, 2008; Jaroonpattanapong and Tachom, 2021).....	46
Figure 2.22: Wave reinforcements of air waves during blasting (Jaroonpattanapong and Tachom, 2021).....	47
Figure 3.1: Layout of the primary crusher plants at Quarry TM (Source: Google earth images)	54
Figure 3.2: Neighbouring facilities around Quarry TM (Source: Google earth images).....	55
Figure 3.3: Geographical map of the quarry (Source: Picture supplied by Quarry TM)	56
Figure 3.4: Example of drilling pattern used for the benches (Source: Picture supplied by Quarry TM)	59
Figure 3.5: Aerial view of the pit showing the location of the seismographs (Source: Image adopted from google earth images).....	60
Figure 3.6: Surface drill rig (Source: Author's picture)	61
Figure 3.7: Measuring of drilled blastholes (Source: Author's picture).....	62
Figure 3.8: (a) Electronic detonator, (b) Insertion of a detonator inside a booster explosive (Source: Author's picture)	64
Figure 3.9: Detonator cord attached to a color-coded connector clip (Source: Author's picture).....	64
Figure 3.10: Charging of holes with emulsion explosives (Source: Author's picture).....	66

Figure 3.11: (a) Observing of gassing of the explosives inside the 400 g cups and (b) Filling the cups with the emulsion explosive (Source: Author's picture)	67
Figure 3.12: Displacement of water from the blasthole during charging (Source: Author's picture)	68
Figure 3.13: (a) Mega-mite 50 x 580 cartridges, and (b) Charging of 50 x 580 cartridge explosives with a detonator (Source: Author's pictures)	68
Figure 3.14: (a) Example of a typical measuring tape (Source: Better Blasting, 2021) and (b) Measuring of blasthole stemming length with measuring tape (Source: Author's picture)	69
Figure 3.15: Honey sucker (Source: Author's picture)	70
Figure 3.16: Varistem® stemming plugs of diameter 102 mm (Source: Author's picture)	71
Figure 3.17: Installation of the Varistem® stemming plug into a blasthole (ERG Industrial, 2020)	72
Figure 3.18: Crushed aggregates used for the stemming of blastholes (Source: Author's picture)	73
Figure 3.19: (a) Stemming of blastholes with crushed aggregates, (b) Buckets used to stem holes (Source: Author's picture)	74
Figure 3.20: Tamping rod used to tamp the aggregates during stemming (Source: Author's picture)	74
Figure 3.21: (a) AXXIS™ titanium logger, (b) slot where the detonator is to be inserted, (c) detonator, and (d) illustration of how the scanning of detonators is done (Source: Author's picture)	75
Figure 3.22: (a) Unrolling of the surface wire and (b) connection of the wire to the electronic delay detonators (Source: Author's picture)	76
Figure 3.23: (a) AXXIS™ titanium blasting box on site, (b) Blasting box connected to a logger, and (c) Logger transferring information to the blasting box (Source: Author's picture)	77
Figure 3.24: (a) Receiving antenna connected to a blasting box on site, and (b) Transmitting antenna connected to a blasting box in the blasting shelter (Source: Author's picture)	78

Figure 3.25: (a) Geophone, (b) Air overpressure transducer, and (c) Control unit (Source: Author's picture)	80
Figure 3.26: (a) Geophone with spikes buried into the ground, and (b) Air overpressure transducer facing the direction of the blast. (Source: Author's picture).....	81
Figure 3.27: (A) Blasting shelter for mine personnel to gather and observe the blast, (B) Controller blasting box is set up in the blasting shelter (Source: Author's picture).....	83
Figure 4.1: Air overpressure levels for the Varistem® blasts at Station A..	89
Figure 4.2: Air overpressure levels for the standard blasts at Station A	90
Figure 4.3: Air overpressure levels at Station A.....	90
Figure 4.4: Air overpressure levels for the Varistem® blasts at Station B..	92
Figure 4.5: Air overpressure levels for the standard blasts at Station B	93
Figure 4.6: Air overpressure levels at Station B.....	93
Figure 4.7: USBM predictor model for the Varistem® blasts at Station A	100
Figure 4.8: USBM predictor model for the standard blasts at Station A...	101
Figure 4.9: USBM predictor model for the Varistem® blasts at Station B	102
Figure 4.10: USBM predictor model for the standard blasts at Station B.	102
Figure 4.11: Mckenzie's predicted air overpressure levels at Station A...	103
Figure 4.12: Mckenzie's predicted air overpressure at Station B.....	105
Figure 5.1: Geological discontinuities present within the rock mass – Field observation by the author at Quarry TM	115
Figure 5.2: Confidence band at 95% significance level for the Varistem® blast at Station A.....	117
Figure 5.3: Confidence band at 95% significance level for the Standard blast at Station A	118
Figure 5.4: Confidence bands at 95% significance level for Station A.....	118
Figure 5.5: Confidence band at 95% significance level for the Varistem® blast at Station B.....	121
Figure 5.6: Confidence bands at 95% significance level for the standard blasts at Station B.....	122
Figure 5.7: Confidence bands at 95% significance level for Station B.....	123

List of Tables

Table 2.1: Air blast levels and their threshold limits (Siskind et al., 1980; Ratcliff et al., 2011; Kabwe and Wang, 2016).....	15
Table 2.2: Coefficients a_0 [in $Pa (m kg^{-1/3})^{-a_1}$] and a_1 [dimensionless] descriptive of the peak overpressure attenuation laws of mass-scaled distances (after Segarra et al., 2010).....	43
Table 3.1: Blast design parameters used in the research study	58
Table 3.2: Specifications of Nomis Blasting Seismographs	79
Table 4.1: Blast recordings from Station A for the Varistem® blasting and standard blasting trials.....	88
Table 4.2: Blast recordings from Station B for the Varistem® blasting and standard blasting	91
Table 4.3: Calculated scaled depths of burial for the Varistem® blasts at both stations	96
Table 4.4: USBM performance indices at Station A.....	101
Table 4.5: USBM performance indices at Station B.....	103
Table 4.6: Mckenzie's predictor model for the Varistem® blasts	104
Table 4.7: Performance indices for Mckenzie's model at Station A	105
Table 4.8: Mckenzie's predictor model for the standard blasts	106
Table 4.9: Performance indices for Mckenzie's model at Station B	107
Table 4.10: Air overpressure levels at the two stations.....	108
Table 4.11: Statistical analysis of variances for air blasts at Station A	109
Table 4.12: Statistical analysis of variance for air blasts at Station B	109

List of Symbols

Symbol	Description [Units]
a_0	Coefficient of the peak overpressure [$Pa (m kg^{-1/3})^{-a_1}$]
a_1	Coefficient of the peak overpressure [-]
A	Asymmetry correction factor [-]
A_f	Bench face factor [-]
A_s	Initiation sequence factor [-]
B	Drilled burden or burden [m]
BH	Bench height [m]
C	Height of the explosive column [m]
D	Blasthole diameter [mm]
D_1	Distance from the monitoring station to the explosive charge [m]
D_n	Distance from the surface to the centre of the stem charge [m]
d_s	Scaled distance [$m.kg^{-1/3}$]
FA	Bench face angle [$^{\circ}$]
f_L	Lower frequency of the transducer [Hz]
H	Bench height [m]
H	Site specific factor representing local topographical conditions [-]
$L+T$	Hole length or blasthole length [m]
L	Length of explosive column [m]

N	Sample size [-]
P	Peak overpressure [Pa or psi]
R_n	Radius corresponding to the diameter of each blasthole [m]
S	Drilled spacing or spacing [m]
SD	Subdrill [-]
SE	Standard error [-]
SL	Stemming height [m]
SPL	Sound pressure level in decibels [dB]
SS_{xx}	Sum of the squares of deviations of data points from their sample mean [-]
S_t	Top stemming length [m]
T	Stemming [-]
T	Fixed default time value per blasting round which is 2500 ms
t_n	Relative initiating time of each blasthole compared to the initiating time of the first blasthole [ms]
t_α	Student's two tailed t-test at 95% confidence level [-]
v_P	Velocity of the sound wave the default value of which is 340 m/s
W	Mass of explosives equivalent to 10 explosive diameters [kg]
W_0	Function of the angle and velocity of the initiation [-]
W_1	Total weight of explosive charge per delay [kg]
x	Scaled distance values [m.kg ^{-1/3}]
X	95% confidence interval [-]
x_m	Average value of scaled distances [m.kg ^{-1/3}]

Y	Predicted air overpressure value [dB]
α	Significance level in hypothesis testing [-]
β	Exponent factor representing geological site conditions [-]
ρ	Average in hole density of explosive [g/cm ³]

List of abbreviations and acronyms

ANOVA	Analysis of Variance
AOp	Air Overpressure
APP	Air pressure pulse
BME	Bulk Mining Explosives
dB	decibels
dB _L	decibels linear
GRP	Gas release pulse
mb	millibars
psi	Pounds per square inch
Pa	Pascals
RMSE	Root Mean Squared Error
RPP	Rock pressure pulse
R ²	Coefficient of determination
s	Standard error
SDoB	Scaled depth of burial
SRP	Stemming release pulse
SPARSH	Stemming Plug Augmenting Resistance to Stemming in Holes
USBM	United States Bureau of Mines
SS	Sum of Squares
Df	Degrees of Freedom
MS	Mean Square
F	F-Ratio

Chapter 1 Introduction

1.1 Background

Rock blasting using explosive energy is one of the most effective methods of breaking rocks in any mining project. The mining operation comes with significant technical and economic implications. For instance, ineffective blast designs and techniques may result in poor blasting performance. This could then have detrimental effects on the environment, the infrastructure in the area, as well as people's health and safety. Ineffective blasting also leads to drawbacks such as severe ground vibrations, air blast, fly rock, blasting fumes and noise (Mpofu et al., 2021). These drawbacks may be exacerbated when quarry operations or surface mines are in the vicinity of urban areas (Fişne et al., 2010; Hidayat, 2021).

Surface mining operations make use of a sequential blasting technique to control the blasting process and enhance efficiency. This technique involves the timed detonation of explosives in a specific sequence rather than all at once which could considerably improve fragmentation and reduce environmental effects. Preparation of a block for blasting requires that explosives are placed into the blast holes and filled with stemming material to the top of the hole collar to confine the explosives. Upon detonation, the explosive energy is released in the form of a shockwave and extremely high gas pressure. The resultant airborne shockwave is known as air blast or air overpressure; it can cause damage to the surroundings and discomfort to human (Segarra et al., 2010). Oates and Spiteri (2021) argue that air blast is an inevitable outcome of blasting in surface mining operations. Air blast is typically managed by ensuring that its intensity is below a permissible threshold limit defined by the jurisdiction the mine falls under. The permissible threshold limit currently applied in South Africa is 134 dB as recommended by the United States Bureau of Mines (Siskind et al., 1980).

Most of the energy generated during the detonation of explosives which is used to fragment the rock is only limited to between 7% to 22%. Regrettably, the fraction of energy lost in the process escapes the blast site in the form of air blast and ground vibrations (Saharan et al., 2017). When done properly, stemming is one of the most efficient ways of minimising air blast in surface mines (Rorke, 2011; Richards, 2013; Bansah et al., 2016). Stemming is the process of putting a non-explosive material on top of the explosive column in a blast hole (Mpofu et al., 2021). Some of the examples of stemming materials in wide use include crushed aggregates, drill chippings, sand or gravel (Patidar, 2017).

Figure 1.1 shows a schematic of the blast design parameters which is representative of the blasting technique used in surface mines.

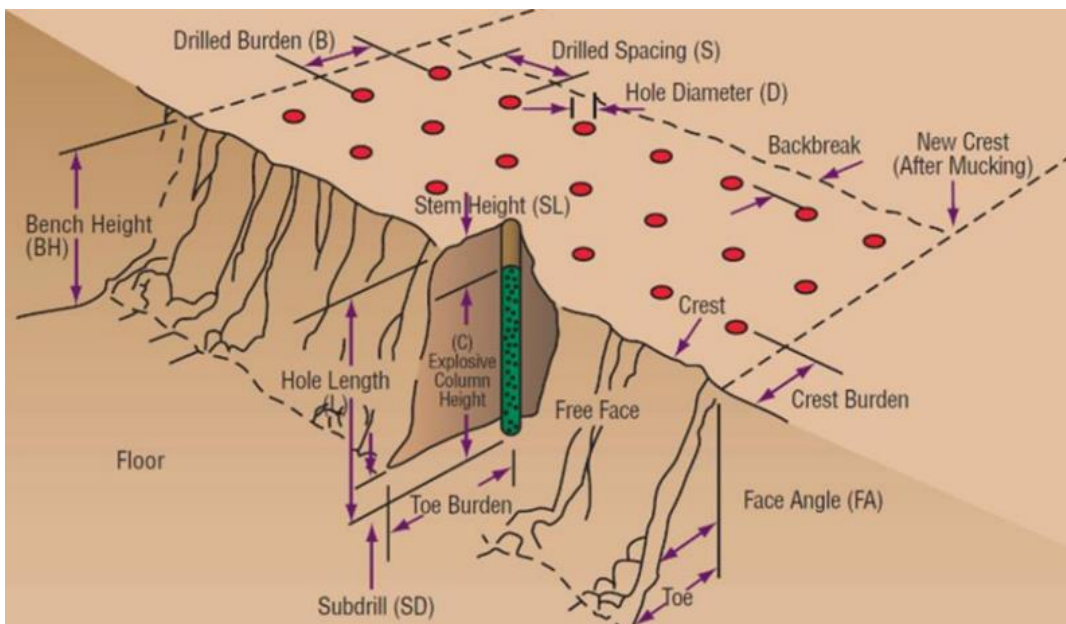


Figure 1.1: Schematic of design parameters for bench blasting (Siamaki, 2022)

Note in Figure 1.1 that drilled burden (B) is the distance of the blast hole from the free face. Drilled spacing (S) is the distance between two blast holes which are fired together in the delay period. Blast holes are normally drilled slightly below the floor level to obtain a clean breakage. The total length of the blast hole is known as hole length (L). The extra length of the hole below the floor or the grade level is called the subdrill (SD). A fraction of the top

length of the drilled blast hole is not filled with explosives. This is known as stemming height (SL).

The mining industry has made some technological advancements with the use of stemming accessories which are gaining popularity. Used in conjunction with stemming materials, these accessories are aimed at minimising air blast experienced during rock blasting. Accessories include stemming plugs, concrete plugs, foam plugs, tulip plugs, and rocklock plugs (Mpofu et al., 2021). This research study focuses on one typical accessory: the stemming plug commercially known as Varistem®.

The Varistem® is a proprietary blast stemming plug designed to hold the blast energy within the rock for longer thereby improving blast efficiency (Shoko, 2021). The basic principle behind this blast-improvement and energy-containment plug is that it increases the efficiency of stemming material in the blasthole. Varistem® plugs operate by directing more energy into the block of rock while allowing less energy upwards and out of the drillhole. As a result of this, the explosive energy is better contained within the rock mass which translates into a more controlled and improved blast. This supports empirical observations where the correct application of stemming plugs has been proven to improve explosive energy utilisation to a great extent (Saharan et al., 2017; Yang et al., 2018).

Ideally, air blast and any other impact of rock blasting must be controlled to reduce the likelihood of any disturbance to nearby residences (Jaroonpattanapong and Tachom, 2020). Shoko (2021) reported that Varistem® stemming plugs have the potential to reduce air blast and improve fragmentation. However, it is yet to be established how effective these Varistem® plugs are in surface mining operations. This research study is set to address the identified knowledge gap for the benefit of the mining industry and the scientific community. To this end, experimental test work was performed at a surface mine in South Africa where standard stemming practices were compared against the Varistem® plugs. Where applicable, evidence of reduced air blast was identified using appropriate statistical tools.

Finally, the data collected was used to model the contribution of the Varistem® plugs from the point of view of air blast.

1.2 Problem statement

Air blast is an inevitable by-product of rock blasting in any surface mining operation. This suggests that proper control measures must always be in place to minimise it. The use of stemming material is generally regarded as one of the most inexpensive yet efficient ways of mitigating against air blasts in surface mines (Rorke, 2011; Richards, 2013; Bansah et al., 2016). This practice helps confine the explosive gases. It also improves rock fragmentation while reducing air blast and flyrock (Rehman et al., 2021). However, due to environmental concerns arising from blasting activities, it has become vital to explore the use of more efficient stemming methods. One anticipated benefit is to improve both energy containment and rock fragmentation during blasting (Oates and Spiteri, 2021). The quest for controlled blasting is even more relevant to quarries located in the vicinity of urban areas where stringent safety regulations are to be complied with (Fişne et al., 2010; Hidayat, 2021). These regulatory requirements specifically apply to the level of air blast and ground vibrations generated from a blast. The problem is that the prediction and control of air blast is generally challenging and complex due to the number of parameters influencing air wave propagation (Khandelwal and Kankar, 2009). Various scholars have proposed predictive models of the level of air blast expected from a blast block (Siskind et al., 1980; Mckenzie, 1990; Sengarra et al., 2010; Jaroonpattanapong and Tachom, 2020). However, to the best of our knowledge, there exists no model specifically applicable to the Varistem® stemming plugs. There are also currently no guidelines available for the design of a blast involving Varistem® plugs in compliance with regulatory standards on air blast. One such standard is from the United States Bureau of Mines (USBM) which sets the upper limit of air blast at 134 decibels (Siskind et al., 1980). It is in this light that the current research is aimed at assessing the potential of the Varistem® stemming plugs in reducing air blast

induced during surface mine blasting. The findings are expected to provide valuable scientific data on the impact of Varistem® stemming plugs on air blast reduction.

1.3 Aim and objectives of the study

The aim of this research is to assess the potential of stemming plugs in reducing the air blast induced during surface mine blasting. Two stemming protocols are used for this purpose, one includes blasting with Varistem® stemming plugs and the other one relies on standard stemming practices involving aggregates. Furthermore, a measure of blast energy confinement known as scaled depth of burial (SDoB) is used to characterise all the blast tests incorporating the Varistem® stemming plugs. The use of the scaled depth of burial is to isolate the contribution of the Varistem® stemming to air blast reduction.

In line with the above, three objectives have been set out for this research project:

- (a) To determine the level of air blast produced during blasting with and without Varistem® plugs.
- (b) To compare the air blast levels produced when incorporating the Varistem® plugs against standard blasting practices.
- (c) To measure the blast energy confinement due to Varistem® stemming plugs and the associated air blast reduction.

From the first objective, the air blast profile is measured for the different production blasts with and without stemming plugs. This is to ensure that the contribution of the stemming plugs in air blast reduction is unambiguously established. The second objective involves performing a comparative evaluation between blasting with and without Varistem® plugs. The aim of this comparative evaluation is to obtain estimates of the contribution of stemming plugs to air blast. Lastly, from the third objective, the blast energy confinement derived from incorporating the Varistem® plugs is measured.

This is to address the question of how effective the Varistem® plugs are at confining the explosive energy during blasting.

1.4 Significance of the study

Blasting operations in surface mines can have a negative impact on the environment and nearby communities. These effects are mostly related to the noise or shockwave produced during a blast. The resulting shockwaves may cause disruptions and damage to infrastructure in neighbouring residential areas. Additionally, air blasts pose a serious health and safety hazard to mine workers (Mckenzie et al., n.d; Khandelwal and Singh, 2005). Surface mines must employ control measures to comply with industry regulatory standards.

The proposed research systematically explores the potential of Varistem® stemming plugs in controlling blast-induced shockwaves. This may potentially offer a solution to improving blast performance through the incorporation of Varistem® plugs. Improved blast performance means better controlled air blast levels which in turn ensures an improvement in the generally strained relationship between mining operations and people living nearby.

Varistem® stemming plugs are blast energy containment accessories that could aid in improving the reduction of air blast in surface mines. Understanding their contribution to blasting operations is expected to add to the body of knowledge by making available data for use by the scientific community. Moreover, this knowledge could be beneficial to mining engineers, construction sites, and government institutions responsible for making policies and laws.

1.5 Structure of the dissertation

This Master's dissertation is organised in six chapters. Chapter 1 covers a background description of the rationale behind the research project. This

background also includes an outline of the problem statement and aims and objectives of the study. Lastly, the significance behind conducting the research project is discussed.

Chapter 2 provides a thorough review of the control and monitoring of air blast in surface mines. This includes parameters that influence air blast generation such as blast design, weather, and terrain conditions. Various techniques for the reduction of air blast including the Varistem® stemming plugs are reviewed. Furthermore, several air blast models that have been proposed by other researchers for predicting and monitoring of air blast are reviewed. This also includes a brief highlight of the results and challenges encountered where these models were applied.

Chapter 3 is devoted to presenting relevant information about how the experimental work was conducted and the equipment used. The data collection and adopted analysis methods are also covered in the chapter. Lastly, the challenges encountered throughout the experimental research and their effects on the findings are discussed.

Chapter 4 presents the key outcomes of the experimental work conducted in Chapter 3. The effects of blast design parameters used in the experimental work is presented. Parameters considered include the mass of explosive per delay and the distance from the source of the blast to the monitoring station. Results on the air blast levels recorded and their respective scaled distances at the two monitoring stations around the selected quarry are then presented.

Chapter 5 provides an interpretation of the results presented in Chapter 4. This interpretation relates the results to the literature reviewed, discusses implications and limitations of the research. Findings from the air blast predictive model which looks at the relationship between the scaled distances and air overpressure levels are presented.

Chapter 6 provides a summary of the key findings from the study and suggests areas for future research.

Chapter 2 Literature review

2.1 Introduction

Drilling and Blasting is one of the most prevalent ways of breaking rocks in surface mining operations. Prior to blasting, the drilled blastholes are charged with explosives and sealed with drill chippings, crushed rocks or other stemming material. These blastholes are then connected and detonated using appropriate initiation systems. The aim of detonating explosives is to break the rock so that it can be easily loaded for further processing (Kuzu et al., 2009).

Whenever an explosive is detonated during blasting, a phenomenon known as air blast is generated (Hajihassani et al., 2014). Air blast is a pressure wave resulting from the detonation of explosive charge loaded in the rock mass (Rodríguez et al., 2007). Air blast can be defined as the impulsive sound generated by an explosive blast which results in rock fragmentation and movement (Siskind et al., 1980).

Air blasts are as a major challenge facing surface mines today due to the heavy regulation around them (Faramarzi et al., 2014). This chapter provides an in-depth review of the control and monitoring of air blast in surface mining operations. Innovative ways of reducing the generation of air blast are identified and presented in detail. The theories around air blast are also reviewed in terms of the tenets associated with the phenomenon. In essence, the first portion of the review considers how air blast is generated while looking at parameters that influence its generation. These parameters include amongst others blast design parameters as well as weather and terrain conditions. Finally, the measurement of air blast and methods of controlling air blast in surface mines are reviewed for their respective strengths and limitations.

In terms of stemming techniques, the Varistem® stemming plugs and other relevant techniques currently in use in the industry are explored. This section

of the review specifically considers previous case studies where the Varistem® plugs have been successfully incorporated into the blasts and the outcome thereof. The review is extended to other types of stemming available in the industry including crushed aggregates, drill chippings and plaster stemming. Furthermore, the significance of blast energy containment and scaled depth of burial are considered. The concept of scaled depth of burial provides a means to comparing blasts under different stemming conditions.

The last section of the review is dedicated to previous research studies on air blast modelling. Several prediction models are discussed in terms of their performance, validity and applications in reported surface mines. In addition to this, regulatory limits from selected jurisdictions on the allowable levels of air blasts for the mining industry are also touched upon. Finally, gaps in knowledge are highlighted in terms of the use of stemming plugs and other techniques as a way of reducing air blast.

2.2 Background on air blast

Air blast or air overpressure is a by-product of rock blasting in surface mines (Mpofu et al., 2021; Şengün and Gül, 2023). The first step in the blasting cycle is the drilling of blastholes through the rock mass. Ideally, several rows of blast holes parallel to the free vertical face of the bench are drilled close enough to loosen the rock in between as exemplified in Figure 2.1.

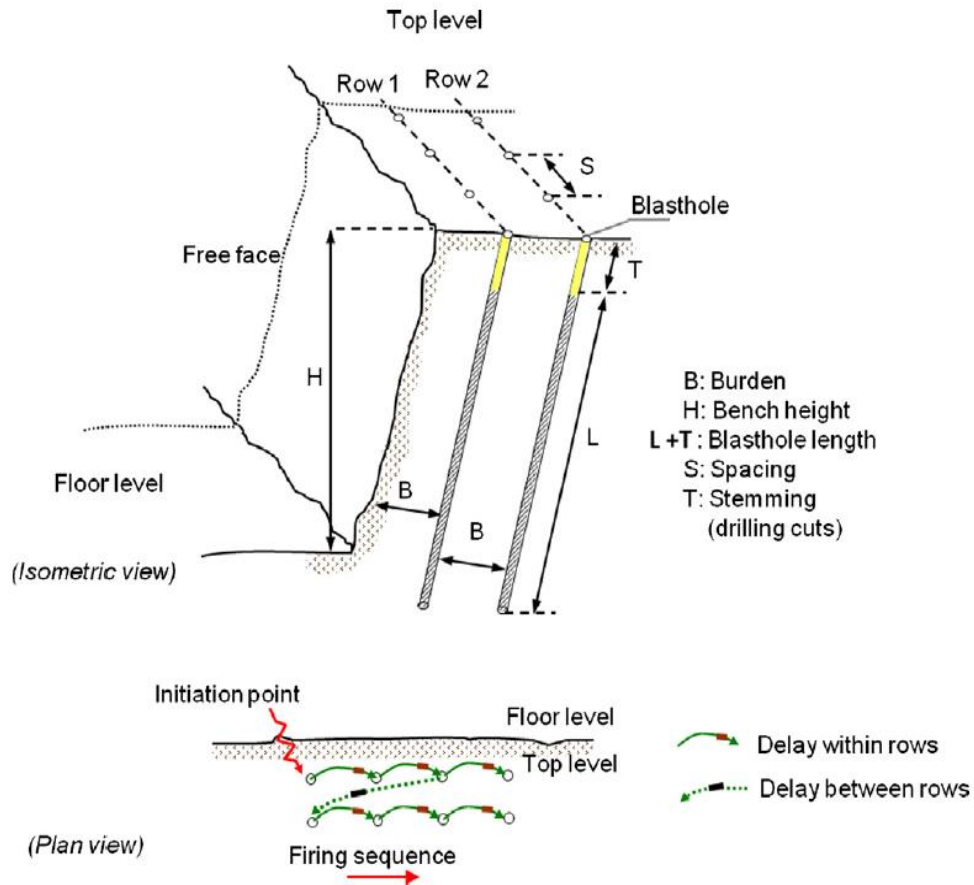


Figure 2.1: A bench showing how blastholes are drilled and connected with initiation systems (adapted from Segarra et al., 2010)

The blastholes can be drilled in either a square or a staggered pattern, depending on the conditions of the rock to be blasted. Once drilling is complete, a detonator which consists of a microchip, a fuse, and primary explosives is inserted into each hole to help activate blasting. Each detonator is programmed and assigned a specific firing time (Gomes-Sebastiao and De Graaf, 2017). Explosives are then used to fill the blastholes before the holes are capped with crushed rocks or other stemming material. The charges of explosives in the blastholes are then initiated for blasting with the help of the detonators fired following a defined timing sequence. The plan view of Figure 2.1 shows a typical blast design for a bench in a surface mine with drillholes connected with initiation systems prior to blasting. Note from the top level in Figure 2.1 that the burden (B) is the distance between the blast hole and free space, i.e., the load that will be moved by the explosives. The spacing (S) is the distance between two blast holes in a row. The blast hole length ($L + T$)

is the entire depth of the blast hole drilled while the extra depth drilled below the floor of the bench to obtain clear breakage is called subdrill. The stemming length (T) is the distance between the explosive charge and the collar of the blast hole which is filled with inert material.

In terms of firing sequence, the detonation of explosives occurs in a row of blastholes, breaking the burden (B) of rock towards the free vertical face of the block first (Segarra et al., 2010). Upon initiation of the explosive charge in each blasthole, a considerable amount of energy is released into the rock to aid in fragmenting the rock. A fraction of this energy is wasted and released into the atmosphere in the form of undesirable environmental side effects like air blast and ground vibration. These side effects can cause damage to structures and buildings located near the blast site. Moreover, air blast causes serious discomfort to local residents and personnel (Faramarzi et al., 2014; Khandelwal and Singh, 2005). According to Hajihassani et al. (2014), air blast is an unwanted by-product of rock blasting that is dependent on blast design parameters (Figure 2.1), weather conditions and type of terrain. These parameters are discussed in detail in Section 2.3. The subsequent sections give a background on how air blast is generated, measured, as well as the human and structural response limits.

2.2.1 Sources of air blast

During blasting, the premature venting of explosive gases in the drilled holes due to inadequate stemming causes air blast. Basically, air blast or air overpressure shockwaves which are generated as a result of rock blasting are produced from four main sources (Segarra et al., 2010; Kuzu et al., 2009; Siskind et al., 1980; Singh et al., 2005). These sources include the rock pressure pulse (RPP) which is produced from vertical ground vibrations. The air pressure pulse (APP) is produced from direct rock displacement at the face or ground swelling at the blasthole collar. Meanwhile, the gas release pulse (GRP) is mainly gas which escapes from the detonating explosives

through rock fractures. Lastly, the stemming release pulse (SRP) is due to gas escaping from the blown-out stemming.

Siskind et al. (1980) argues that APP is a source of air overpressure that is likely to dominate in a properly designed blast. However, this phenomenon is normally absent for cases of total confinement like underground blasts. Furthermore, Siskind et al. (1980) explained that RPP not only has the smallest amplitude amongst the four sources of air overpressure, but it is generally of higher frequency. Figure 2.2 provides a graphical definition of RPP and APP as recorded during a blast.

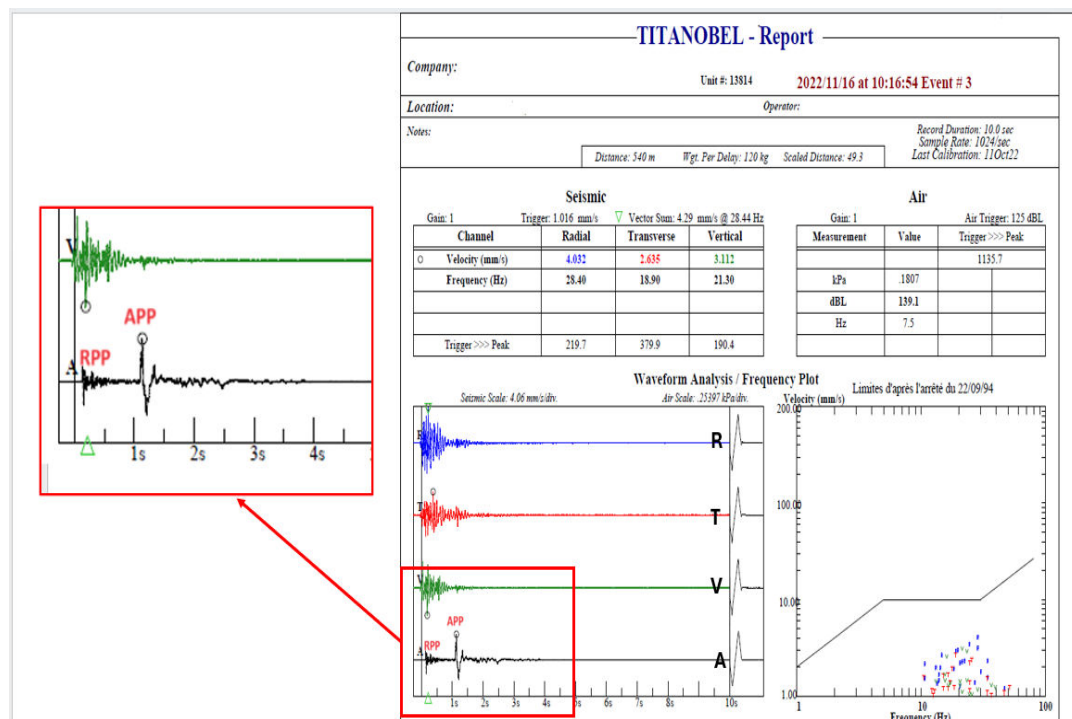


Figure 2.2: Vibration analysis report showing the RPP and APP on the waveform analysis plot (Docrat, 2023)

Note from Figure 2.2 that the waveform analysis plot features four wave plots representing the radial (R) in blue, transverse (T) in red, vertical (V) in green and air (A) in black. The radial, transverse and vertical represents measurements of the ground vibrations. Meanwhile the air wave represents measurements on air overpressure. In case of air overpressure, when a blast is fired, there are vertical ground vibrations within the rock which produces RPP as annotated on Figure 2.2 with the smallest amplitude waves.

Additionally, APP which is annotated with a higher wave amplitude is recorded after RPP as shown on Figure 2.2 and this is as a result of rock displacement. The seismograph responsible for monitoring the blast then records the respective air levels and ground vibrations as captured in the tables labelled as seismic and air as captured in Figure 2.2.

Moreover, Segarra et al. (2010) also highlighted the fact that APP and RPP are unavoidable sources of air blast in bench blasting. On the other hand, GRP and SRP are controllable sources of air overpressure that greatly depend on the blast design. Indeed, insufficient stemming can result in premature gas escape into the atmosphere thereby generating excessive air blast (Siskind et al., 1980; Singh et al., 2005). According to Segarra et al. (2010), GRP and SRP are the primary cause of disturbance near the blasting site. These two mechanisms produce high frequency waves superposed to the air pressure pulse. Frequencies lower than 20 Hz are what define the blast-induced air blast frequency spectrum (Pyra and Kłaczyński, 2019). Siskind et al. (1980) further highlighted that other factors that may contribute to GRP and SRP are small diameter holes, high propagation velocities of the rock, wet holes, and long columns.

2.2.2 Measurement of air blast

Surface mines make use of blasting seismographs to measure both air blast and ground vibration (Rorke, 2011; Kabwe and Wang, 2016; Ratcliff et al., 2011). These seismographs have a built-in control unit, a geophone sensor and a microphone in the same casing. The geophone sensor is used to measure ground vibrations while the microphone picks up the propagation of the air blast and record it over time.

Prior to a blast being initiated, the seismograph is placed in a location which is in proximity of the area being blasted. The control unit is then used to set the appropriate trigger levels for the geophone and microphone to avoid false recording from unrelated events like wind noise and blast sirens (Kabwe and

Wang, 2016). Each of these units shown in Figure 2.3 is set to trigger and start recording for vibrations and air blast once a blast is initiated.

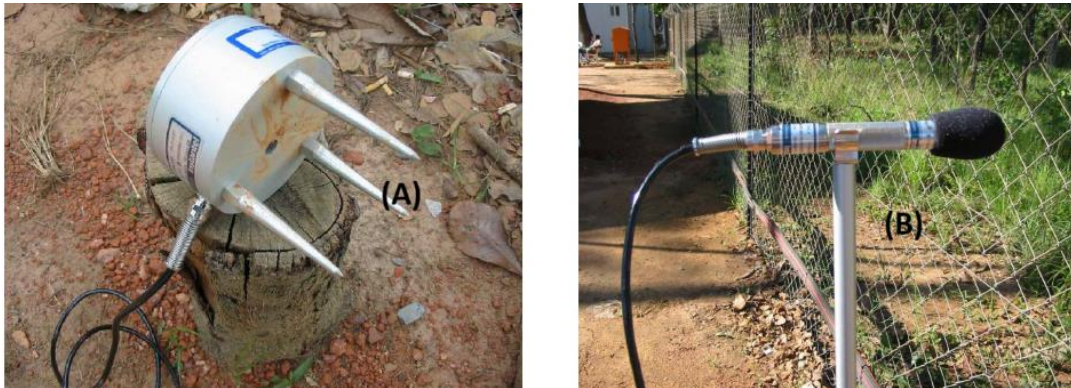


Figure 2.3: Parts of the seismograph units illustrating (A) Geophone sensor and (B) Microphone (Kabwe and Wang, 2016)

As exemplified in Figure 2.3, the geophone has spikes which are inserted into the ground to measure ground vibrations. On the other hand, the microphone is positioned in a direction facing the blast to record the air blast levels.

Air blast is commonly reported in decibels (dB) when it is actually measured as pressure expressed in millibars (mb), pounds per square inch (psi) or Pascals (Pa). The formula for converting pressure in psi to dB is provided as indicated in Equation 2.1 (Ratcliff et al., 2011):

$$\text{SPL dB} = 20\text{Log}_{10} P + 170.8 \quad (2.1)$$

Where SPL dB is the sound pressure level in decibels (dB).

P is the measured air pressure in psi.

According to Ratcliff et al. (2011), decibels are generally based on a logarithmic scale for sound pressure which also considers levels of human hearing.

2.2.3 Human and structural response to air blast

Under optimal circumstances, the human hearing frequency range is between 20 and 20 000 Hz, and it decreases over the course of a lifetime. At frequencies higher than 20 Hz, air blast may be heard by the human ear and is referred to as sound or noise; at frequencies lower than 20 Hz, air blast is inaudible and is more frequently known as a concussion (Ratcliff et al., 2011).

In terms of structural response, the most important sign of air blast that could be problematic or harmful is how buildings, especially residential ones, react to it (Siskind et al., 1980). In the 1970s, the United States Bureau of Mines (USBM) conducted extensive research on air blast (Siskind et al., 1980; Ratcliff et al., 2011). A series of surface mine blasts was carried out while the response of residential structures for potential damage and nuisance was monitored. From the results of the study, safe levels of air blast were recommended that would ensure a low probability of damage to structures. The results of the study recommended monitored air blast amplitudes of up to 135 dB to be safe, provided the monitoring instrument is sensitive to low frequencies (down to 1 Hz) (Siskind et al., 1980). The USBM recommended safety limits of air blast are widely accepted over the world and are commonly applied in South Africa (Goncalves and Tose, 2009; Kuzu et al., 2009; Ratcliff et al., 2011; Faramarzi et al., 2014; Kabwe and Wang, 2016).

The recommended limits of human and structural response to different air blast levels are given below in Table 2.1.

Table 2.1: Air blast levels and their threshold limits (Siskind et al., 1980; Ratcliff et al., 2011; Kabwe and Wang, 2016)

Level	Description
120 dB	Threshold of pain for continuous sound
>130 dB	Resonant response of large surfaces (roofs, ceilings). Complaints start.
134 dB	USBM recommended limit for human irritation
150 dB	Some windows break

170 dB	Most windows break
180 dB	Structural damage

2.3 Factors influencing the level of air blast in surface mining

Several theories exist regarding factors that affect and/or influence air blast in surface mines. This section reviews the effect of controllable blast design parameters on air blast. Specific focus is made for a review of parameters considered to be controllable since they can be altered. The effects of weather and topography on the generation of air blast are also discussed.

2.3.1 Effects of controllable blast design parameters on air blast

2.3.1.1. *Burden and spacing*

Lusk and Worsey (2013) observed that blast designs with a small burden make it easier for gases to escape during blasting. Gaseous energy is released prematurely into the atmosphere without performing any meaningful work if the burden is less than ideal (Hidayat, 2021). This can push the blasted rock in an uncontrolled manner with high speed thereby causing high air blast and flyrock. In contrast, a wider burden can result in inadequate fragmentation, excessive ground vibrations, and toe problems.

Khandelwal and Kankar (2009) reported that a burden which is smaller than the designed burden will cause a large fraction of the explosive energy to be dispersed into the atmosphere. This leads to inefficient use of explosive energy thereby resulting in significant air blast levels. A concordant study by Hidayat (2021) also supports this assertion by noting that gaseous energy dissipates into atmosphere without doing useful work. This of course was observed in instances where the burden is less than the optimum length required.

A similar principle applies with regards to the spacing between blast holes. Smaller spacing has been found to result in cratering and crushing between

holes (Lusk and Worsey, 2013). Meanwhile, widely spaced holes result in poor rock fragmentation. The concept of cratering and crushing is illustrated in Figures 2.4 and 2.5 below. Additionally, a change in spacing can influence air blast outcome by interacting with stemming techniques. An incorrect hole spacing that is coupled with insufficient stemming can worsen air blast effects (Mpofu et al., 2021; Hosseini et al., 2023). As such, the stemming length should be at least as long as the burden

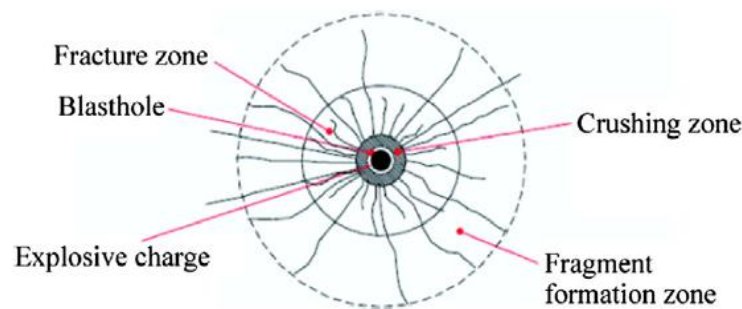


Figure 2.4: A section of the blasthole showing the crushing zone (After Silva, 2019)

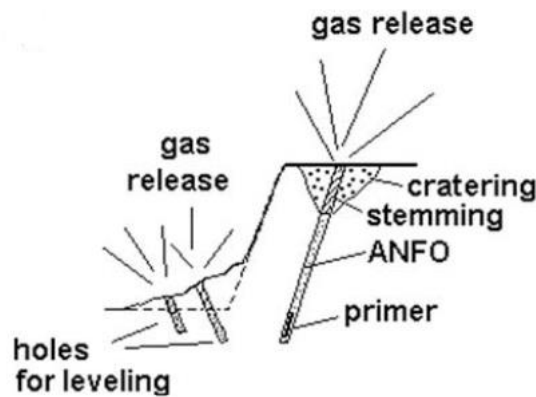


Figure 2.5: Illustration of cratering around a blasthole on a bench (Kuzu et al., 2009)

In addition to producing shock waves, the energy generated from an explosive charge also causes compressive forces that causes crushing within the rock mass (Hosseini et al., 2023). This effect then results in fracturing as illustrated in Figure 2.4. The detonation of the charge load in the collar zone, as well as the type and length of the stemming material, causes cratering to develop on top of the bench (Szendrei and Tose, 2023).

2.3.1.2. Stemming length

Stemming is the process of putting a non-explosive material on top of explosive column in a blast hole (Mpofu et al., 2021). Stemming allows for more effective use of energy for rock breaking while also preventing gases from escaping when explosives are detonated. Figure 2.6 illustrates a typical layout of a bench blast with blastholes filled with stemming material and one without stemming material.

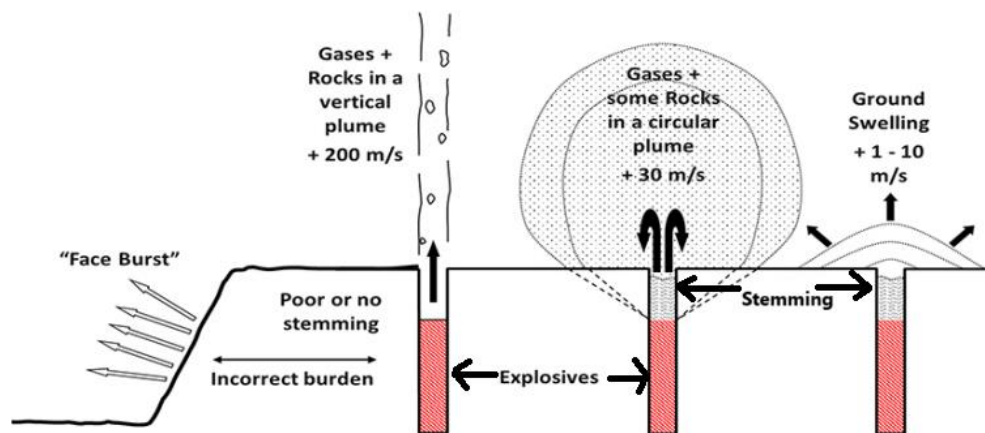


Figure 2.6: Typical layout of a bench blast (Adapted from Szendrei and Tose, 2024)

Stemming length is dependent on several elements including the power of explosives used, blast-hole diameter, burden, spacing, stemming material, and the quality of adjacent rocks (Mpofu et al., 2021; Neale, 2010; Oates and Spiteri, 2021). If stemming is not done correctly, explosive gases will be released into the atmosphere, causing air overpressure (AO_p) and noise. According to Lusk and Worsey (2013), stemming lengths that are shorter than $0.7B$, with B being the burden in metres, can result in high levels of air blast, flyrock, noise, and overbreak.

2.3.1.3. Charge weight per delay

In bench blasting (see Figure 2.7), charged blast holes are detonated in a sequence of rows, to allow the rock to move towards the free face (Prasad

et al., 2017). Normally, the detonation of explosives is carried out in a precisely timed sequence to maximise energy release and reduce environmental effects. In order to achieve the appropriate fragmentation while managing flyrock and air blast, the timing of detonations is crucial. As exemplified in Figure 2.7, the first hole to be detonated will be the one marked 0 milliseconds (ms). Thereafter the other holes will detonate at inter-hole delay timing of 17 ms and an inter-row delay timing of 25 ms.

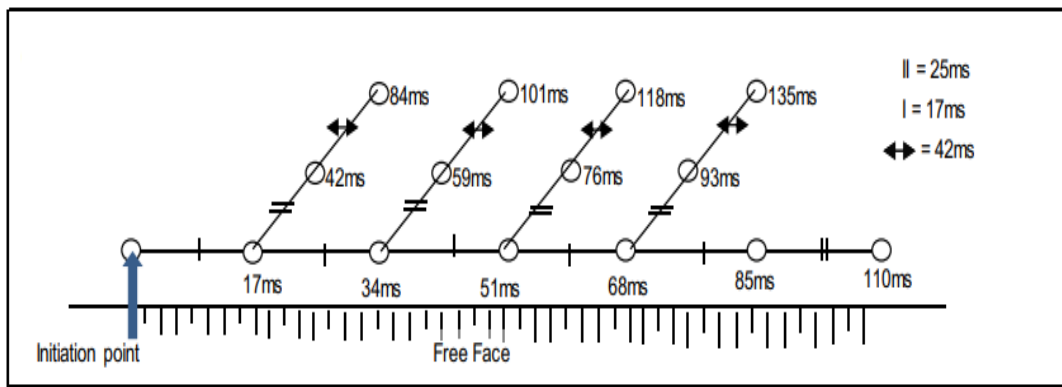


Figure 2.7: An illustration of timing sequence of blastholes in a bench (Choudhary et al., 2021)

A blasting round that uses a large amount of explosive per delay, produces a large air blast compared to one using small volume of explosives (Khandelwal and Kankar, 2009). Singh et al. (2006) defined charge weight per delay as the maximum explosive that can detonate in a hole. The charge weight per delay differs from the total amount of explosives, in that the latter involves the overall explosives charged per blasting round on a bench (Ghosh et al., 2024). Figure 2.7 consists of 15 drilled hole bench, the total amount of explosives in this case will be the total explosives charged in all 15 holes. However, the charge weight per delay will be the maximum explosive charge that detonates out of the 15 in each delay. Air blast levels increase with increased charge weight per delay (Richards, 2013). The larger the charge weight per delay, the higher the amplitude of the vibration (Kabwe and Wang, 2016; Hidayat, 2021). The control of charge weight per delay can be effectively managed by timing blasts so that holes fire one at a time or by reducing the blast hole diameters (He et al., 2022).

2.3.1.4. Monitoring distance

The effect of AOp tends to diminish if the air blast monitoring station is placed at a distant location away from the blast site due to energy dissipation into the atmosphere (Khandelwal and Kankar, 2009). In their study, Singh et al. (2005) also reported that air blast decays with distance because of geometric spreading. Geometric spreading has to do with how the energy from a blast explosion disperses over a larger area as it travels. Reed (1972) found that the air blast pressure amplitude is inversely proportional to distance raised to the power of 1.2, which implies that as distance increases, the pressure decreases significantly. Ideally, air blast decreases as the distance from the blast site increases in an inverse power function relationship (Richards, 2013; Reed, 1972). However, the relationship between the logarithm of the air overpressure and logarithm of scaled distance is linear which is deduced from linear regression (Marín et al., 2022).

2.3.2 Influence of weather on air blast

Air blasts are caused by detonation of explosives in blastholes; they travel at the speed of sound in all directions as a wave front. This is the reason why wind speed and direction, atmospheric pressure and other weather conditions affect the speed of the wave front as dictated by basic physics (Singh et al., 2005).

Weather conditions such as wind speed generally increases with height (Griffiths et al., 1978; Legesse et al., 2017). This means that as wind speed increases with height, the propagation of air blasts becomes more noticeable. A study by Zheng et al. (2010) indicates that the amplitude of wind speed from impact waves increases with the height of falling rock, leading to stronger air blasts. Additionally, as highlighted in Section 2.3.1.4, air blast intensity typically decreases with distance due to geometric spreading, where a finite amount of energy fills an increasing volume of

space. However, wind alters this decay rate; higher wind speeds can reduce the normal rate of air blast decay, allowing for greater distances to be affected by the blast (Singh et al., 2005). This variation in wind speed causes the sound generated from a blast to refract back to ground level and hence giving an increase in the expected level of sound at a distant point. Figure 2.8 is a typical illustration of how wind affects sound propagation in air.

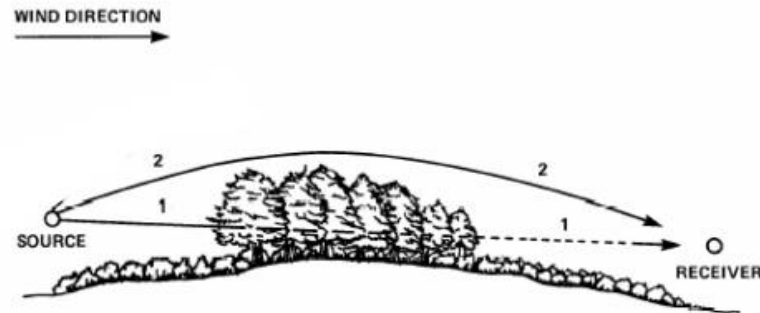


Figure 2.8: Effect of wind speed on sound diffraction (Hannah, 2007)

Note from Figure 2.8 that in the absence of wind, the principal sound wave arrives at the receiver by travelling horizontally from the source through path 1. Along this path, the ground, vegetation, and trees can absorb some of the sound (Hannah, 2007). During downward windy conditions, however, the path (2) sound (which normally travels upward into the sky and does not return to earth) is bent down and returns to the earth, sometimes passing above the attenuation from ground surface and vegetation. This process of waves returning to the ground is known as refraction and thus yields higher sound levels at the receiver. The receiver in this case can be the air blast monitoring equipment or structures on surface.

Temperature inversion is another factor that may be a concern during blasting. A study by Ozer et al. (2020) found a strong correlation ($R^2 = 0.79$) between air temperature and air overpressure propagation, indicating that as temperature increases, air density decreases, facilitating shock wave travel. In essence, higher temperatures cause the air to become less dense, which promotes the propagation of shock waves. On the other hand, lower temperature environments cause the air density to increase, which potentially results in slower shockwave propagation and less effective blasts

(Huynh et al., 2017). In light of this, a phenomenon known as temperature inversion can happen when a layer of warm air traps cooler air at the surface. This usually occurs during certain weather patterns, such as clear nights when heat reflects off the ground, forcing the air above to stay warmer while the surface air cools quickly.

During a temperature inversion, air blast waves are refracted back to the earth surface (Ratcliff et al., 2011). As this happens, the air overpressure is then concentrated on a particular structure which may be at a further distance. In a previous study, Griffiths et al. (1978) equally argued that part of the sound emanating from a blast can be refracted back to the ground level when a temperature inversion exists.

According to Singh et al. (2005), temperature inversions occur in the morning and evening as the ground surface and air get warmer and cooler at different rates. This is plausibly one of the reasons why some surface mines prefer to blast around mid-day when inversions are absent. Singh et al. (2005) also reported that an inversion can increase air blast by 10 dB over the level normally expected from a given blast at a given distance. Figure 2.9 below is an illustration of how temperature inversion occurs.

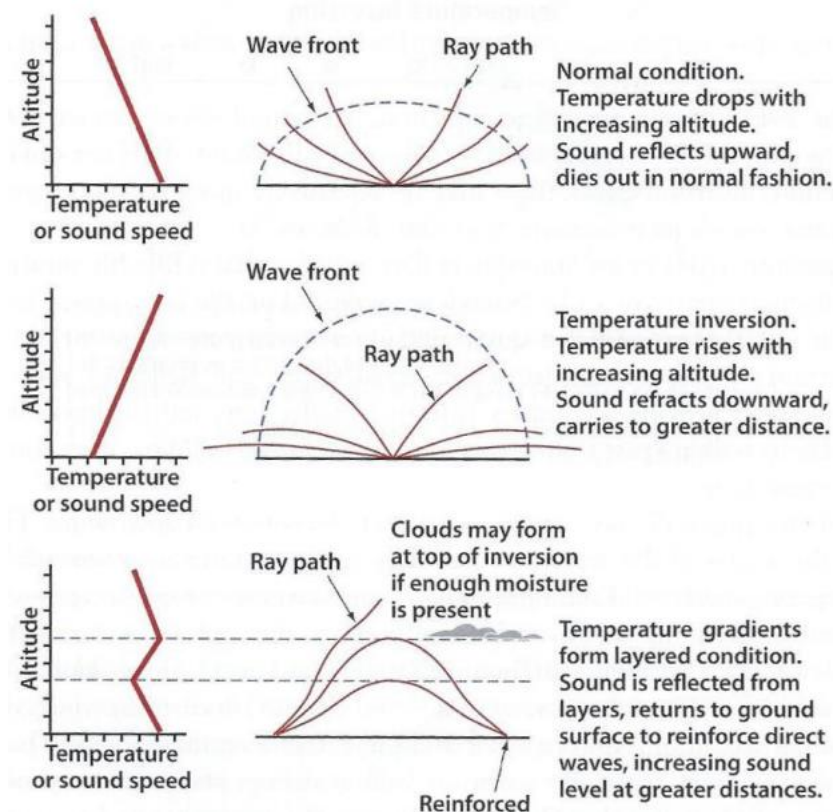


Figure 2.9: Effect of temperature inversion on sound transmission (After Ratcliff et al., 2011)

It can be seen from Figure 2.9 that during normal atmospheric conditions, temperature will decrease with an increase in altitude. Sound waves then reflect outwards and eventually die out without returning on the ground. On the other hand, when there is a temperature inversion, the atmospheric temperature increases with an increase in altitude. As such, sound waves are refracted back to the ground and spread over a greater distance. A similar principle occurs in cases of cloudy conditions due to temperature gradients which formed layered conditions. Here the sound waves are reflected from those layers and return to the ground to reinforce direct waves.

Lastly, rainy weather can extensively influence air blast levels during blasting as compared to blasting on a clear day (Ratcliff et al., 2011). Rain alters air conditions, which can improve the way blast-generated sound waves travel. In wet conditions, air blasts may be more intense and have a wider range because of changes in the way sound travels caused by variables like

humidity and air density. An increase in humidity during rainy conditions can enhance the propagation of air blast waves, leading to higher air over-pressure levels (Tran et al., 2021). Alternatively, rain can alter wind patterns, affecting how air blasts disperse. Higher wind speeds can lead to more significant air pressure fluctuations, intensifying the blast effects (Roy et al., 2011). Tran et al. (2021) further stated that rainy conditions often lead to lower temperatures, which influences the density of air and consequently the behaviour of air blasts.

2.3.3 Influence of topography on air blast

The rate of decay of air blast with distance can be influenced by the topography of the landscape. Ratcliff et al. (2011) observed that air blast levels are higher in valleys than around the hills. This is because valleys can increase the intensity of air blasts by influencing the direction of airflow and generating a noticeable deflection of air to become more parallel to the valley (Bullard et al., 2000). In contrast, hills may disperse air pressure waves more broadly, reducing their intensity in surrounding areas. When blasting in a hilly terrain, air blast levels occurring in the surrounding area are lowered by topographic shielding as exemplified in Figure 2.10. The phenomenon known as topographic shielding occurs when natural features like hills, mountains, or structures block or lessen the intensity of air pressure waves.

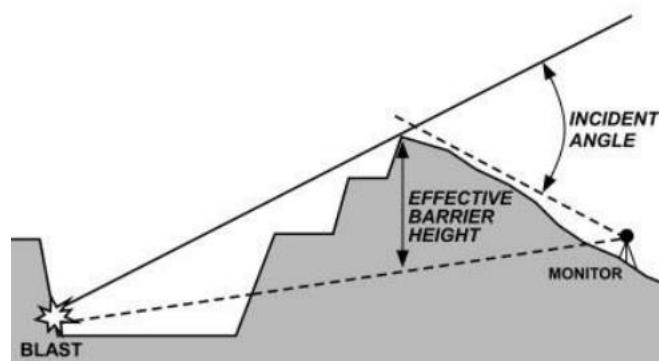


Figure 2.10: Typical illustration of topographic shielding in blasting (Richards, 2013)

Figure 2.10 illustrates that air pressure waves (e.g., sound or seismic) can be partially or fully blocked by topographical features as they travel through a medium. Features like hills can significantly reduce the impact of air blasts on nearby structures and community (Ratcliff et al., 2011). This obstruction diminishes the energy and intensity of the wave at the monitoring location.

The topography of the landscape in surface mines influences air blast levels by producing shadowing effects (Singh et al., 2005). Shadowing involves the presence of geological features such as hills and valleys which hinder the spread of air blast waves. Because of this barrier, less energy reaches some places, which lowers the air blast levels there (Ratcliff et al., 2011). Ideally, the factors discussed in this section all influence air blast levels to a certain extent. For controllable blast design parameters, surface mines can alter the parameters to optimize the blast performance. Similarly for effects such as weather and topography, care should be taken to ensure that such conditions are avoided during blasting, or proper mitigation plans are put in place.

2.4 Review of stemming techniques available in the mining industry

This section of the review provides an in-depth overview of the different stemming techniques employed in the mining industry. Firstly, the review looks at the conventional stemming material used to optimize blasting. This includes the common types of stemming material used, their physical characteristic, as well as the benefits involved with their application. Secondly other stemming techniques such as the use of deck-charge blasting, Varistem® plugs and SPARSH are reviewed. This part of the review looks at their principle of operation and the benefits involved with their application. Lastly an overview of some successful case studies where these stemming techniques were applied as highlighted by other researchers is included.

2.4.1 Conventional stemming material

In the blasting cycle, once drilled blastholes are charged with explosives and detonators amongst others, surface mines make use of inert material called stemming to fill the top of blastholes. This practice aids in confining explosive gases thereby producing better rock fragmentation. Proper stemming of blastholes has been established to be effective at reducing the occurrence of flyrocks as well as the amount of air blast produced by surface blasting activities (Rehman et al., 2021; Oates and Spiteri, 2021; Richards, 2013). The type of stemming material also plays an important role in the effectiveness of the stemming. Normally, the choice of stemming material is informed by availability and cost (Mpofu et al., 2021; Oates and Spiteri, 2021). The following stemming materials are commonly used in surface mines: drill cuttings, crushed aggregates, and plaster stemming. They are covered in the subsequent sub-sections.

2.4.1.1 *Drill cuttings*

During the drilling of blastholes, a drill bit is used to cut through the rock and penetrate the ground until the desired depth is reached. During this process, small pieces of rock, dirt and other materials are broken off and extracted from the blasthole as the drill bit penetrates. These materials that accumulate around the hole collar after drilling are known as drill cuttings or drill chippings.

Drill cuttings are the most easily accessible and least expensive stemming material that can be readily found at blast sites. As such, they tend to be most frequently utilised in open pits and quarries (Cevizci, 2012). However, dry drill cuttings eject from blastholes relatively easily and provide little barrier to the upwards explosion. As a result, a significant portion of the blast energy is wasted and lost to the environment. Konya and Konya (2018) reported that the use of drill cuttings is the most common practice; however, it is the most inefficient form of stemming material. The inherent issues with drill cuttings as a stemming material are their non-uniform particle size and poor

compaction (Rehman et al., 2021). Occasionally, these two issues cause blowouts from the stemming section. Blowouts are premature escape of explosive gases into the atmosphere. If the amount of stemming material is inadequate, it may not provide enough resistance to contain the explosive gases, leading to a blowout (Konya and Konya, 2018).

In South Africa and throughout Africa, drill chips are still used as stemming material in the mining sector, albeit their efficacy is being evaluated against other materials. Because drill cuttings are readily available at blast sites during charging operations, they are frequently used in quarries and open pits (Cevizci, 2013). However, significant improvements in fragmentation have been observed when crushed aggregate are used to replace drill chippings (Oates and Spiteri, 2021). Observations from other research indicate that alternative stemming materials like crushed aggregate might perform better in terms of rock fragmentation and explosive energy utilisation (Mpofu et al., 2021; Konya and Konya, 2018; Richards, 2013). In this light, surface mines are increasingly exploring alternative stemming materials like crushed aggregates which is discussed in the next section.

2.4.1.2. *Crushed aggregates*

In the mining context, aggregates refer to coarse material such as crushed stone, gravel, sand, and concrete. These materials are generally extracted as raw material at quarries and are then processed to the desirable product size. Crushed aggregates of uniform particle size are the most common and highly recommended stemming material (Oates and Spiteri, 2021). A uniform particle size distribution is important because it influences how pressure waves propagate through the stemming material (Konya and Konya, 2020). As such, this can help mitigate environmental impacts such as air overpressure by absorbing and dissipating energy more effectively. Figure 2.11 illustrates the typical size range of crushed aggregates used for stemming in surface mines. When applying crushed aggregates for stemming in blasting operations, the typical effective size range is between

5 mm to 20 mm (Fomina and Polyanskiy, 2019). This size range offers adequate packing density and interlocking capabilities to withstand explosive pressures (Chung and Mustoe, 2002)



Figure 2.11: (a) Crushed aggregates; (b) Blasthole filled with crushed aggregates (Own picture taken by the author at Quarry TM)

Mpofu et al. (2021) pointed out that crushed aggregates are a cost-effective type of stemming that can be typically produced on quarry operations and at a desirable rate. The cost of crushed aggregates in South African surface mines is affected by a number of operational elements, such as transportation, blasting, and drilling. By increasing blasthole diameter from 89 mm to 102 mm, total unit costs can be reduced by about 0.091\$/m³ (Bilim et al., 2020).

Ideally, in a typical open pit mine, the stemming material needs to be sourced from a quarry and transported to the mine which can incur non-negligible costs. In terms of the performance of crushed aggregates over drill cuttings, studies have revealed significant differences in their effectiveness for rock fragmentation and operational efficiency. A study by Sharma and Rai (2015) found a better muckpile throw of 21.2% and an 18% increase in loading and hauling productivity when crushed aggregate was used instead of drill chippings. Additionally, crushed aggregate stemming resulted in smaller average fragment sizes (i.e., K_{50} values of 0.45–0.59 m) compared to drill cuttings (K_{50} = 0.58–0.77 m). In another study, crushed aggregates were found to enhance explosive energy confinement, resulting in reduced wear on crushing equipment and improved mill performance (Kojovic, 2005).

2.4.1.3. Plaster stemming

Plaster stemming is a newly developed stemming material made of a thick paste, which hardens in less than 25 to 30 min of application. Figure 2.12(a) illustrates how the plaster paste is poured into the blasthole collar and Figure 2.12(b) shows the hardened plaster paste. This stemming technique has been found to be more effective than traditional dry drill cuttings (Cevizci, 2012). When applied in a blasthole, the hardened plaster creates a strong plug that confines the blast energy better, resulting in better fragmentation and slightly higher ground vibrations. In a follow-up study, Cevizci (2019) compared plaster stemming with drill cuttings. The researcher found that blast-induced vibration was increased when using plaster stemming compared to drill cuttings. This is an indication that more of the blast energy is transferred and used to break the rock as the plaster confines blast-induced pressure.



Figure 2.12: (a) Application of plaster paste into the blasthole collar; (b) Blasthole filled with hardened plaster (Cevizci, 2013)

The comparison between plaster stemming and drill cuttings in surface mines reveals significant differences in efficiency, cost, and environmental impact. Cevizci (2019) observed that plaster stemming can achieve higher maximum pressure (11 945 MPa) compared to drill cuttings (7 395 MPa), indicating better energy utilization. Previous studies (Cevizci, 2013 & 2014) as well showed that blasting costs can be reduced by 15-16% with plaster stemming

due to increased burden and spacing distances. And while plaster stemming was reported to increase vibration and air shock slightly, corresponding values remain within acceptable limits.

2.4.2 Deck-charge blasting

The process of deck charging involves dividing the explosive charge within a single deep blast hole into multiple columns, with each column being separated by a specific length of stemming or air cushion. This is illustrated in Figure 2.13. The type of stemming material used on top of the explosive column is either drill cuttings or crushed aggregate.

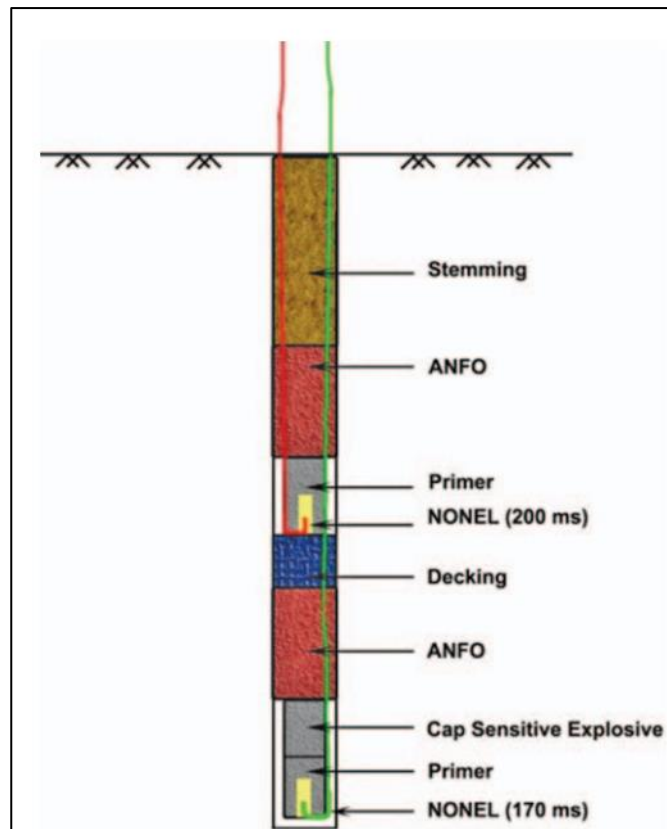


Figure 2.13: Deck-charge arrangement for a quarry blast (Balamadeswaran et al., 2018)

Deck charge technology has been proven to effectively improve the utilization of explosive energy (Balamadeswaran et al., 2018; Zhang et al., 2018). In addition to this, deck-charging has two major benefits: improved

distribution of the explosive energy and reduced explosive charge per delay. The improved distribution of explosive energy within the rock mass results in better rock fragmentation while reduced explosive charge per delay leads to lower ground vibrations (Singh et al., 1991; Persson et al., 1993; Jhanwar, 2011; Zhang et al., 2018). Kabwe (2017) reported a 94% reduction in oversized fragments, with a mean fragment size of 264.81 mm. This led to improved efficiency of loading and hauling. All these benefits were realised from the use of deck charge blasting technique.

Deck-charging is generally employed when the strength of the rock varies significantly throughout the length of the blasthole (Balamadeswaran et al., 2018). There are three possible locations where an air-deck can be placed in a blasthole; namely, at the top of explosive charge, in the middle of the explosive column, and at the bottom of the blast hole below the explosive charge (Jhanwar, 2011). Each deck in the blasthole is initiated by a unique primer containing an individual delay detonator which is in turn activated by the passing detonation front from the detonating cord (Persson et al., 1993).

Deck charge stemming significantly contributes to air blast reduction in surface mines by optimizing the explosive energy distribution and minimizing undesirable side effects. Implementing top air decks has been shown to reduce flyrock by 50% and back break by 38%, which are critical factors in air blast generation (Monjezi et al., 2022). Deck charge stemming also comes with its own drawbacks which may hinder its adoption in some surface mines. In deck charge stemming, the necessity for certain materials and methods may result in increased operating expenses that are not always outweighed by the advantages (Zhang et al., 2018). Moreover, to the best outcome, the top, middle, or bottom charge placement must be carefully considered when implementing deck charge stemming. Misplacement may result in increased ground vibration and inefficient blasting (Monjezi et al., 2022).

2.4.3 Varistem® plugs

The Varistem® technology is a patented stemming plug designed for use in mining, quarrying, and civil blasting. These plugs were patented by MOCAP, a company based in the United States of America, under the patent number US5936187A (Miller and Brown, 1999). ERG Industrial (Pty) Ltd is the official distributor of the suite of Varistem® stemming plugs across South Africa, Africa, and the world at large. The manufacturing process used to produce Varistem® stemming plugs is known as dip moulding (Varistem, 2023). During this process, a mould typically made from a metal is heated into a specific temperature. The heated mould is then dipped into a liquid polymer or plastic material. This material coats the interior surface of the mould, forming a layer that will become the plug.

These plugs typically consist of wedge-shaped material made from suitable plastics, which are designed to lock into place within a blast hole upon the initiation of explosives. The plugs are manufactured from durable plastics, which provide the necessary tear strength and flexibility to withstand the forces generated during blasting (Bruce, 2017).

According to ERG Industrial (2023), Varistem® blast stemming plugs are available in various sizes to fit blasthole diameters ranging from 45 mm to 251 mm as illustrated in Figure 2.14 below.



Figure 2.14: Different sizes of Varistem® plugs available for use in blasting (ERG Industrial, 2023)

Once the charging of blastholes is complete, stemming plugs are inserted between the explosive column charge at the bottom and the stemming material to be filled on top as illustrated in Figure 2.15.

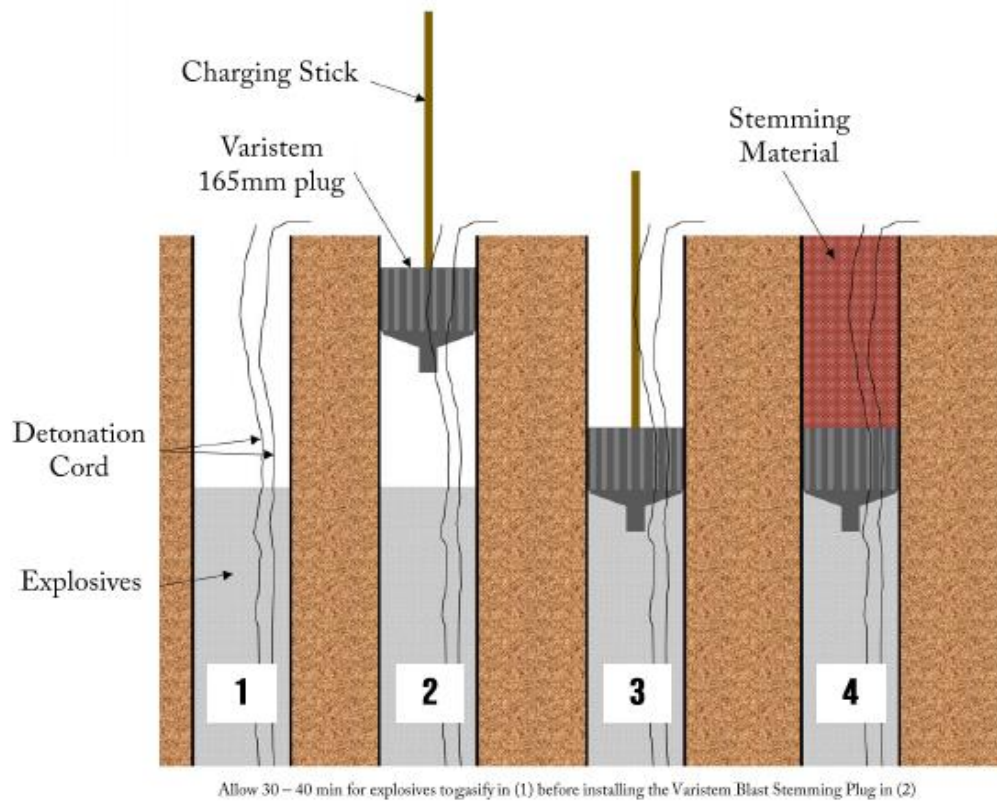


Figure 2.15: Schematic showing the installation of a Varistem® stemming plug into a blasthole (ERG Industrial, 2020)

According to ERG Industrial (2023), the shockwave created by the denotation of the explosive charge forces the plugs upward into the stemming material. This then creates a temporal pressure seal in the blasthole. The temporary pressure locks the plug in place and retain the explosive energy for a short time while directing it into the rock mass to weaken the rock. The sealing effect is crucial for enhancing the efficiency and effectiveness of the blasting operation. As such, the Varistem® plug operates by directing most of the shockwave/explosive energy into the rock mass (Modern Mining, 2021). This prevents the explosive gases from escaping and venting through the blasthole. It is therefore anticipated that Varistem® stemming plugs may potentially lead to improved fragmentation,

reduced occurrence of flyrocks, reduced noise and air blast, and increased energy retention (ERG Industrial, 2023).

A coal mine in the Mpumalanga province of South Africa has been using Varistem® stemming plugs at their operations since November 2019. Prior to adopting the plugs, the coal mine was faced with challenges of significant air blast. ERG Industrial then proposed the Varistem® as a way of reducing air blast. The Varistem® plugs were tested and successfully reported to have reduced air blast by 61% to 71% (Modern Mining, 2021).

Another successful case study exists at AfriSam's Rooikraal quarry. AfriSam is a leading supplier of construction material such as cement, aggregates and ready-mix concrete material. Their Rooikraal quarry is located within Brakpan, in the Gauteng province. In 2021, a trial was undertaken by ERG Industrial at AfriSam's Rooikraal quarry. The intention of the trial was to demonstrate the energy retention capabilities of the Varistem® blast stemming plugs by means of a split blast conducted on the production blocks. The blocks were split into two sections: the first incorporated the 102 mm Varistem® plugs while the other used crushed aggregates only for standard stemming. Figure 2.16 illustrates this setup and the performance of the trial blast upon initiation.

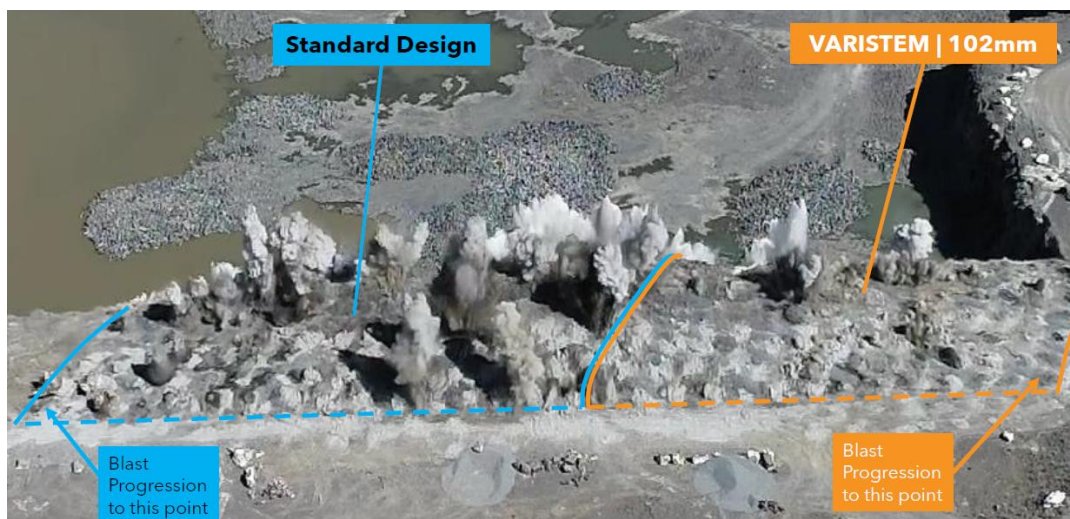


Figure 2.16: Performance of the standard versus Varistem® blast at Rooikraal quarry (ERG Industrial, 2021)

A visual analysis of the two blasts in Figure 2.16 suggests an improvement in overall energy retention for the Varistem® plugs (ERG Industrial, 2021). This is because the Varistem® operates by directing most of the shockwave/explosive energy into the rock mass. It is also evident that the Varistem®-plugged block took a significantly longer time to release the explosive energy into the atmosphere than the standard stemmed side. The enhanced energy retention that was observed on site results in decreased noise and vibration, decreased flyrocks, and improved fragmentation

Given the review covered above, it is important to note that there are currently very few scientific publications on the Varistem® plugs. Selected internal reports from the supplier, ERG Industrial, provide some insights on the performance of Varistem® plugs. This database also contains a small number of publicly available reports that are questioned for their scientific validity. To fill this knowledge gap and validate some of the empirical data on the performance of the plugs, a scientific investigation is necessary.

2.4.4 SPARSH

Stemming Plug Augmenting Resistance to Stemming in Holes (SPARSH) is another commercial stemming plug available for use in engineering blasting. Sazid (2014) reported that SPARSH can be efficiently applied to most practical blasting conditions such as blasthole of any diameter, watery blastholes, and blasthole in any direction or inclination. According to Saharan et al. (2017), SPARSH does not restrict the type of stemming material and stemming length. Moreover, it can be effectively used with air-decking above the explosive column. Indeed, the combination of SPARSH and air-decking has been found to be an effective way of enhancing explosive energy utilisation (Sazid, 2014; Mel'nikov et al., 1979; Marchenko, 1982).

The design of the SPARSH is comprised of a base plate and stemming spikes that exerts an outward pressure on the wall of the blasthole when inserted. This outward pressure locks in any blasthole pressure that might arise from the detonation of the explosive column. Figure 2.17 shows a

schematic of the arrangement of SPARSH while Figure 2.18 provides a graphical comparison of the standard stemming method with the SPARSH arrangement.

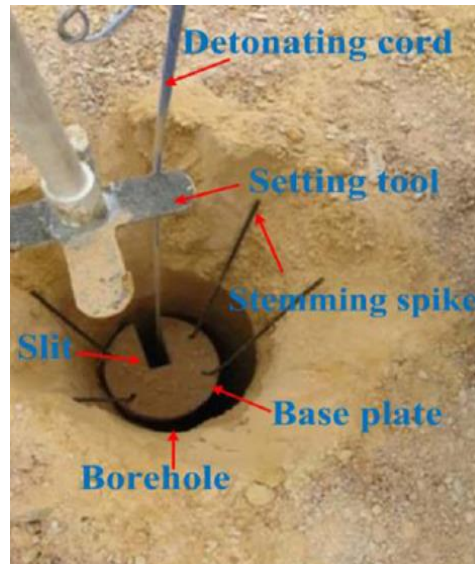


Figure 2.17: Arrangement of the SPARSH (Sazid, 2014)

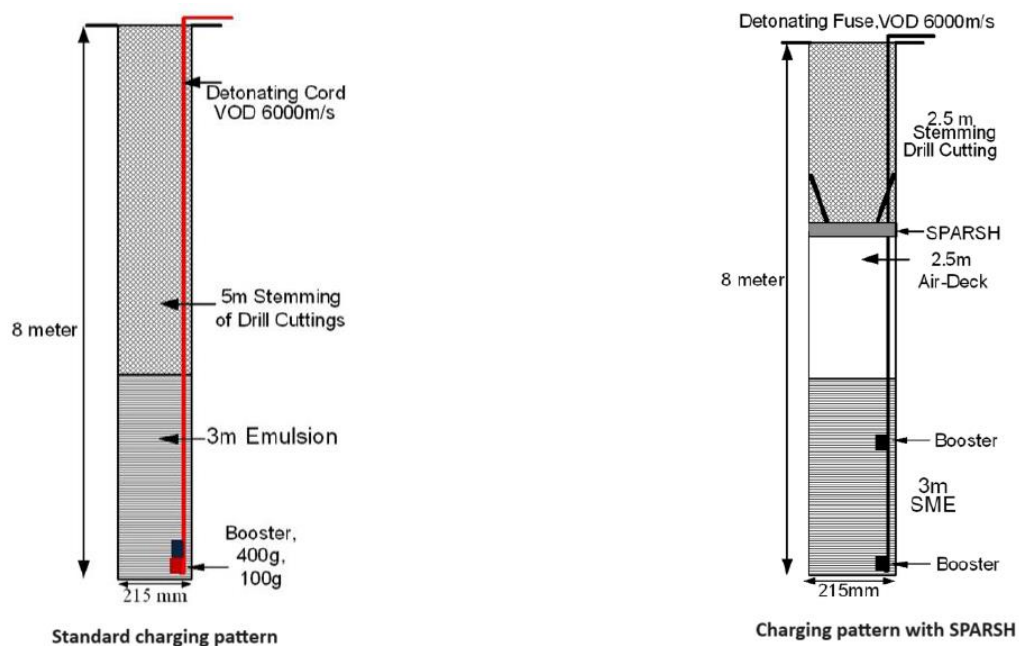


Figure 2.18: A comparison between standard stemming arrangement versus SPARSH (Saharan et al., 2017)

Note the difference in stemming arrangements in Figure 2.18 for a similar geometry of the two blastholes: 8 m in depth and 215 mm in diameter. The

standard charging pattern made use of a detonating cord with a 400g and 100g booster which was first inserted inside the hole. An emulsion explosive of up to 3 m was used to charge the blasthole. Thereafter, drill cuttings were used to stem the hole up to 5 m. On the other hand, charging with SPARSH involved leaving a 2.5-m air gap above the 3-m explosive column by inserting the SPARSH in place. The remaining blasthole column was stemmed with drill cuttings. Sazid (2014) conducted several experiments on four different mines comparing the SPARSH to conventional/standard stemming. One key benefit observed with the application of SPARSH was the elimination of boulders at all four mines investigated. The introduction of the SPARSH subsequently led to the reduction of the mean fragment size by over 30% in the muckpile. Additionally, a 30% reduction in explosives required for blasting was achieved while improving the fragmentation.

Finally, Saharan et al. (2017) reported that the SPARSH can lower stemming ejection velocity by approximately 41.27%. This means a reduction in stemming ejection velocity of about 0.65 times compared to conventional stemming was achieved. This reduction is essential as it minimizes the loss of explosive energy due to gas venting, thus improving the overall blasting efficiency. Additionally, SPARSH also provided an increased energy retention time of approximately 5 times that of conventional stemming practices.

2.5 Significance of energy containment during a blast

In surface mining operations, blast energy confinement is essential to obtaining efficient and safe blasting results. Ensuring that blast energy is properly contained minimises harmful environmental impacts such as air overpressure, flyrocks, and ground vibrations while optimising the beneficial work done in fragmenting and displacing the rock mass (Tobin, 2013). Based on the literature reviewed in the previous sections, it is evident that stemming has an important role to play in the containment of the explosive energy in a blasthole. Oates and Spiteri (2021) states that “stemming retains useful

explosive gas energy that is wasted in the case of unstemmed holes”. Furthermore, understanding the mechanisms of air blast generation and the risks involved is crucial for developing effective control measures.

Successful blasting is the result of optimized blast design and most importantly, reduced environmental impacts. This can be achieved by considering factors such as rock properties, geology, and confinement conditions in the design of the blast (Lopes et al., 2022; Himanshu et al., 2023). The concept of Scaled Depth of Burial (SDoB) was introduced in blasting engineering to optimize explosive charge design and enhance the effectiveness of blasting operations.

The SDoB is an empirical measure of blast energy confinement. Scaled depth can be described as the ratio of the stemming material to the amount of explosives within a space equivalent to 10 hole diameters (Tobin, 2013). Figure 2.19 shows a schematic of the concept of SDoB. Using this concept, blast design parameters such as stemming, burden, and spacing can be optimized (ERG Industrial, 2023). This can help mining operations to accomplish the desired rock fragmentation and displacement. In addition to this, mining operations may be able to minimize environmental impacts and meet regulatory standards around air blasts.

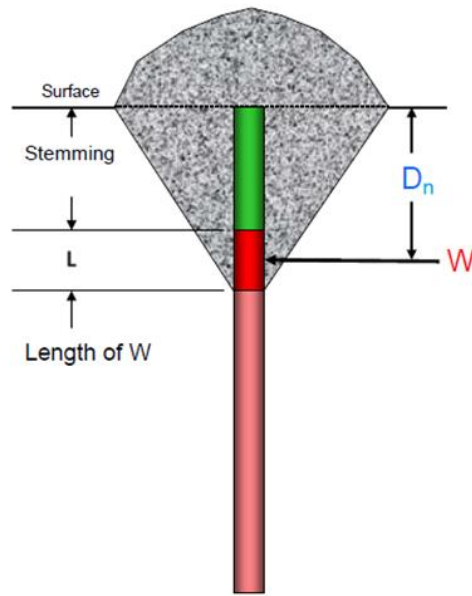


Figure 2.19: Schematic illustrating the scaled depth of burial concept (Chiappetta, 2010)

A common rule of thumb used when doing SDoB calculations states that if a blasthole has a diameter less than 100 mm, a maximum value of 8 should be used to calculate L and if the blasthole diameter is greater than 100 mm, a value of 10 should be used (Chiappetta, 2010; Tobin, 2013). The scaled depth of burial (SDoB) can be calculated using Equation 2.2 below (Chiappetta, 2010):

$$SDoB = \frac{D_n}{W^{1/3}} \quad (2.2)$$

$$\text{Where } D_n = S_t + 0.5 L \quad \text{and} \quad W = \frac{\rho d^2}{1273} L.$$

From Equation (2.2) and Figure 2.18 above, D_n represents the distance from the surface to the centre of the stem charge (in m); W is the mass of explosives equivalent to 10 explosive diameters (in kg); and L is the length of explosive (in m). S_t represents the top stemming (m), d is the hole diameter (mm) and ρ is the average in-hole density of explosive (g/cm³).

Figure 2.20 illustrates the significance of the SDoB by portraying how the ratio of stemming to explosives influences the level of blast energy confinement.

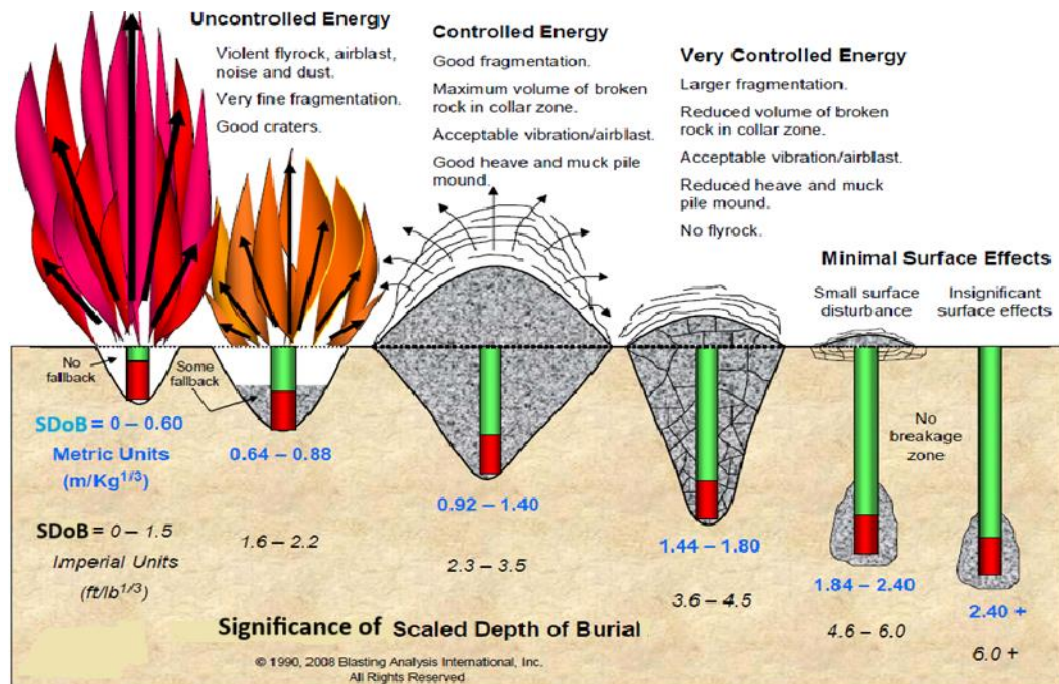


Figure 2.20: Pictorial definition of the scaled depth of burial (Chiappetta, 2010)

It can also be seen that deeper burial depths are indicated by higher *SDoB* values, which lead to more controlled energy release and minimal surface impacts. Tobin (2013) stated that ‘if the stemming height is inadequate (that is, the ratio of stemming material to explosives in 10 diameter holes is low), the energy release is uncontrolled, with the majority of the blast energy manifesting itself in nuisance such as fly rock and noise and the minority of the energy applied to rock breaking’.

2.6 Previous studies on air blast reduction

The environmental impacts caused by blasting activities must be monitored and controlled to minimize any disturbance to nearby residents. Several researchers have studied air overpressure (AOp) and proposed various generalized models. These models generally built using scaled distances as well as linear and multiple regression have since registered varying degree of success as control tools for blast-induced AOp.

As highlighted earlier in Section 2.2.3, the USBM has studied air blast from several surface mining operations and has come up with safe regulatory limits for air blasts. In addition to this, the USBM developed an empirical model for predicting air blast (Siskind et al., 1980). The USBM predictor model makes use of the cube-root scaled distance method to predict AOp. This method is widely accepted in surface mines and quarries (Kuzu et al., 2009; Hajihassani et al., 2015; Segarra et al., 2010; Siskind et al., 1980). The scaled distance (d_s) method captured in Equation (2.3) below is popular in surface mines and can be applied in the absence of monitoring instrument to predict AOp (Hajihassani et al., 2015). The cube-root scaled distance formula used for predicting air blast is indicated in Equation 2.3 (Siskind et al., 1980, Ratcliff et al., 2011):

$$d_s = \frac{D_1}{W_1^{1/3}} \quad (2.3)$$

Where D_1 denotes the distance (in m) from the monitoring station to the explosive charge; W_1 is the explosive charge weight per delay (in kg); and d_s is the cube-root scaled distance expressed (in m.kg^{-1/3}).

Since the intensity of air blast decreases with distance more rapidly than ground vibrations, the cube root of the charge weight, instead of square root, is more useful for predicting air blast intensity (Gou et al., 2020). It should be noted that the scaled distance (d_s) is different from the scaled depth of burial (SDoB) discussed in Section 2.5. The latter relates to the confinement and energy release of the blast. The scaled distance on the other hand is associated with the distance from the blast site to the monitoring point (D_1) divided by a scaling factor based on the explosive charge weight (W_1) (Ratcliff et al., 2011).

To come back to the USBM predictor model, using Equation (2.3) above, a site specific AOp attenuation formula was established to predict air blast levels. This is done through statistical analysis techniques such as least squares regression analysis and the resultant USBM predictor equation is given below (Kuzu et al., 2009):

$$AOp = H (d_s)^{-\beta} \quad (2.4)$$

Where AOp is the air overpressure (in dB); H and β are dimensionless site-specific factors; and d_s is the scaled distance factor in Equation (2.3) above expressed (in $\text{m.kg}^{-1/3}$).

In a study by Alaba et al. (2023), Equation (2.4) was tested along with other empirical models to predict air blast levels at a mine. The comparative analysis looked at the performance of each model in terms of their respective accuracy and precision. The USBM model (Equation 2.4) was found to be more reliable compared to other empirical models. Equation (2.4) recorded a coefficient of determination $R^2 = 0.9913$, a root mean squared error RMSE = 0.2729, and a standard error SE = 9.60. In essence, an R^2 of 0.9913 means that Equation (2.4) can account for 99.13% of the air blast data collected at the mine where the study was undertaken. Meanwhile, a RMSE of 0.2729 indicates that Equation (2.4) is a better model fit and has yielded an almost accurate prediction of air blast at the mine. However, the standard error suggests that there is a slight deviation of 9.60 when comparing the predicted data to the measured data. Basically, a model is considered an ideal fit when $R^2 = 1$, RMSE = 0, and $s = 0.0\%$ (Khemlani and Trafton, 2014; Sapra, 2014; Larry and Taylor, 1997).

Kuzu et al. (2009) also explored the use of the industry accepted cube-root scaled distance method outlined in Equation (2.3). However, Kuzu et al. (2009) realised that the use of the SD method alone provided a limitation because it restricted the mass of explosives to be used per delay. To address this limitation, Kuzu et al. (2009) modified the empirical formula and infused it in Equation (2.4). In doing so, the researchers were able to take site-specific factors such as the geological properties of the rock mass into account. Afterwards, they discovered that their predicted AOp levels were still high probably due to stemming. Indeed, their blast design incorporated small length of blast holes making the available length of stemming to be short. As a result, the blast holes often blew out the stemming material resulting in high air pressure waves. The role of the discontinuities present

in the rock structures probably also had an impact on the outcome of their results. The researchers then recommended that the most sensible course of action for future enquiry would be to set blasting parameters adequately at the source of the blast. It is important to note that recorded deviations less than 7% from the measured air blast levels on site.

In another study, Segarra et al. (2010) investigated air overpressure in quarry blasting by introducing a new prediction model. The model was based on the peak overpressure from blasting and air blast data gathered from 41 blasts monitored at two quarries. Here also, Segarra et al. (2010) made use of the scaled distance method (i.e., Equation 2.3) to develop their own empirical model of air blast. They then established that peak overpressure (P) is related to the scaled distance as indicated in Equation 2.5 (Segarra et al., 2010):

$$P = a_0 d_s^{a_1} \quad (2.5)$$

Where a_0 and a_1 are coefficients of the peak overpressure attenuation laws of mass-scaled distances as given in Table 2.2 below.

Table 2.2: Coefficients a_0 [in $\text{Pa} (\text{m kg}^{-1/3})^{-a_1}$] and a_1 [dimensionless] descriptive of the peak overpressure attenuation laws of mass-scaled distances (after Segarra et al., 2010)

Source	Description of the tests	f_L (Hz)	a_0	a_1
USBM (1980)	Quarry blasts. Behind face	0.1	622	-0.515
	Quarry blasts. Direction of the initiation	0.1	19,010	-1.12
	Quarry blasts. Front of face	0.1	22,182	-0.966
ISEE (1998)	Confined blasts for air blast suppression	n.s.	1906	-1.1
	Blasts with average burial of the charge	n.s.	19,062	-1.1

Kuzu et al. (2009)	Quarry blasts in competent rocks	2	261.54	-0.706
	Quarry blasts in weak rocks	2	1833.8	-0.981
	Overburden removal	2	21,014	-1.404
Hustrulid (1999)	Detonation in air. Unconfined	n.s.	185,000	-1.2
f_L is the lower frequency of the transducer. n.s. stands for “not specified”.				

To build the model, Segarra et al. (2010) introduced a new parameter A , which resulted from accounting for asymmetrical propagation of air blast:

$$P = A d_s^{a_1} \quad (2.6)$$

Where A is an asymmetry correction factor defined as the product of the coefficient a_0 in Equation (2.5), the bench face factor A_f , and the initiation sequence factor A_s . By replacing all these three factors into Equation (2.6), the below can be obtained:

$$P = a_0 A_f A_s d_s^{a_1} \quad (2.7)$$

Segarra et al (2010) went further and accounted for the directional effect of rock displacement. They proposed that factor A_f in Equation (2.7) is an amplifier of air overpressure at the bench floor level. This was expressed as follows:

$$A_f = \exp(a_2 \cos\theta) \quad (2.8)$$

The initiation sequence A_s factor, on the other hand, which accounted for wave superposition in the direction of the initiation was defined as:

$$A_s = \exp(a_3 W_0) \quad (2.9)$$

Where W_0 is a function of the angle and velocity of the initiation.

By combining Equations (2.8) and (2.9), the following predictive equation was formulated:

$$P = a_0 Z^{a_1} \exp(a_2 \cos\theta + a_3 W_0) \quad (2.10)$$

A linear type of microphones connected to the blasting seismographs were used to measure AOp. These measurements were taken around the blasted blocks at distances ranging from 45 m to 394 m for the 41 blasts. The measured peak overpressures ranged from 482 Pa to 6 Pa with a relative expanded uncertainty of 13.1% (Segarra et al., 2010). Using the model in Equation (2.10) resulted in a coefficient of determination of 0.87. This means that the model accounted for 87% of the variance in overpressure and was found to be statistically meaningful. The mean of the absolute values of the relative errors for the data set was found to be 32%. This value measures how accurate the model is by comparing the predicted and measured overpressures.

In a more recent work, Jaroonpattanapong and Tachom (2021) studied blast-induced AOp by focusing on two controllable parameters: the delay time between rows or circuits and the anticipated direction of the blast. The work involved making use of a wavefront reinforcement model to describe AOp. The researchers chose this model because they wanted to test the theory stating that AOp levels increase at locations where air wavefronts are reinforced. Figure 2.20 illustrates the principle of wave reinforcement from blastholes.

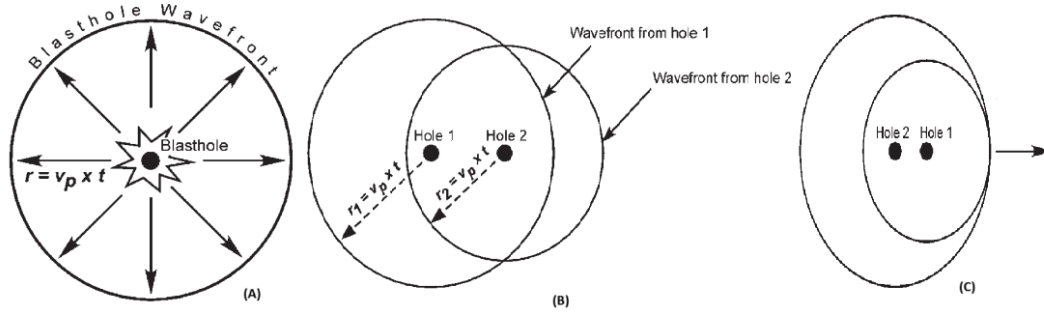


Figure 2.21: (A) Wavefront propagation from a blasthole; (B) wavefronts from two blastholes with time delay between initiations; (C) reinforcing wavefronts from two blastholes with time delay between initiations (Richards, 2008; Jaroonpattanapong and Tachom, 2021)

The wavefront reinforcement model in Figure 2.20 is a framework that works on the principle that when a single blasthole is fired, an air-transmitted vibration wavefront occurs. The wavefront then spreads uniformly in all directions and propagate at the speed of sound v_p . At any period after the blast, the wavefront will be at a radius r from the blasthole, which is proportional to time t based on the relationship $r = v_p t$. If two blastholes are initiated with a time delay between holes, the wavefronts will be of different radii because of the delay time and different centres. Wavefronts from two blastholes with time delay between initiations coincide and reinforce in the same direction (see Figure 2.20C). The researchers applied this AOp wavefront reinforcement model to 54 blasts. Coordinates of each blast hole, drill pattern, burden, spacing, and delay time between blast holes were collected to aid in determining the radius of each blast hole as shown in Equation (2.11) below (Jaroonpattanapong and Tachom, 2021):

$$R_n = \frac{v_p (T - t_n)}{1000} \quad (2.11)$$

Where R_n is a radius of the diameter of each blasthole (in m); v_p is the velocity of the sound wave the default value of which is 340 m/s; T is the fixed default time value per blasting round which is 2 500 ms; and t_n is the relative initiating time of each blasthole compared to the initiating time of the first blasthole (in ms).

To determine the wavefronts reinforcements, data relating to the coordinates of blast holes, drill pattern, burden, spacing, and delay time between blast holes of the blasts were collected. This data was recorded, and Equation (2.11) was used to calculate R_n for the different blastholes. The coordinates of the blastholes and radii data were then transferred to AutoCAD® software and processed through a script file (Jaroopattanapong et al., 2018). Using this software, wavefront circles were then generated from the first blasthole to the last. Once these wavefront circles overlap, two locations if reinforcement and non-reinforcement are identified on the wavefront. A handheld GPS is then used to locate these identified areas on site using their coordinates. Seismographs are then placed at these locations to record vibrations.

Out of the 54 blasts that were conducted for their study, only 37 blasts generated wave reinforcements. And from the 37 experimental blasts, 29 blasts (or 78.4%) recorded higher AOp levels at the areas where the wavefront reinforcement occurred while 8 blasts did not follow the wavefront reinforcement. Moreover, the researchers observed that the wavefront reinforcement areas are generally clustered in two areas: the front and the back of the blasting direction as exemplified in Figure 2.22. The parallel red lines indicate reinforcement areas.

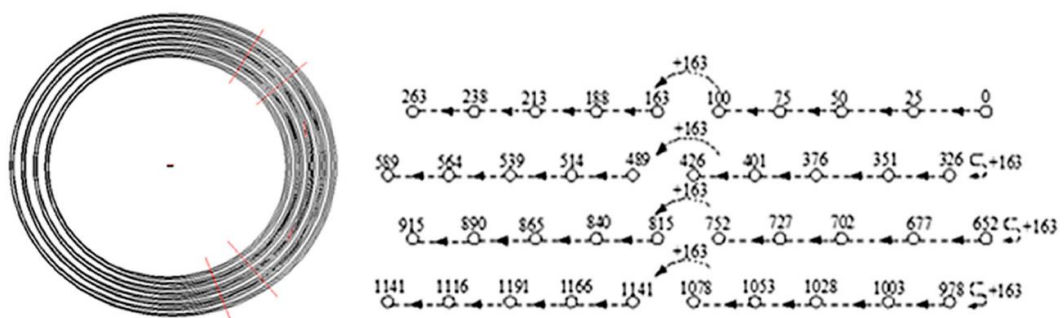


Figure 2.22: Wave reinforcements of air waves during blasting (Jaroopattanapong and Tachom, 2021)

In essence, Jaroopattanapong and Tachom (2021) found that the wavefront reinforcement model offers an alternative solution to reducing the blast-induced air overpressure.

One simple empirical formula for predicting AOp was proposed by the National Association of Australian State (NAAS). The mathematical model applicable to confined blasthole charges is given by (NAAS, 1983; Hajihassani et al., 2015; Alaba et al., 2023):

$$AOp = \frac{140}{D_1} \left(\sqrt[3]{\frac{W_1}{200}} \right) \quad (2.12)$$

Where AOp is the air overpressure (in dB); W_1 the mass of charge per delay (in kg); and D_1 the distance from the free face (in m).

Alaba et al. (2023) evaluated the performance of Equation (2.12) at a mine in Ghana and compared it with other existing models. The NAAS model yielded $RMSE = 0.8482$ and $R^2 = 0.5312$. These values did not indicate a good fit of the NAAS model when the USBM model in Equation (2.4) and the model by McKenzie (1990) performed better.

Mckenzie (1990) conducted a study on air blast monitoring from quarry mines. The scope of his research was to understand the generation of air overpressure from production blasts. In his assertion of the phenomenon, he indicated that the air overpressure pulse is likely caused by the shock wave created by the detonation of the explosive charge, rather than the initial movement of the blast face. In order to make accurate predictions of AOp, the following empirical formula was then proposed (Mckenzie, 1990):

$$AOp = 165 - 24 \log \left(\frac{D_1}{\sqrt[3]{W_1}} \right) \quad (2.14)$$

Where AOp is the air overpressure (in dB); W_1 is the explosive charge weight per delay (in kg); and D_1 is the distance from the free face (in m).

In testing Equation (2.14), Alaba et al. (2023) found that Mckenzie's model yielded $R^2 = 0.9886$ and $RMSE = 0.2982$. Ideally, an $R^2 = 0.9886$ means that Equation (2.14) can account for 98.86% of air overpressure data collected at the mine operation where the study took place. Meanwhile, a $RMSE$ of 0.2982 indicates that Mckenzie's model is a better model fit on the data set

with an almost accurate prediction of air blast. Despite its usefulness, McKenzie's air blast prediction model has several limitations. Its development mostly relied on empirical site-specific data. The model also does not take into consideration factors such as blast geometries and geological conditions, which might have a substantial influence on air overpressure (Szendrei and Tose, 2023). The impact of air resistance and other physical elements that are essential to the precise forecasting of air blast are not included in the model (Mishra et al., 2023). In addition to the above, variations in input parameters, including charge size and delay timing, can affect the predictive ability of the model. This could then produce inconsistent outcomes if the underlying assumptions are not true for various blasting operations (Marto et al., 2014). Finally, it is worth noting the lack of sufficient scientific papers that tested McKenzie's model at various mine sites.

The review presented above is a summary of relevant empirical models of air blast; however, the effect of stemming is yet to be captured. This research study attempts to address this by testing the contribution of the Varistem® stemming plugs to the reduction of air overpressure in surface mining operations.

2.7 Concluding remarks

Air blast is a byproduct of blasting in surface mines. Whenever explosives are detonated during blasting, environmental impacts such as air blast and ground vibration are generated. Air blast is produced from four sources: the rock pressure pulse (RPP), air pressure pulse (APP), gas release pulse (GRP), and stemming release pulse (SRP). APP and RPP are unavoidable air blast sources in bench blasting, with APP being the most dominant. In contrast, GRP and SRP are controllable sources. They are also the main cause of annoyance near the blasting site.

Surface mines make use of blasting seismographs to measure air blast and ground vibration. These seismographs have a built-in microphone for

measuring and recording air blast as well as a geophone for ground vibrations. The United States Bureau of Mines (USBM) studied air blast across surface mines and recommended an industry safe limit of 134 dB to avoid human irritation. Several blast design parameters influence air blast generation in surface mines. They include specifically burden, spacing, stemming length, and charge weight per delay. Weather conditions such as wind speed and direction as well as atmospheric pressure are also factors that affect the speed of the air blast wavefront. In addition to this, the occurrence of temperature inversions refracts air blast waves back to the ground and focuses the air overpressure towards existing infrastructures. The rate of decay of air blast with respect to distance can be influenced by topography. As such, air blast levels may be higher in valleys because of terrain conditions.

Mining operations also utilize different stemming material and technologies to aid in containing blast energy. One of such technologies is the Varistem® plugs which is the object of this postgraduate research study. Additionally, understanding blast design concepts such as scaled depth of burial can aid in blast energy confinement and result in a more efficient blasts. A well confined explosive charge tends to produce a more controlled energy blast leading to reduced air blast pressure. Alternatively, insufficient explosive charge confinement can lead to an uncontrolled energy blast thereby leading to high levels of air blast. To the best of our knowledge and based on the literature review conducted, no model was found that considered the stemming types and technologies.

Lastly, this review looked at currently existing air blast prediction models and their testing at different surface mines. From the review, two of the most common prediction models in use are the USBM model and McKenzie's model. These models were found to have better performance indices (R^2 , RMSE and s) when applied at certain blasting operations. These performance indices indicated that the models were a good fit and a more accurate predictors of air blast. In light of this, the applicability of these two

models is explored later in Chapters 4 and 5. This dissertation proposes to explore the potential of the Varistem® plugs at reducing air blast during blasting in surface mines. Understanding the contribution of the plugs to blasting operations can add to the body of knowledge by making available data for use by the scientific community. Moreover, this knowledge could be beneficial to mining engineers, construction sites, and government institutions responsible for making policies and laws. The review highlighted the lack of scientific studies on the contribution of Varistem® plugs. This gap in knowledge requires a scientific enquiry to confirm some of the empirical evidence on the performance of the Varistem® plugs.

Chapter 3 Experimental work and data collection

3.1 Introduction

This chapter includes pertinent information about the equipment utilized, the experimental design plan, and the standard operating procedure for monitoring air blast. The technique and data gathered are presented in line with the goals of the dissertation. The challenges encountered throughout the experimental research and their effects on the findings are also discussed.

3.2 Overview

The aim of this research was to assess the potential of the Varistem® stemming plugs in reducing blast induced air blast at a surface mine. To fulfill the purpose of the study, blasting seismographs were used to monitor the air blast on site. Blasting seismographs are specialized instruments that allow easy and accurate monitoring of air overpressures produced during blasting. The seismographs used in this work were located at distances ranging from 100 m to 700 m away from the pit. And air blast monitoring was carried out for several blasts over a period of five months. During this period, data relating to the blast design as well as the air blast levels produced for each blast were collected and recorded for further analysis. The blast designs were provided by the planning department at the quarry. However, implementing the blast designs involved carrying out certain activities for each blast in order to complete the blasting process.

Marking and drilling of holes on a bench using the surface drill rig was the first activity carried out. Secondly, measuring the drilled hole depth to confirm if it matches the plan outlined on the design followed. Inserting detonators and boosters on each blasthole was then carried out. Charging blastholes with emulsion explosives then took place. After charging, Varistem® plugs

were inserted inside the holes using a tamping rod. Crushed aggregate stemming material were then used to fill the holes up to the hole collar. Blasting seismographs were then positioned at two locations around the pit to facilitate monitoring of air blast levels. Blasting was then initiated and facilitated through the use of blasting boxes near a close proximity to the pit. Detailed descriptions of each procedure are discussed in the subsequent sections. The section below gives an overview of the quarry where the data was collected. Lastly, a site description of the quarry where data was collected is also presented.

3.2.1 Overview of the quarry

This research study was carried out in a South African quarry in the Gauteng province. The real name of the mine site will not be disclosed for this research at the request of the mining company. As a result, the mine site is referred to in this dissertation as “Quarry TM”.

Quarry TM is an established operational mine in operation since 1962. Open-cast mining is used in the quarry to extract granite for further processing. The aggregates mined are then produced in different grades, mostly for ready-mix applications in the road building and construction industries. Drilling and blasting is used to fragment the rock of value for processing. The fragmented muckpile is then loaded onto haul trucks for transportation to the crushing and screening plant available on site.

The maximum footprint of the quarry has been reached in the southern and northern sections of the pit. So, current mining is undertaken in the northern end of the pit while medium and long-term expansion of the pit are being planned for the eastern side.

The exposed granite is mined by conventional drilling and electronic blasting. The blasted material is hauled and dumped into one of two primary crushers located South (A-Plant) and West (B-Plant) of the pit as illustrated in Figure 3.1.



Figure 3.1: Layout of the primary crusher plants at Quarry TM (Source: Google earth images)

The run-of-mine material is then crushed and screened to produce various types of aggregates and sands.

There are two operational Ready-mix plants located on Quarry TM. These plants make use of some of the aggregate material generated by the mine to produce ready-mix.

The neighbouring facilities near the quarry include taxi rank, industrial warehouses, residential settlements, and corporate offices as shown below in Figure 3.2.



Figure 3.2: Neighbouring facilities around Quarry TM (Source: Google earth images)

As such, the mining company thrives to adhere to US Blast Management and Consulting standards in view to limit the impact of drill and blast operations on the neighbourhood. In addition to this, all its operations are managed in accordance with the ISO 9001 Quality Management standards. This includes making use of electronic blasting technology which enables the Mine Planning Department to simulate and appropriately design the blasts. The latter ensures that ground vibrations are kept below 22 mm/s, or below 25 mm/s if the frequency is above 14 Hz, and below the 125 dB for air blast limit. The US Office of Surface Mining and Reclamation Enforcement specifies a safe overpressure level of 133 dB and below for impulse air-blast in a frequency range of at least 2 – 200 Hz (Singh et al., 2005). Furthermore, the company takes precautions to limit fly rocks and noise generation during blasting by judicious stemming all blast holes. Numerical simulations of blast designs also help verify the expected blast outcome.

One of the main objectives of this research is to measure the air blast profile of Quarry TM with and without Varistem® plugs as part of the stemming arsenal.

3.2.2 Site description

The type of rock found in the mine area is mainly granite, with an average uniaxial compressive strength of 133 MPa. This local rock has an average density of 2 650 kg/m³.

Figure 3.3 shows a geological map of the quarry with the area to be blasted for the duration of the study enclosed in the black circle. The main rock type which makes up most of the pit is represented in blue. A shear zone represented in green colour cuts across the pit. There is also the presence of a dolerite dyke on the far right of the area to be blasted. This highly variable formation is characterised by discontinuities in the rock mass that can give rise to a wide range of air blast vibration levels. Most importantly, the map shows residential areas, a taxi rank facility and distribution warehouses surrounding Quarry TM.

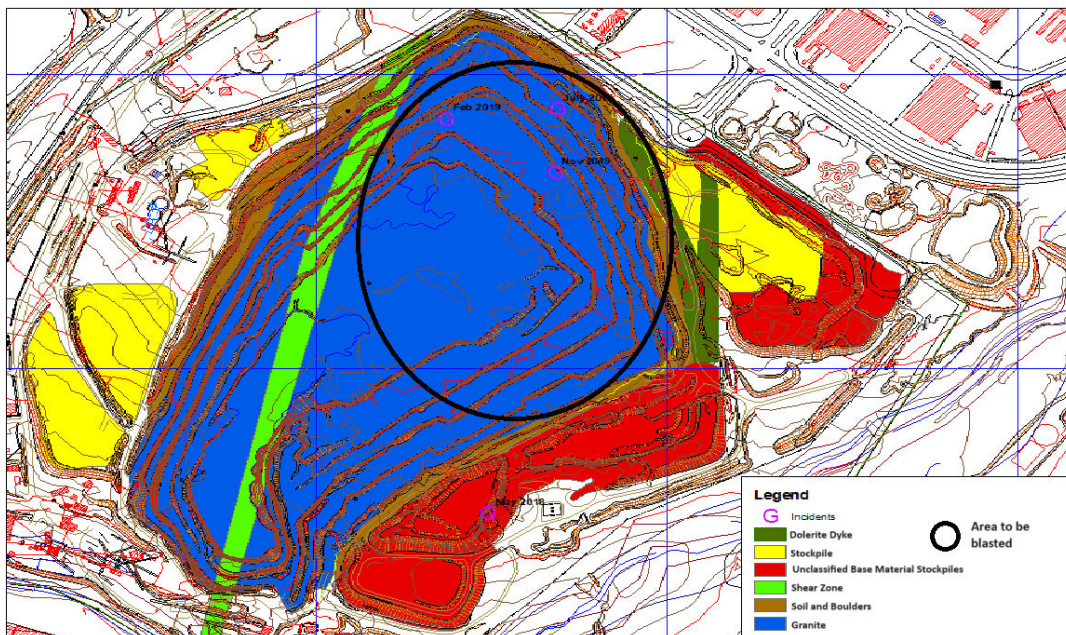


Figure 3.3: Geographical map of the quarry (Source: Picture supplied by Quarry TM)

In terms of the blast designs used, crushed aggregates produced on site were used for stemming with and without the 102 mm Varistem® plugs depending on the experimental programme. Blastholes of diameter 102 mm

are drilled in staggered pattern for a burden of 2.8 m and a spacing of 3.0 m. The benches had an average height of 12 – 13 m, with a stemming length of 1.9 – 3 m. The blasthole depth was at an average of about 15 m, with a subdrill of 0.50 m.

3.3 Experimental work and equipment used for collecting data

This section outlines the actual experimental work that was carried out for the purpose of this study. Firstly, the data acquisition and experimental set up of the study are presented. Secondly, the equipment and tools used in collecting data are also presented. The drilling, charging, and blasting procedures were observed at the mining site for five months. Data gathered during the observations included the blast location, bench and hole conditions, date and time, basic weather conditions, stemming parameters, and the air blast level.

3.3.1 Data acquisition and experimental setup

One of the main objectives of this study was to measure the air blast at various locations during blasting. At Quarry TM, the main instrument used for air blast is the Nomis seismograph. Air-overpressure (AOp) in dBL, distance (D_1) from the blast face to the monitoring station and the explosive charge weight (W_1) were all output data obtained from the instrument. This data was acquired from the benches circled as the area to be blasted as identified in Figure 3.3 above.

To start the experiment, data related to the blast design patterns; coordinates of drill holes, numbers of blastholes to be drilled per round, hole depth, stemming length and explosive charge weight per blasthole were collected. For this experimental work, a series of tests were conducted and organized as follows.

- First tests involved 15 blasts incorporating the Varistem® stemming plugs while their respective air blast profile was monitored from two locations, namely, Station A and Station B.
- Second tests entailed 12 blasts with standard stemming while air blast was also monitored from two locations, namely, Station A and Station B.

In terms of the second group of tests, historical data had to be relied upon to fulfil the objectives of the study. Blast data spanning for a period of five months was collected as part of the results highlighted in Chapter 4.

Table 3.1 provides a summary of technical information on the adopted blast design with and without Varistem® stemming plugs.

Table 3.1: Blast design parameters used in the research study

Description	Proposed parameters
Pattern	Staggered
Hole diameter	102 mm
Burden and spacing	2.8 x 3.0 m
Average bench height	12 – 13 m
Stemming length	1.9 – 3 m
Average explosives mass per hole	±112 kg/hole
Technical powder factor	±1.15 kg/m ³
Stemming material	10 mm of aggregates
Explosive	INNOVEX 100 + INNOPACK cartridges

The GPS Tremble system was employed to determine the correct depth and position of each hole. The information was rendered on a computer as exemplified in Figure 3.4 below.

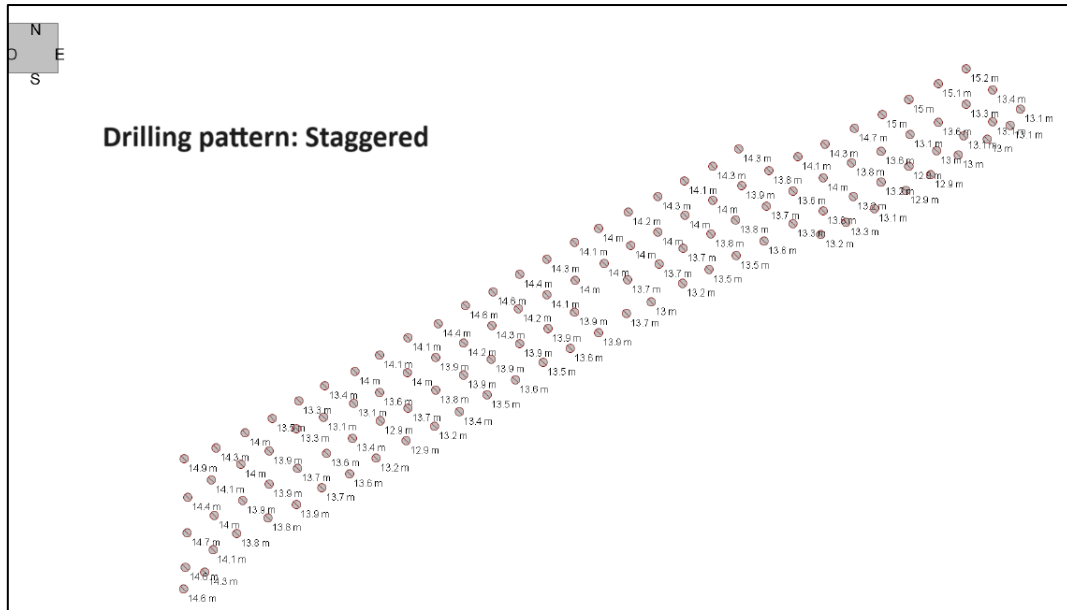


Figure 3.4: Example of drilling pattern used for the benches (Source: Picture supplied by Quarry TM)

To accommodate the overburden and avoid oversize fragmentation, angled holes were drilled on certain holes identified on the blast design. The angled holed were identified and informed by the presence of geological discontinuities such as faults or wedges on the blast design of certain areas.

INNOVEX 100 base type bulk emulsion was used as the preferred explosive. Set at a density of 1.2 g/cm^3 , the emulsion was primed with INNOPACK cartridges. And as per Table 3.2, the mass of explosives by design required for effective fragmentation is 1.15 kg per cubic meter of rock. An electric initiation system with delaying detonator was used to conduct the blasting rounds (shots). Additional data on the hole depths before and after charging for all the blasts was collected. The actual mass of explosives loaded per hole and the corresponding stemming length were also recorded. This information is available in the Appendices while relevant data are later processed in Chapter 4.

In terms of air blast data, the blasts on the quarry were organized in such a way that each shot was monitored from two separate stations; namely, Station A and Station B. Figure 3.5 below shows an aerial view of the pit and

the features annotated as “vibro” represent the two locations of the blasting seismographs.



Figure 3.5: Aerial view of the pit showing the location of the seismographs (Source: Image adopted from google earth images)

Quarry TM has several nearby facilities in its neighbourhood as explained in Section 3.2.1 above. This situation not only justified the choice of locations for the seismographs, but it also motivated the inception of this research study.

The two monitoring stations were located respectively about 100 m and 700 m away from the blast. A mobile Nomis seismograph was set up at each station. These seismographs were positioned at each station about 30 min prior to a blast. They were then programmed to start recording 15 min prior to a blast. The data pertaining to the recorded blast events by the seismographs are discussed in Chapters 4 and 5. Finally, the vibration reports and associated raw data are available in the Appendices.

3.3.2 Equipment and tools used for the collection of data

For this study, the experimental data was collected using the following equipment: surface drill rig, electronic detonators, boosters, emulsion, and cartridge explosives, measuring tape, Varistem® plugs, crushed aggregates, logger, surface wire, blasting box, antennas and blasting seismographs. All the relevant information pertaining to the above equipment is provided in the subsequent sections.

3.3.2.1 Surface drill rig

The first step of the blasting cycle is drilling holes through the rock mass. Ideally, four rows of blast holes parallel to the free vertical face of the bench with a burden of 2.8 and spacing of 3m were drilled close enough to loosen the rock in between.

At Quarry TM, before drilling could take place, a Global Positioning System (GPS) Trimble system was employed to determine the accurate drill hole depth and drill pattern. Once the quality control was done, a surface drill rig machine (Figure 3.6) fitted with 102 mm drill bits was utilised to carry out the drilling of the blastholes across the benches.



Figure 3.6: Surface drill rig (Source: Author's picture)

After drilling was complete, the blasthole length had to be re-measured by means of a measuring tape. The re-measured blasthole length was at an average of 12-15m for the different benches per blast with a subdrill of 0.50m. Additionally, the number of drilled blastholes per blast were at an average of 30 to 200 holes depending on the size of bench being blasted. The remeasuring of blastholes was done to ensure that the length of each drilled hole was consistent with the blast design layout. An illustration of how this was done can be seen in Figure 3.7 below. This critical task of quality control was executed in close collaboration with the drill and blast team. Each blasthole depth was recorded across the bench on a field workbook. The template of the field workbook is included in the Appendices at the end of this dissertation.



Figure 3.7: Measuring of drilled blastholes (Source: Author's picture)

3.3.2.2 *AXXIS™ electronic delay detonator*

The detonators that were used to initiate blasting are AXXIS™ electronic delay detonators. These are manufactured and supplied to the quarry by Bulk Mining Explosives company trading as BME.

The following specifications of the AXXIS™ electronic delay detonators used in this work should be noted:

- They have a delay time range of 0 to 35 s (35 000 ms) in 1 ms increments.
- This type of detonator shell is made up of aluminium magnesium or copper alloy.
- The detonators have a nominal outer diameter of 7.5 mm and a nominal length of 88.9 mm.
- The dynamic shock resistance is 80 MPa.

It should also be noted that these AXXIS™ detonators only function with the AXXIS™ blasting boxes covered in Section 3.3.2.9. In addition to this, special security PIN codes are required to operate the system. In situation where a blast needs to be aborted at short notice, a deadman's switch is available to disarm all detonators.

After measuring the length of the drilled holes, the next step was to prepare the electronic delay detonators. Figure 3.8 shows the type of electronic delay detonators that were used and how they were inserted into a booster before being taken down the blastholes.

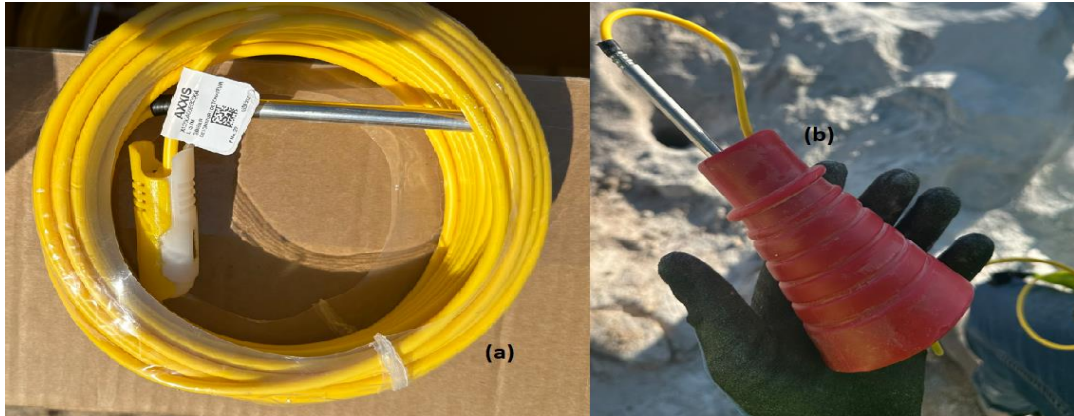


Figure 3.8: (a) Electronic detonator, (b) Insertion of a detonator inside a booster explosive (Source: Author's picture)

A detonator is a device that typically comes with a tiny amount of explosives, a signal transmitter, and perhaps a timing mechanism, all of which are housed inside of a cylindrical metal shell (Orica, n.d.). The detonator was equipped with a colour-coded connector clip (Figure 3.9a) that made it simple to connect it to other shock tube assemblies and to the surface wire (Figure 3.9b).



Figure 3.9: Detonator cord attached to a colour-coded connector clip (Source: Author's picture)

At Quarry TM, AXXIS™ detonators can be connected to denotating cords usually 5 m to 20 m in length depending on the depth of the blastholes. These detonating cords are made from a specific length of shock tubing that had an

ultrasonic seal at one end and a millisecond delay detonator crimped to the other. Within 10 cm of the seal, the shock tube is attached to a label that has the precise delay written on it. Colour-coded labels were used to distinguish between various delay assemblies as shown in Figure 3.9.

3.3.2.3 *Emulsion explosives*

INNOVEX 100 base emulsion is the type of explosives usually charged into the blast holes at Quarry TM. The emulsion explosives used for the purpose of this research are manufactured and supplied to the quarry by BME (Bulk Mining Explosives) company. INNOVEX 100 base emulsion is a class 5.1 oxidizing agent with UN classification number 3375. A class 5.1 oxidizing agent refers to substances that can enhance the combustion of other materials (Vladimirovich et al., 2014; Fei et al., 2020). Moreover, a UN classification number 3375 refers to “Emulsions, explosive, water-resistant” indicating that these emulsions are designed to maintain stability and performance in wet conditions (Raines and Doup, 2023).

Gassing agents play an essential role in the formulation and performance of emulsion explosives. This gassing agent creates bubbles within the emulsion. The presence of gas bubbles improves the detonation velocity of the explosive (Mishra et al., 2017). In essence, absence of gassing agent or gas bubbles within the emulsion means that the explosive may not achieve optimal detonation velocity (Mishra et al., 2017). When sensitised with the gassing agent, INNOVEX 100 becomes a booster-sensitive emulsion designed for opencast mines. INNOVEX 100 is a low viscosity black emulsion specially formulated using recycled oil and alternative fuel. It is sensitised to a cup density of 0.9 – 1.2 g/cm³ by using a suitable sensitising agent. A cup density of 0.9 – 1.2 g/cm³ ensures that the explosive is neither too insensitive nor too sensitive, balancing safety and effectiveness (Anders and Borges, 2011). INNOVEX 100 sensitisation entails the use of an appropriate sensitising agent, usually sodium nitrite (NaNO₂). Ammonium nitrate (NH₄NO₃) as the main ingredient of the emulsion reacts with this

sensitising agent. Within the emulsion, bubbles are formed by the nitrogen gas that results. The overall density of the emulsion is successfully decreased by the gassing agent through the formation of gas bubbles. Optimising the performance of the explosive requires this reduction.

Upon sensitising the emulsion explosives, the sensitised slurry was pumped into the blastholes as shown in Figure 3.10. The quarry makes use of emulsion because it is water-resistant. To prevent overcharging the holes, the team leader provides the person operating the truck carrying explosives with the mass of explosives needed per hole. A second-round of tape measurement of the stemming is performed as part of quality assurance protocols to check if blastholes were correctly charged. Where holes are found to be overcharged, a honey sucker (see Figure 3.15 in Section 3.3.2.4) is used to extract the excess emulsion.



Figure 3.10: Charging of holes with emulsion explosives (Source: Author's picture)

It is important to charge and allow for the gassing of the explosives inside the hole. Transparent cups 400 g in size were also used as the charging was carried out (Figure 3.11b). These cups were filled with the emulsion to

observe the gassing process as shown in Figure 3.11(a). Gassing was allowed to take place to determine whether it was safe to apply stemming to the blastholes. Based on the gassing observed in the 400 g cups, the gassing process inside blastholes was allowed for a period of 30 to 40 min.



Figure 3.11: (a) Observing of gassing of the explosives inside the 400 g cups and (b) Filling the cups with the emulsion explosive (Source: Author's picture)

There was serious water seepage present across the pit which caused some holes to be filled with water. To address this inconvenience, the explosive hose was pushed to the bottom of the hole before pumping could proceed. This allowed the water-resistant emulsion to settle from the bottom of the hole and displace the water as shown in Figure 3.12 below.



*Figure 3.12: Displacement of water from the blasthole during charging
(Source: Author's picture)*

In the case where a toe of a bench or a big boulder had to be blasted, Mega-mite 50 x 580 cartridges shown in Figure 3.13 were used to charge the blastholes and perform secondary blasting. These cartridge explosives are also manufactured and supplied by BME but they have less energy compared to the emulsion. They are also suitable for charging the toe of a bench.



Figure 3.13: (a) Mega-mite 50 x 580 cartridges, and (b) Charging of 50 x 580 cartridge explosives with a detonator (Source: Author's pictures)

3.3.2.4 Measuring tape

After charging the blastholes with explosives was complete, a measuring tape similar to the one shown in Figure 3.14 was used to measure the length of stemming required across the blast block. Two stemming lengths were measured, one straight after charging and the second one after gassing of the explosives. The second stemming length assisted the blast team in determining whether the holes were overcharged or not. This was done for all the holes across the blast block. Measuring and checking of the required stemming length was important to ensure that the designed stemming length was implemented. Every blast block to be blasted had a specific stemming length defined during the blast design process. In a situation where the stemming length was shorter and blastholes were overcharged, a certain portion of the explosive was pumped out using the honey sucker in Figure 3.15 to remedy the situation.



Figure 3.14: (a) Example of a typical measuring tape (Source: Better Blasting, 2021) and (b) Measuring of blasthole stemming length with measuring tape (Source: Author's picture)



Figure 3.15: Honey sucker (Source: Author's picture)

3.3.2.5 Varistem® stemming plugs

The main aim of this research study was to establish how effective Varistem® plugs are at reducing blast-induced air overpressure in surface mines. A sample of the plugs used is shown in Figure 3.16. These plugs were used in conjunction with crushed aggregate stemming material.



Figure 3.16: Varistem® stemming plugs of diameter 102 mm (Source: Author's picture)

In terms of the setup, once the emulsion explosive had gasified inside the blasthole, a Varistem® stemming plug was then inserted into the hole. A tamping rod (see Figure 3.20 in Section 3.3.2.6 below) was then used to push the plug down the hole.

Varistem® plugs are locally supplied by ERG Industrial company which acquired distribution rights from MOCAP, a company based in the United States of America. Varistem® plugs are available for all blasthole diameters ranging between 45 mm and 251 mm. Quarry TM makes use of Varistem® stemming plugs of diameter 102 mm for their benches. The size of the plugs is in line with the diameter of drilled blasthole presented in Section 3.3.1, that is, 102 mm.

For each blasthole, a Varistem® stemming plug was placed on top of the explosive column charge before the stemming material could be placed. The procedure is illustrated in Figure 3.17.

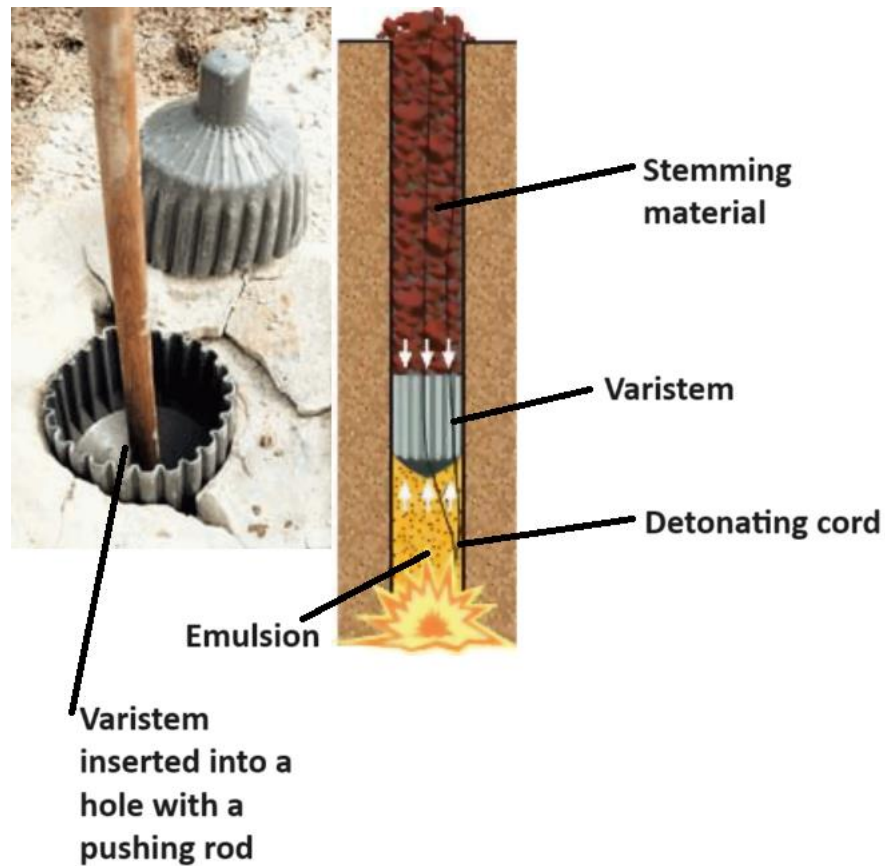


Figure 3.17: Installation of the Varistem® stemming plug into a blasthole (ERG Industrial, 2020)

When a single blast hole is fired, these plugs work by containing the explosive energy and directing it into the rock mass. The plugs effectively lock against the walls of the blasthole instead of allowing the explosive energy to escape in the form of high-pressure gas and air blast (Modern Mining, 2021). It is the benefit of this working principle on air blast reduction that is tested as part of the research study.

3.3.2.6 Crushed aggregates

Aggregates of average size 10 mm were used as stemming material. Aggregates are typically placed inside a blasthole to prevent explosive gases and energy from escaping into the atmosphere. Most surface mines prefer to use crushed aggregates as they interlock making them most effective for

stemming (Oates and Spiteri, 2021). For this reason, the crushed aggregates in Figure 3.18 and produced on site were adopted for this study.



Figure 3.18: Crushed aggregates used for the stemming of blastholes (Source: Author's picture)

Buckets like the one shown in Figure 3.19(b) were filled with crushed aggregates for an easy and controlled pour in the blasthole. A tamping rod as illustrated in Figure 3.20 was used to compact the aggregates to enhance energy containment during blasting. Stemming was considered complete once the aggregates reached the collar of the blasthole as shown in Figure 3.19(a).



Figure 3.19: (a) Stemming of blastholes with crushed aggregates, (b) Buckets used to stem holes (Source: Author's picture)

If stemming is not done correctly, explosive gases will be released into the atmosphere, causing air overpressure and noise. That is why all holes were tamped with the type of tamping rod shown in Figure 3.20 below for effective stemming. The Varistem® plugs work in conjunction with stemming material to help contain the explosive gases within the blast hole for a longer duration thereby preventing premature escape of gases.



Figure 3.20: Tamping rod used to tamp the aggregates during stemming (Source: Author's picture)

3.3.2.7 AXXIS™ titanium logger

Upon completion of stemming, the detonating cords inserted inside the blastholes were scanned by means of the AXXIS™ titanium logger shown in Figure 3.21(a). The colour-coded end of the detonating cord (Figure 3.21c) was placed on the logger as shown in Figure 3.21 (b and d) to perform a scan. The purpose of scanning was to record the electronic delay detonators in each blasthole across the bench and allocate individual initiation timings to each of the holes.



Figure 3.21: (a) AXXIS™ titanium logger, (b) slot where the detonator is to be inserted, (c) detonator, and (d) illustration of how the scanning of detonators is done (Source: Author's picture)

The AXXIS™ titanium logger used in this study was manufactured by Trimble company and supplied to the quarry by BME. This type of device has an Android 8.1 operating system, a screen of size 635 mm, and a resolution of 1280 x 720 pixels. The logger uses a 10.8-Volt lithium-ion battery. It also has a touch screen interface and a numeric keypad (see Figure 3.21). Finally, during scanning, the logger allocates a connector ID and firing time to each detonator down the explosive column in the blasthole. All the logged data is

stored and then transferred to the blasting box through a USB cable. The blasting box is covered later in Section 3.3.2.9 below.

3.3.2.8 *Surface wire*

After scanning and recording the detonators with the logger, the surface wire (Figure 3.22a) was unrolled and spread across the bench. This was done to connect the detonators from all the blastholes as shown in Figure 3.22(b). This activity was important as it had to do with finalising the actual implementation of the designed pattern. As exemplified in Figure 3.22(b), the yellow ultra-sonic seal that is attached on one end of the shock tube was clipped on the surface wire.

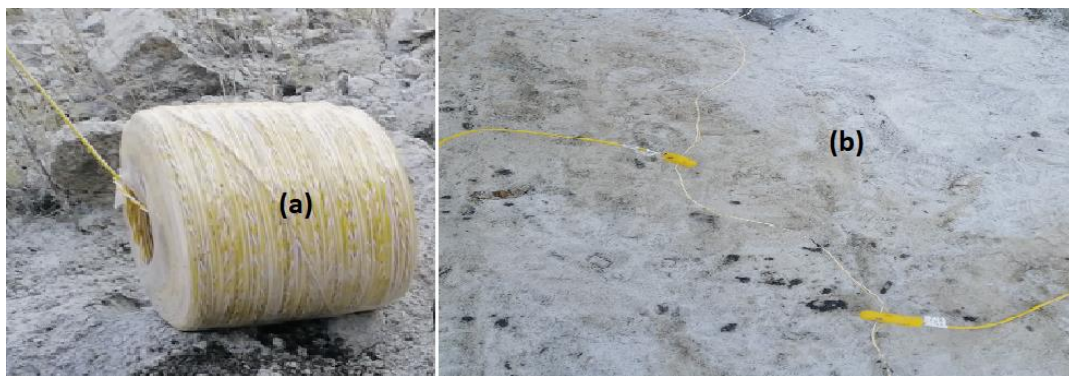


Figure 3.22: (a) Unrolling of the surface wire and (b) connection of the wire to the electronic delay detonators (Source: Author's picture)

3.3.2.9 *AXXIS™ titanium blasting box*

Quarry TM makes use of AXXIS™ titanium blasting boxes manufactured by BME. Some of their specifications are as follows: a user interface of LCD colour with variable intensity and contrast setting, a screen of resolution 2000 x 1500 pixels with a 24-Volt rechargeable lithium-ion battery of capacity 12000 mAh, and a capability of handling 1000 detonators when in blaster box mode.

Proceeding with the preparation for the blast, it should be recalled that the detonators were connected to the surface wire harness in Section 3.3.2.8.

Upon completion of connecting the detonators with the surface wire harness, the AXXIS™ titanium blasting box (Figure 3.23a) was placed at the blast site and connected to one end of the surface wire harness. Once this was complete, the logger in Figure 3.23(c) was connected to the blasting box (see Figure 3.23b). This enabled the transfer of information about the scanned detonators in the blastholes to the blasting box. At this point, the blasting box was also used to verify whether all the detonators were connected to the surface wire according to the data received from the logger. As a confirmation, the logger generated a one-time PIN to configure the blasting box. This PIN was later used to initiate firing of the blastholes.



Figure 3.23: (a) AXXIS™ titanium blasting box on site, (b) Blasting box connected to a logger, and (c) Logger transferring information to the blasting box (Source: Author's picture)

It is important to say that the blasting box in Figure 3.23 is positioned near the bench where it must connect wirelessly and send signals to another controller blasting box positioned at the blasting shelter. The controller blasting box and its setup are discussed in detail under Section 3.3.2.12.

3.3.2.10 Antenna and antenna stand.

Once the data from the logger was transferred into the blasting box, the antenna in Figure 3.24(a) was then set up on a stand to form a two-way communication. This box was positioned inside the pit at approximately 100m away from the bench. Then, an antenna was placed near the bench to establish a signal connection with the second antenna set up in the blasting shelter.

The antenna consists of a metal conductor that conveys radiofrequency (RF) waves between two points in space. This device can either transmit or receive a signal. In this case, the antenna in Figure 3.24(a) was set up to act as a receiver. Similarly, another antenna was set up in the blasting shelter to act a transmitter as shown in Figure 3.24(b).



Figure 3.24: (a) Receiving antenna connected to a blasting box on site, and (b) Transmitting antenna connected to a blasting box in the blasting shelter (Source: Author's picture)

When it was time to initiate the blast, a blasting box connected to the transmitting antenna under the shelter was activated. This generated power in the form of a radio signal that travelled to the receiving antenna. This is where the signal was converted back into electrical energy containing the

required blasting information. The receiving antenna captured this as a command to set off the blast.

In summary, each blast set off as part of this research study required the use of one transmitting antenna, one receiving antenna, and two blasting boxes.

3.3.2.11 Nomis Seismographs

At Quarry TM, a specific model of seismographs called Nomis seismographs was used to measure and record air blast and ground vibrations. These seismographs are manufactured by Nomis Seismographs Inc. in Birmingham, Alabama. They are locally distributed in South Africa and in the region by Blast Analysis Africa CC. The specifications of the Nomis seismograph are detailed in Table 3.2.

Table 3.2: Specifications of Nomis Blasting Seismographs

Seismic monitoring:	Specifications
Range	0 – 254 mm/s
Resolution	0.005 in/s
Accuracy	±3%
Frequency response	2 – 400 Hz (1 Hz optional)
Weighting scales	Linear (flat)
Linear range	88 – 148 dB

The air overpressure transducer embedded into the Nomis seismograph records AOp values ranging from 88 dB up to 148 dB. The resolution, accuracy, trigger levels are 0.1 dB above 120 dB (0.25 Pa), 0.2 dB at 30 Hz and 100 – 148 dB in 1 dB steps respectively. The blasting air overpressure transducer or microphone as it is often called is responsible for measuring and recording the air blast.

Following the set-up and configuration of the blasting boxes and the antennas, the Nomis blasting seismographs were positioned in a near field distance ranging about 100 m to 700 m away from the pit. The blasting

seismograph makes use of an air overpressure transducer (Figure 3.25b) to record air vibration levels from a blast. The other channel of the seismograph is the geophone with metallic spikes (Figure 3.25a) used to measure ground vibrations. Lastly, the seismograph has a control unit (Figure 3.25c) which records and stores the data from the air overpressure transducer and geophone during a blast.



Figure 3.25: (a) Geophone, (b) Air overpressure transducer, and (c) Control unit (Source: Author's picture)

The units in Figure 3.25 above, critical to the research study, are configured together as exemplified in Figure 3.26 below to record and store data during a blast.

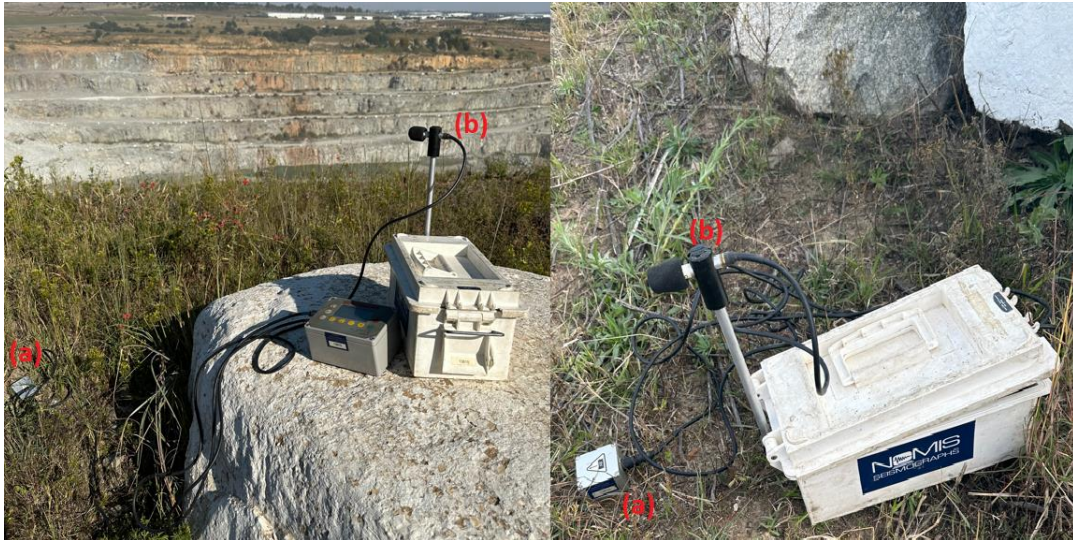


Figure 3.26: (a) Geophone with spikes buried into the ground, and (b) Air overpressure transducer facing the direction of the blast. (Source: Author's picture)

Best practice requires that the geophone spikes be buried into the ground to measure the vibrations as illustrated in Figure 3.26 above. The air-overpressure transducer, on the other hand, must face the direction of the blast.

The Nomis Seismographs are mobile; they were placed around the quarry relative to the closest infrastructure. Approximately 30 min before the blast, the seismographs were positioned at their respective locations and set up to start recording 15 min before the blast. Two fixed locations were established as monitoring stations: Station A and Station B. These stations were approximately 100 m to 700 m relative to the bench being blasted at a certain period around the pit.

Seismographs were employed to monitor all blasts with and without Varistem® plugs. The recording devices inside the Nomis Seismograph were activated once the particle velocity of the ground surpassed 0.5 mm/s (Preskitt and Cornelius, 1979). This functionality of surpassing 0.5 mm/s is crucial for capturing significant vibration events while reducing unnecessary data from lower vibrations. It is for this reason that these machines are designed to only record blast related air blast levels. When it comes to air

overpressure, the trigger level was set at 125 dB(L), with the letter L after the units dB signifying linear. The reason for setting this specific trigger level was because the quarry wanted to ensure that their blasts are kept below a noise limit of 125 dB as guided by Table 2.1. Once blasting was complete, the seismographs were removed from their respective locations and taken for battery charging and safekeeping.

Seismographs generally measure data continuously and trigger only when a pre-set threshold value is exceeded (Kuzu et al., 2009). The threshold values set by the quarry for ground vibration and air blast were guided by the international USBM standards. The USBM has established a regulatory safety air blast level limit to be 134 dB (Siskind et al., 1980). Furthermore, Siskind et al. (1980) also reported that safe levels of ground vibrations were established to be 12.7 mm/s. However, it should be noted that ground vibrations were not part of the scope of this study.

3.3.2.12 *Blasting shelter*

A blasting shelter is a specific housing where all personnel around the mine gather prior to firing a blast. This is done to observe a blast as well as ensure that all personnel are safety and accounted for during the blast. The quarry has two blasting shelters located about 500 m from the pit: see Figure 3.27(A) showing one of the two shelters used in this study.



Figure 3.27: (A) Blasting shelter for mine personnel to gather and observe the blast, (B) Controller blasting box is set up in the blasting shelter (Source: Author's picture)

The team leaders make use of their internal telecommunication systems to clear everyone from the pit. All the machinery which might have been present in the pit are also cleared out. Once everyone from the pit has been accounted for, the second blasting box connected (Figure 3.27B) to the transmitting antenna is set up in the blasting shelter. The antenna in the blasting shelter serves as a transmitter to the receiving antenna that is positioned in the pit as was shown in Figure 3.26 in the previous section.

3.3.2.13 Mobile laptop

One of the main equipment needed during this experimental investigation was a mobile laptop. The laptop helped with the logging and storage of all the data collected for the purpose of the research study. This device ensured that all important data/events and observations were documented as they occurred on a day-to-day basis.

3.4 Data analysis used for the study

This section provides a brief overview of the data analysis methods adopted for this research study. The in-depth analysis is presented later in Chapter 5.

The USBM predictor model and Mckenzie's predictor model were the two empirical prediction models used to model air blast as part of the analysis. Equations (2.3), (2.4) and (2.12) were used to model the air blast profile for Quarry TM at both monitoring stations. Blast information such as the explosive charge weight (W_1) and the distance from the blast to the monitoring station (D_1) were used to calculate the cube-root scaled distances (d_s). Furthermore, these values were used to get new air overpressure levels as demonstrated later in Sections 4.3.3.1 and 4.3.3.2 of Chapter 4. This was to identify the most suitable models for Quarry TM. The Root Mean Squared Error (RMSE) and the coefficient of determination (R^2) were used in the process of identification of the best models.

In terms of studying the performance of the Varistem® stemming plugs, it was decided to resort to hypothesis testing. This statistical tool mainly focused on comparing blasts with and without Varistem® plugs assuming all other parameters were kept constant. This was to establish whether the mean air blast level produced would exceed 134 dB in either stemming setup.

From a modelling point of view, air blast data was analysed using a systematic approach, considering that seismographs only record for a limited duration (such as 2 min). This involved understanding the characteristics of the recorded data and the nature of the air blast. Furthermore, the Microsoft® Excel® analysis toolpack known as "solver" were used to fit the recorded data and generated the line of best fit for the two blasts at Station A and B. Factors that influence air blast generation as highlighted in Section 2.3 of Chapter 2 were also considered for the analysis. Additionally, statistical analysis such as ANOVA test and bootstrapping were used to extract meaningful insights from the data.

3.5 Challenges encountered during the research study

Upon commencement of the project, the research design had to be modified. Initially, the plan was to run concurrent tests and collect data of the blasts with and without the stemming plugs simultaneously. Due to safety reasons presented by the quarry of preferring not to exclude the plugs from the blast design, historical data without stemming plugs had to be relied upon to fulfil the objective of the study.

One of the challenges encountered with working with shock tubes and detonators was their high propensity to explode. Precautions had to be taken to ensure they are handled with care which required time. Furthermore, if the shock tubes were not connected properly to the surface wire, the data would be loaded with an error on the blasting boxes. This meant that more time had to be spent to locate where the error originated from.

Meteorological conditions, such as air humidity and wind, are known to have a great effect on blast-induced air over-pressure. Indeed, these agents can cause high frequency air overpressure and dust pollution (Hieu et al., 2021). As such, for the purpose of this research, blasting had to take place in sunny conditions when the skies were clear which we had no control over.

The presence of cracks in the rock mass influenced the mass of explosives charged thereby causing variability in blast performance. Due to the presence of fractures on the highwall of the bench, some holes had to be drilled at an angle and incorporated in the blast design. Geological joints were also present in some highwall areas with visual evidence of fractured faces. Angled holes had to be drilled in areas where geological joints were present to avoid having oversize fragmentation. The charging of these angled holes had to be distributed in segments, a booster charge was placed at the lower section of the hole to initiate and produce better fragmentation at the base. Thereafter, emulsion explosives were used to fill the rest of the column charge. In terms of timing, electronic detonators with millisecond delays were used to initiate the angled drilled holes, thereby ensuring controlled energy distribution. Additionally, some benches around the quarry had an uneven

terrain with some loose material on the top and edge of the crest of the highwall. Other areas also showed evidence of weathered rock material. The challenge with this was that the timing of the blast had to be slowed down in some areas thereby making the tests longer. This was because weathered material breaks easily and tends to cause high fly rock and increase air overpressure. Heavy rains experienced on the site caused the blocks to be muddy and in cases where blastholes were drilled, they would be filled with water. Rainy conditions can increase the air humidity and cause the air overpressure to be higher than in dry conditions (Tran et al., 2021). As such, the weather forecast was consulted ahead of time so that blasting was scheduled for favourable weather conditions like on sunny days.

Clearing employees from the blast area was sometimes a challenge. Since the drilling machines also had to be evacuated to safety during blasting, some operators waited until the last minute to heed the call to evacuate the site. This meant that blasting would be delayed.

Chapter 4 Estimation of the contribution of stemming plugs to air blast reduction

4.1 Introduction

This chapter outlines the resultant outcome of the test programme outlined in Section 3.3.1 of Chapter 3. Firstly, the results of the air blast profile from Station A and Station B are presented. while also highlighting the observations made from the calculated scaled depth of burial. Secondly, the resultant estimations from modelling air overpressure as a function of scaled distance using the USBM predictor model and McKenzie's model are also presented. Lastly, results derived from the comparison of air blast with and without stemming plugs using ANOVA statistical analysis are presented.

4.2 Air blast profile from Station A and Station B

4.2.1 Air blast profile from Station A

A Nomis Seismograph was set up at Station A to record the blast events for the Varistem® and standard blasts as outlined in Section 3.3.1 of Chapter 3. This seismograph was set up 30 minutes prior to a blast and it was configured to start recording 15 minutes before firing of each blast. The blast design parameters used for this station are given in Table 3.1 of Chapter 3. These blasts were organized in such a way that each blast was monitored separately in near field about 100 – 700 m of the blast block as highlighted in Table 4.1 below. As highlighted in Section 2.6 of Chapter 2, Equation (2.2) was used to calculate the cube root scaled distances for each blast. Blast designs for each block were used to calculate the explosive charge weight per delay.

The recorded data gathered from Station A is captured in Table 4.1 below. The blast reports generated from the Nomis Seismograph are included as part of Annexure A of the report. This data consists of the test results from

blasting with and without the stemming plugs. It should be noted that this test work was not carried out concurrently, since historical data had to be relied upon when it came to the standard blasts. Since the same station was used to monitor and record the blast events, this section outlines the blast results recorded but for different benches. Table 4.1 shows the air blast level results denoted as (AOp) and their respective monitoring distances. The cube-root scaled distance was captured for each blast since it is utilised when estimating the peak air blast overpressure levels at a specific distance from the blast (Şengün and Gül, 2023).

Table 4.1: Blast recordings from Station A for the Varistem® blasting and standard blasting trials

	Station A: Varistem® blast			Station A: Standard blast		
Blast Number	Distance (m)	Scaled distance (m/kg ^{1/3})	AOp (dB)	Distance (m)	Scaled distance (m/kg ^{1/3})	AOp (dB)
1	411	91.7	103.5	325	45.4	135.4
2	370	47.3	128.9	341	84.8	130.0
3	235	31.4	134.8	360	91.5	128.0
4	151	34.8	119.1	258	61.2	135.1
5	220	28.1	133.8	352	51.5	136.7
6	128	27.1	132.7	320	77.6	131.6
7	320	41.0	124.5	305	45.1	137.8
8	470	97.8	88.0	186	25.6	143.1
9	168	21.3	141.3	209	45.0	145.3
10	383	47.7	123.3	220	30.7	142.6
11	215	33.6	125.0	215	47.1	144.8
12	434	60.2	116.0	330	69.9	132.6
13	265	35.0	135.0			
14	210	25.0	135.3			
15	250	35.0	136.9			

Plotting the data sets in Table 4.1 on a logarithmic scale produced the scatter plot in Figure 4.1 below for the Varistem® blasts. The line 134dB corresponding to the air blast threshold limit recommended by the United States Bureau of Mines (USBM) was also introduced on the plot area. This air blast threshold limit line is denoted as 134 dB to signify the literature review covered in Section 2.2.3 of Chapter 2 and aid in establishing whether the blasts were within regulatory standards.

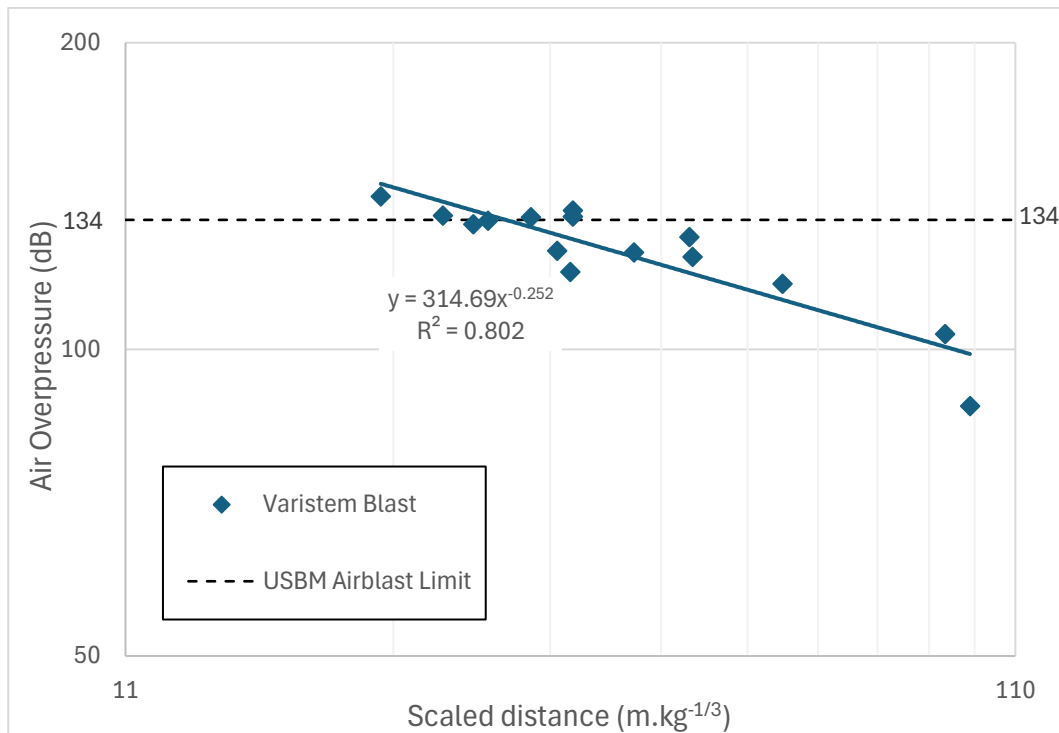


Figure 4.1: Air overpressure levels for the Varistem® blasts at Station A

Meanwhile, the logarithmic graph plot for the standard blast is illustrated in Figure 4.2 below. The USBM air blast threshold limit of 134 dB was also drawn on the plot area for reference.

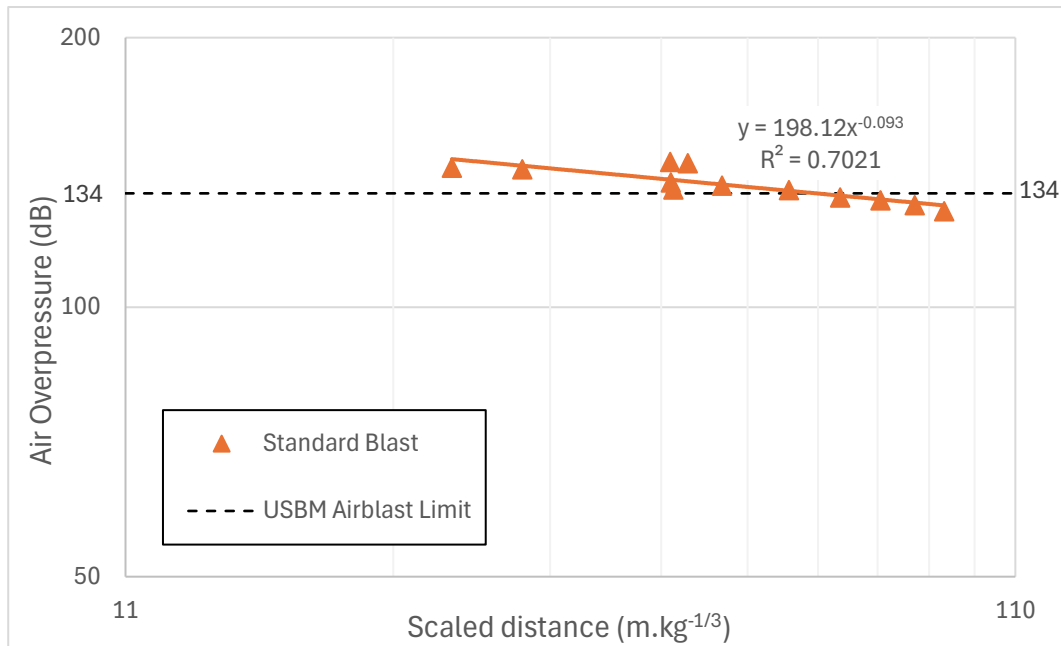


Figure 4.2: Air overpressure levels for the standard blasts at Station A

Plotting Figures 4.1 and 4.2 on the same set of axes produced Figure 4.3. This resultant graph plot (i.e., Figure 4.3) provides a better visual comparison of the performance of the Varistem® and standard blasts for Station A.

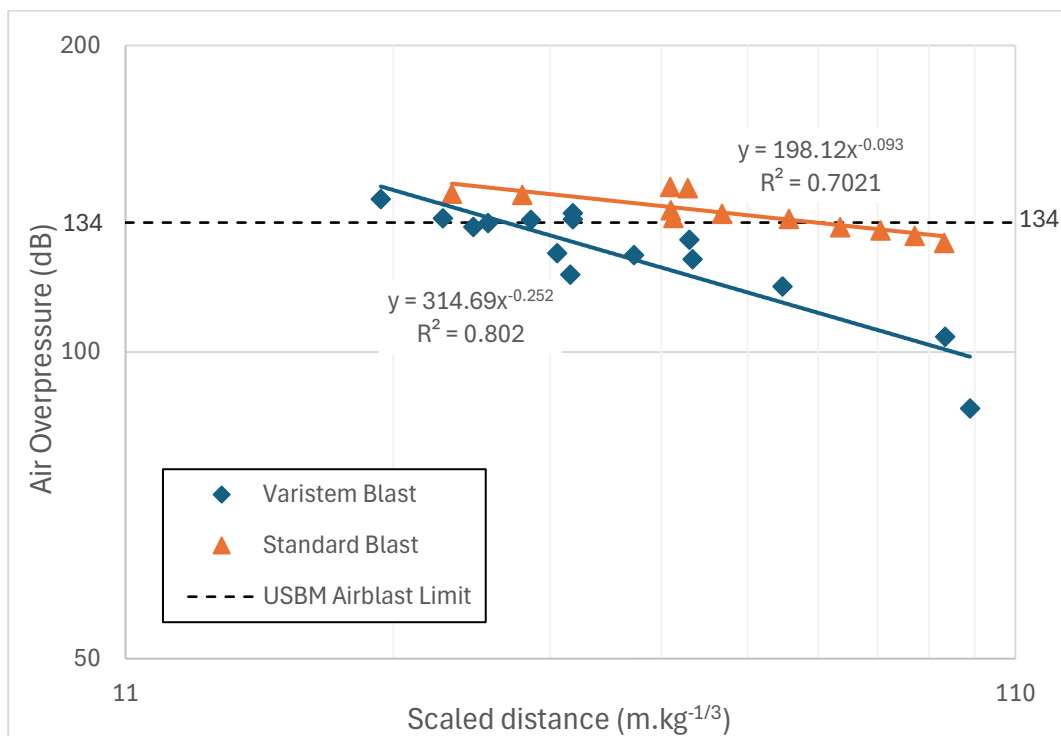


Figure 4.3: Air overpressure levels at Station A

The line of best fit for the Varistem® blasts produced an R^2 of 0.8020 at Station A as evidenced in Figure 4.3 above. This implies that the line of best fit accounts for 80.20% of the air overpressure (AOp) data collected. Additionally, visual inspections of Figure 4.1 suggest that 5 out of the 15 Varistem® blasts produced AOp levels above 134 dB. On the other hand, the line of best fit for the standard blasts produced an R^2 of 0.7021. In this case, the line of best fit can only account for 70.21% of the AOp data collected at Station A. Visual inspections (see Figure 4.2) also suggest that 8 out of the 12 standard blasts were above the 134 dB threshold limit.

4.2.2 Air blast profile from Station B

The same test programme was conducted at Station B using the experimental setup highlighted in Section 4.2.1 above and Section 3.3.1 of Chapter 3. The recorded blast events for Station B are captured in Table 4.2 below.

Table 4.2: Blast recordings from Station B for the Varistem® blasting and standard blasting

Blast no.	Station B: Varistem® blasts			Station B: Standard blasts		
	Distance (m)	Scaled distance (m/kg ^{1/3})	AOp (dB)	Distance (m)	Scaled distance (m/kg ^{1/3})	AOp (dB)
1	327	73.0	120.0	345	48.2	132.1
2	322	41.2	119.8	293	72.9	142.3
3	456	60.9	122.7	465	118.1	120.3
4	553	127.3	114.0	585	138.7	135.2
5	392	50.1	121.3	315	46.1	140.0
6	585	123.6	116.0	430	104.3	129.3
7	585	75.0	110.0	420	62.1	131.1
8	286	59.5	118.5	295	40.5	136.7
9	312	39.6	127.5	660	142.2	127.7

10	540	67.3	117.9	345	48.1	132.3
11	427	66.7	120.0	620	135.9	125.2
12	314	43.6	113.5	470	99.6	129.1
13	299	39.5	126.6			
14	110	13.1	129.7			
15	342	47.9	122.1			

Similarly to Section 4.2.1, the recorded data in Table 4.2 was plotted on a logarithmic graph as shown in Figures 4.4 and 4.5 below. The Varistem® blast graph plot (see Figure 4.4) had all the data points below the 134-dB USBM air blast limit at this station. On the other hand, the standard blast (see Figure 4.5) had two recorded blasts which were above the 134dB USBM limit.

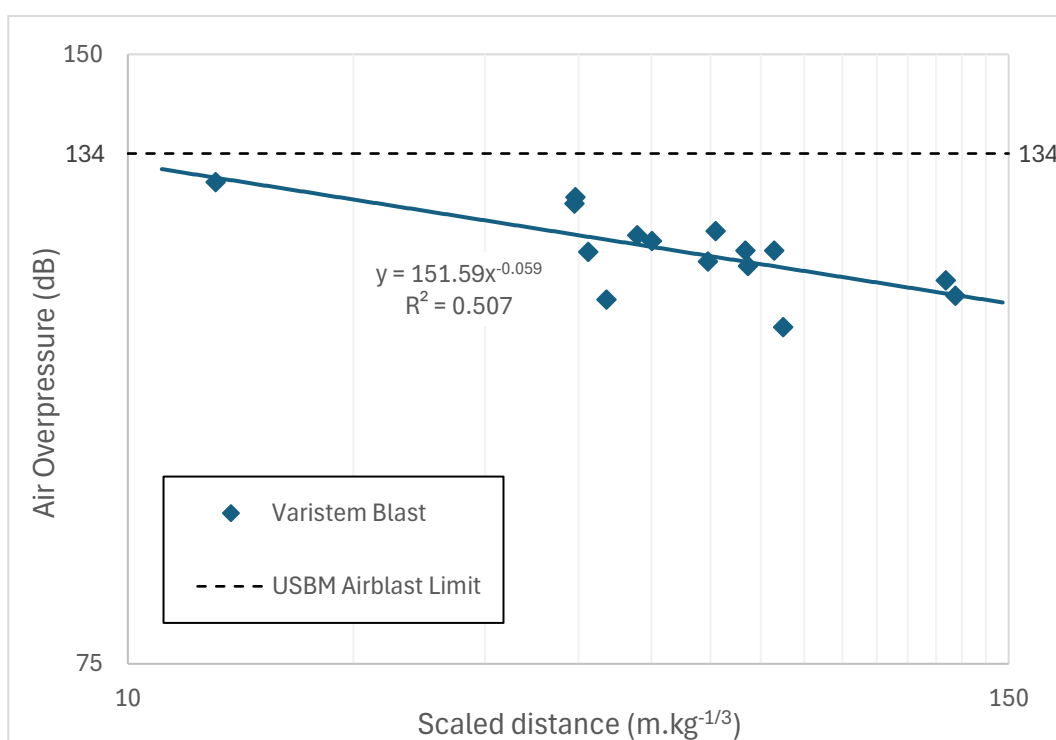


Figure 4.4: Air overpressure levels for the Varistem® blasts at Station B

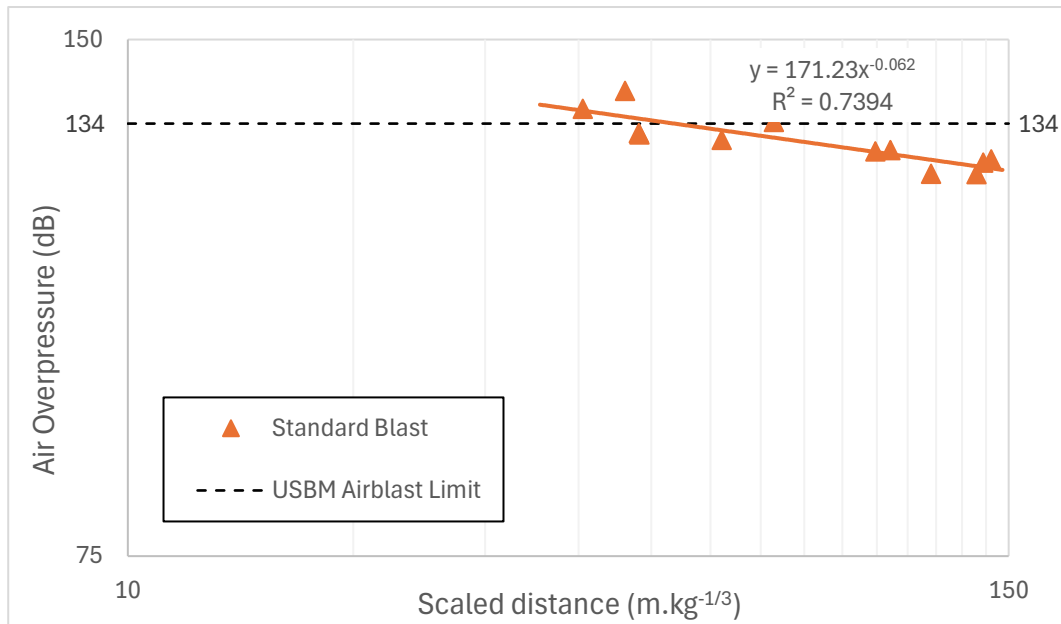


Figure 4.5: Air overpressure levels for the standard blasts at Station B

For better comparison, Figures 4.4 and 4.5 were plotted on the same set of axes and the resultant line chart is illustrated in Figure 4.6 below. Both graph plots for the Varistem® blast and the standard blast had a negative slope angle which supports the literature covered about air overpressure decreasing with an increase in distance.

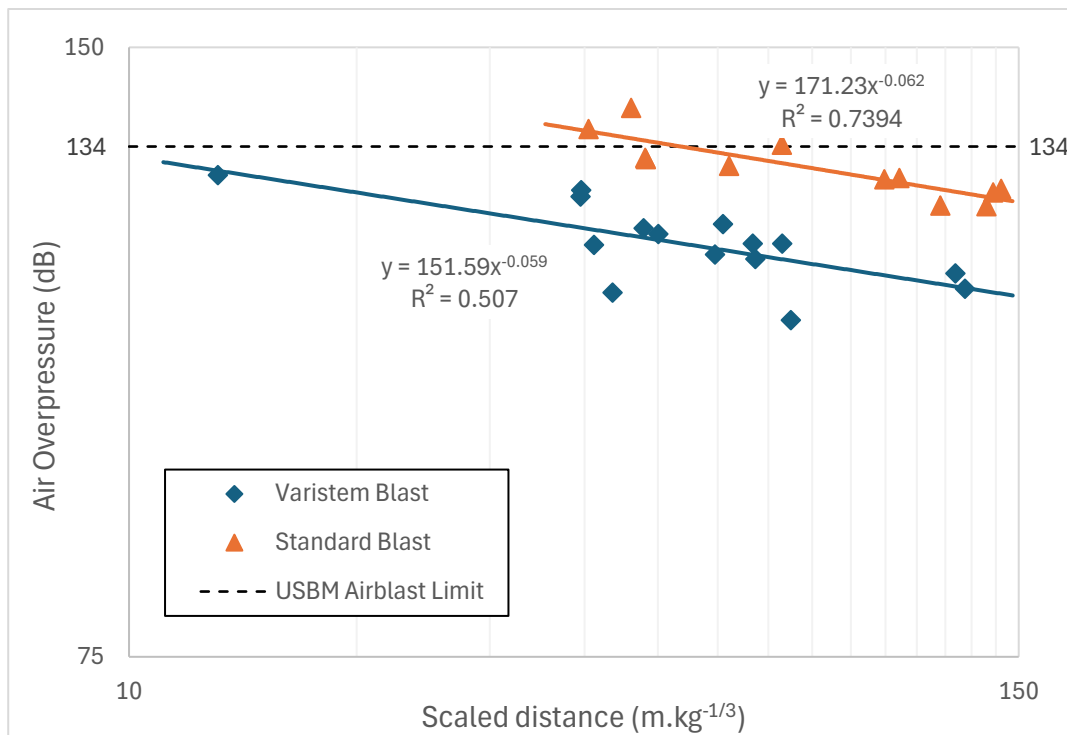


Figure 4.6: Air overpressure levels at Station B

A comparative analysis of Figure 4.6 shows that the line of best fit for the Varistem® blasts produced an R^2 of 0.5070 at Station B. An R^2 value of 0.5070 imply that the line of best fit for the data set can account for only 50.70% of the air overpressure data collected. Additionally, visual inspections suggest that all the 15 blasts carried out for the Varistem® were below the 134-dB air blast threshold limit. On the other hand, the line of best fit for the Standard blast produced an R^2 of 0.7394. This value implies that only 73.94% can be accounted for of the air overpressure data collected at Station B. Visual inspections also suggest that 3 out of the 12 standard blasts were above the 134-dB threshold limit.

4.2.3 Calculated scaled depth of burial – Observations

As highlighted in Chapter 3, calculations pertaining to the scaled depth of burial (SDoB) were carried out only for the Varistem® blasts. This is because the Varistem® blasts were the only data set with sufficient information to perform the calculations. The calculation of the scaled depth of burial involved parameters like top stemming, explosive density, explosive diameter, and length of 10 explosive diameters. As such, the blast parameters as captured in Tables 4.1 and 4.2 was used for this study. An average hole density of explosive (ρ) of 1.15 g/cm³ was used across all the blasts. The formulae presented in Section 2.5 of Chapter 2 were used as part of this study and they are highlighted in Equation (4.1) below:

$$SDoB = \frac{D_n}{W^{\frac{1}{3}}} \quad (4.1)$$

$$\text{where } D_n = S_t + 0.5 L \quad \text{and} \quad W = \left(\frac{\rho d^2}{1273} \right) L$$

From Equation (4.1), D_n represents the distance from the surface to the centre of the stem charge (in m); W is the mass of explosives equivalent to 10 explosive diameters (in kg); and L is the length of explosive (in m). Moreover, S_t represents the top stemming (m), d is the hole diameter (in mm) and ρ is the average in hole density of explosive (in g/cm³).

The length of 10 borehole diameters was specifically used because of the literature presented Section 2.5. As a result, the length L was calculated as

$$L = \frac{102 \text{ mm}}{1000} \times 10 = 1.02 \text{ m}$$
 and this value was the same across all blasts. Table

4.3 shows the calculated scaled depth of burial for each blast.

Table 4.3: Calculated scaled depths of burial for the Varistem® blasts at both stations

Blast No	Stemming Length	Scaled depth of burial
1	$S_t = 2.4 \text{ m}$	$D_n = 2.91$ $W = 9.587$ $SDoB = \frac{D_n}{W^{\frac{1}{3}}} = \frac{2.91}{9.587^{\frac{1}{3}}} = 1.37 \text{ m/kg}^{\frac{1}{3}}$
2	$S_t = 2.0 \text{ m}$	$D_n = 2.51$ $W = 9.587$ $SDoB = \frac{D_n}{W^{\frac{1}{3}}} = \frac{2.51}{9.587^{\frac{1}{3}}} = 1.18 \text{ m/kg}^{\frac{1}{3}}$
3	$S_t = 2.3 \text{ m}$	$D_n = 2.81$ $W = 9.587$ $SDoB = \frac{D_n}{W^{\frac{1}{3}}} = \frac{2.81}{9.587^{\frac{1}{3}}} = 1.32 \text{ m/kg}^{\frac{1}{3}}$
4	$S_t = 2.4 \text{ m}$	$D_n = 2.91$ $W = 9.587$ $SDoB = \frac{D_n}{W^{\frac{1}{3}}} = \frac{2.91}{9.587^{\frac{1}{3}}} = 1.37 \text{ m/kg}^{\frac{1}{3}}$
5	$S_t = 2.0 \text{ m}$	$D_n = 2.51$ $W = 9.587$ $SDoB = \frac{D_n}{W^{\frac{1}{3}}} = \frac{2.51}{9.587^{\frac{1}{3}}} = 1.18 \text{ m/kg}^{\frac{1}{3}}$
6	$S_t = 1.9 \text{ m}$	$D_n = 2.41$ $W = 9.587$ $SDoB = \frac{D_n}{W^{\frac{1}{3}}} = \frac{2.41}{9.587^{\frac{1}{3}}} = 1.13 \text{ m/kg}^{\frac{1}{3}}$
7	$S_t = 2.3 \text{ m}$	$D_n = 2.81$ $W = 9.587$ $SDoB = \frac{D_n}{W^{\frac{1}{3}}} = \frac{2.81}{9.587^{\frac{1}{3}}} = 1.32 \text{ m/kg}^{\frac{1}{3}}$
8	$S_t = 2.2 \text{ m}$	$D_n = 2.71$ $W = 9.587$

		$SDoB = \frac{D_n}{W^{\frac{1}{3}}} = \frac{2.71}{9.587^{\frac{1}{3}}} = 1.28 \text{ m/kg}^{\frac{1}{3}}$
9	$S_t = 2.3 \text{ m}$	$D_n = 2.81$ $W = 9.587$ $SDoB = \frac{D_n}{W^{\frac{1}{3}}} = \frac{2.81}{9.587^{\frac{1}{3}}} = 1.32 \text{ m/kg}^{\frac{1}{3}}$
10	$S_t = 2.2 \text{ m}$	$D_n = 2.71$ $W = 9.587$ $SDoB = \frac{D_n}{W^{\frac{1}{3}}} = \frac{2.71}{9.587^{\frac{1}{3}}} = 1.28 \text{ m/kg}^{\frac{1}{3}}$
11	$S_t = 2.0 \text{ m}$	$D_n = 2.51$ $W = 9.587$ $SDoB = \frac{D_n}{W^{\frac{1}{3}}} = \frac{2.51}{9.587^{\frac{1}{3}}} = 1.18 \text{ m/kg}^{\frac{1}{3}}$
12	$S_t = 1.9 \text{ m}$	$D_n = 2.41$ $W = 9.587$ $SDoB = \frac{D_n}{W^{\frac{1}{3}}} = \frac{2.41}{9.587^{\frac{1}{3}}} = 1.13 \text{ m/kg}^{\frac{1}{3}}$
13	$S_t = 2.3 \text{ m}$	$D_n = 2.81$ $W = 9.587$ $SDoB = \frac{D_n}{W^{\frac{1}{3}}} = \frac{2.81}{9.587^{\frac{1}{3}}} = 1.32 \text{ m/kg}^{\frac{1}{3}}$
14	$S_t = 2.2 \text{ m}$	$D_n = 2.71$ $W = 9.587$ $SDoB = \frac{D_n}{W^{\frac{1}{3}}} = \frac{2.71}{9.587^{\frac{1}{3}}} = 1.28 \text{ m/kg}^{\frac{1}{3}}$
15	$S_t = 2.0 \text{ m}$	$D_n = 2.51$ $W = 9.587$ $SDoB = \frac{D_n}{W^{\frac{1}{3}}} = \frac{2.51}{9.587^{\frac{1}{3}}} = 1.18 \text{ m/kg}^{\frac{1}{3}}$

4.3 Modelling air overpressure as a function of scaled distance

4.3.1 USBM predictor model

The USBM empirical model was chosen for this study because it is the most frequently used and widely accepted formula for predicting air blast from blasting operations as discussed in literature (i.e., Chapter 2). This empirical model was developed by the United States Bureau of Mines (USBM). The model aims to estimate the air overpressure (AO_p) induced from blasting operations, which can affect nearby structures and communities. It generally assists in assessing potential damage and ensuring safety protocols are in place. Typically, the USBM model includes a link between the amount of explosive utilised, the distance from the blast to the monitoring location, and air blast overpressure. The USBM empirical formula is generally given as indicated in Equation (4.2) below (Siskind et al., 1980):

$$AOp = H (d_s)^{-\beta} \quad (4.2)$$

Where AOp is site air blast levels (dB); H and β are site specific factors which are dimensionless; and $d_s = D_1 W_1^{-1/3}$ is the cube root scaled distance factor (m.kg^{-1/3}). D_1 denotes the distance [in m] from the monitoring station to the blast block and W_1 is the explosive charge weight per delay (in kg).

4.3.2 Mckenzie's predictor model

Mckenzie's predictor model was the second model used as part of the study to predict air overpressure levels at the two monitoring stations. Mckenzie (1990) conducted a study on air blast monitoring from quarry mines. From his study, Mckenzie (1990) proposed an empirical model for forecasting air blast levels, which are essential for evaluating possible effects on delicate locations close to blasting operations. In order to avoid causing excessive disruption to neighbouring homes and delicate structures, the model offers acceptable air blast thresholds, which are commonly expressed in decibels

(dB). As highlighted in Section 2.6, the empirical formula as proposed by Mckenzie (1990) is as indicated in Equation (4.3):

$$AOp = 165 - 24 \log \left(\frac{D_1}{\sqrt[3]{W_1}} \right) \quad (4.3)$$

Where AOp is the air overpressure (in dB); W_1 the explosive charge weight per delay (in kg); and D_1 is the distance from the free face of the blast block to the monitoring station (in m).

The estimation results derived when modelling air blast using both the USBM model and Mckenzie's model at Quarry TM are outlined in the subsequent section.

4.3.3 Comparison of the two predictor models

4.3.3.1 *USBM predictor model*

Using Equation (4.2), the USBM model for Quarry TM was tested at both monitoring stations as follows. The experimental data captured in Table 4.1 was used to calculate site constants for the quarry as well as the new AOp values by curve fitting. In this case, H in Equation (4.2) is the site-specific factor representing the local topographical conditions at Quarry TM whereas β is the exponent factor representing the geological site conditions at the quarry.

The calculated site constants for Station A for the Varistem® blasts were found to be $H = 295.3$ and $\beta = 0.235$. The resultant site specific USBM equation for the Varistem® at Station A was found to be:

$$AOp = 295.3 (d_s)^{-0.235} \quad (4.4)$$

For a better comparison study, the USBM predictor model captured in Table 2.1 was adopted for both stations. The USBM predictor model chosen for this purpose was for quarry blasts in front of the face as highlighted in Chapter 2. The adopted USBM predictor equation used was as follows:

$$AOp = 622 (d_s)^{-0.515} \quad (4.5)$$

From Equation (4.5), H is given as 622 and $\beta = 0.515$ respectively to make up Equation (4.2). Figure 4.7 illustrates the outcome for the Varistem® blasts when the USBM predictor model was applied at Station A. Details of the calculations are included as part of the Appendices (see Annexure B) at the end of the dissertation.

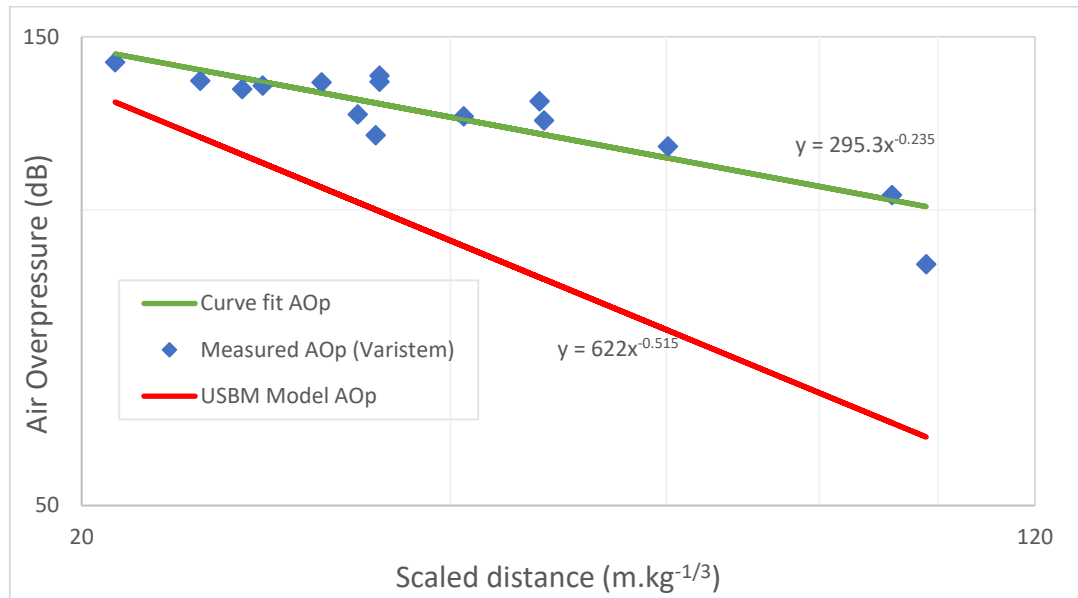


Figure 4.7: USBM predictor model for the Varistem® blasts at Station A

The same curve fitting calculations were performed for the standard blasts at Station A which led to the generation of Figure 4.8. The resultant site constants at Station A for the standard blasts were then found to be $H = 196.6$ and $\beta = 0.091$. As such, the resultant site specific USBM equation for the standard blasts at Station A was expressed as follows:

$$AOp = 196.6 (d_s)^{-0.091} \quad (4.6)$$

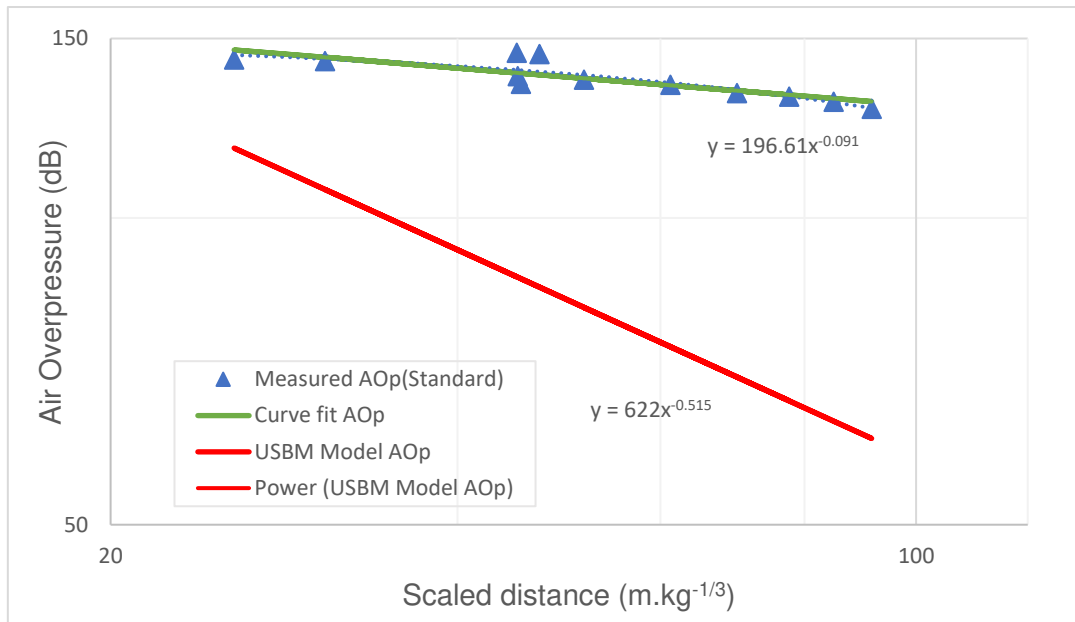


Figure 4.8: USBM predictor model for the standard blasts at Station A

The coefficient of determination (R^2) and the root mean squared error (RMSE) in Table 4.4 were used as performance indices for the quality of the curve fits done at Station A using the USBM model.

Table 4.4: USBM performance indices at Station A

	R^2	RMSE
Varistem® blast	0.8649	6.067144
Standard blast	0.7636	3.085334

Similar tests and calculations were also performed for the monitoring Station B. The curve fitting method gave the following site constants for the Varistem® blast: an H value of 151.6 and a β value of 0.059. The resultant site specific USBM equation for the Varistem® at Station B was found to be:

$$AOp = 151.6 (d_s)^{-0.059} \quad (4.7)$$

Figure 4.9 illustrates the resultant graphical plot for the Varistem® blasts when the USBM predictor model was applied at Station B.

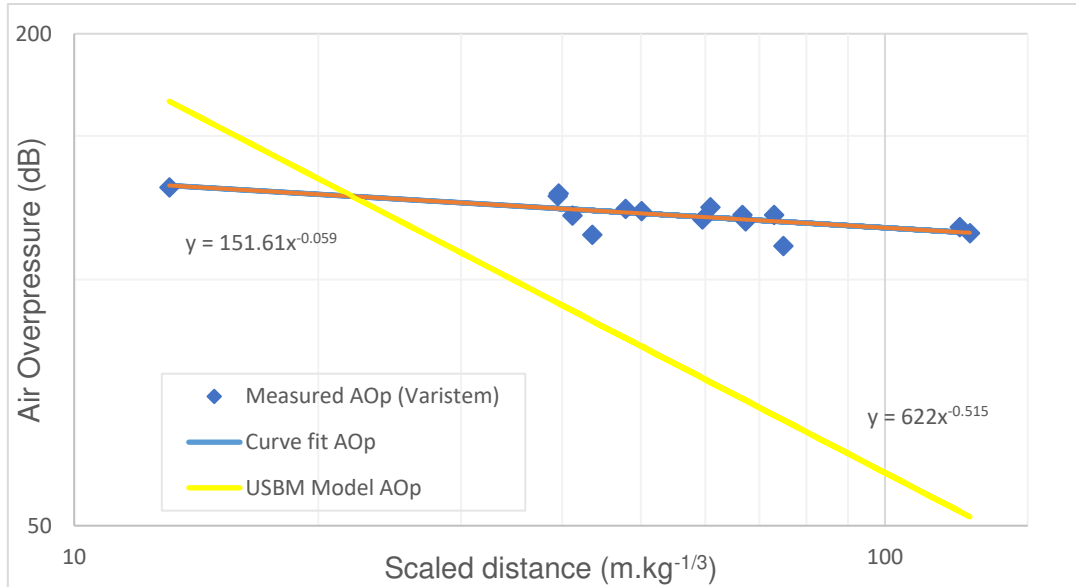


Figure 4.9: USBM predictor model for the Varistem® blasts at Station B

Meanwhile, the Standard blast produced the following site constants for Station B: $H = 168.3$ and $\beta = 0.056$. The resultant site specific USBM equation for the standard blasts at Station B was found to be:

$$AOp = 168.3 (d_s)^{-0.056} \quad (4.8)$$

Figure 4.10 illustrates the resultant graphical plot for the standard blasts when the USBM predictor model was applied at Station B.

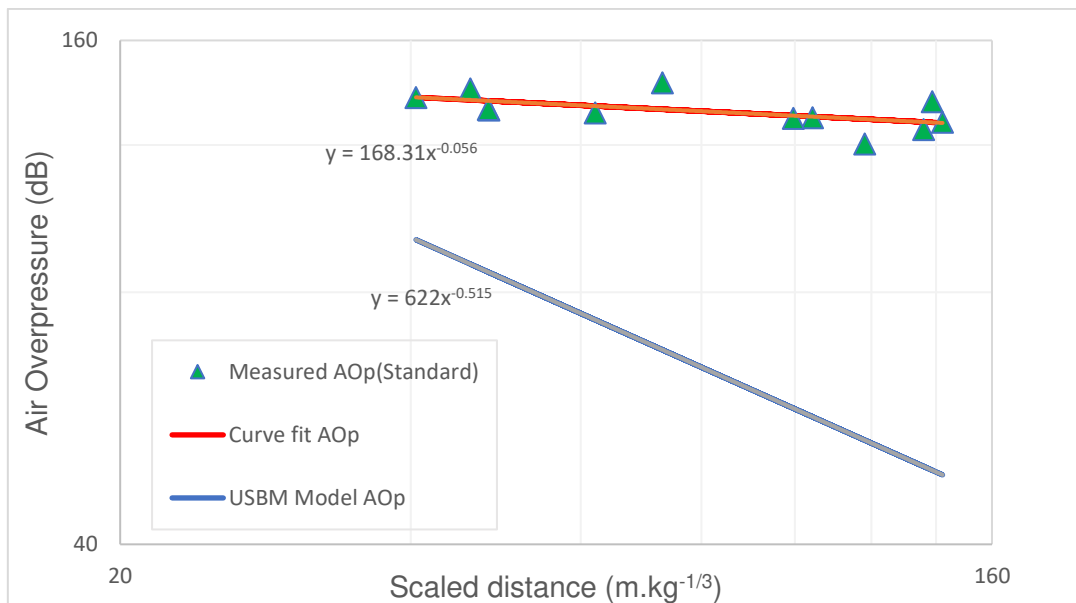


Figure 4.10: USBM predictor model for the standard blasts at Station B

The coefficient of determination (R^2) and the root mean squared error (RMSE) in Table 4.5 were used as performance indicators of the quality of curve fitting done with data from Station B using the USBM model.

Table 4.5: USBM performance indices at Station B

	R^2	RMSE
Varistem® blast	0.8070	3.663068
Standard blast	0.6303	4.841641

4.3.3.2 Mckenzie's predictor model

As highlighted in Section 3.4 of Chapter 3, Tables 4.6 and 4.8 below provide an overview of the calculations carried out for Station A. The resultant scaled distances were plotted against the new predicted air overpressure as exemplified in Figure 4.11 below. The measured air overpressure data points were also included in the same plot area for both the Varistem® and standard blasts.

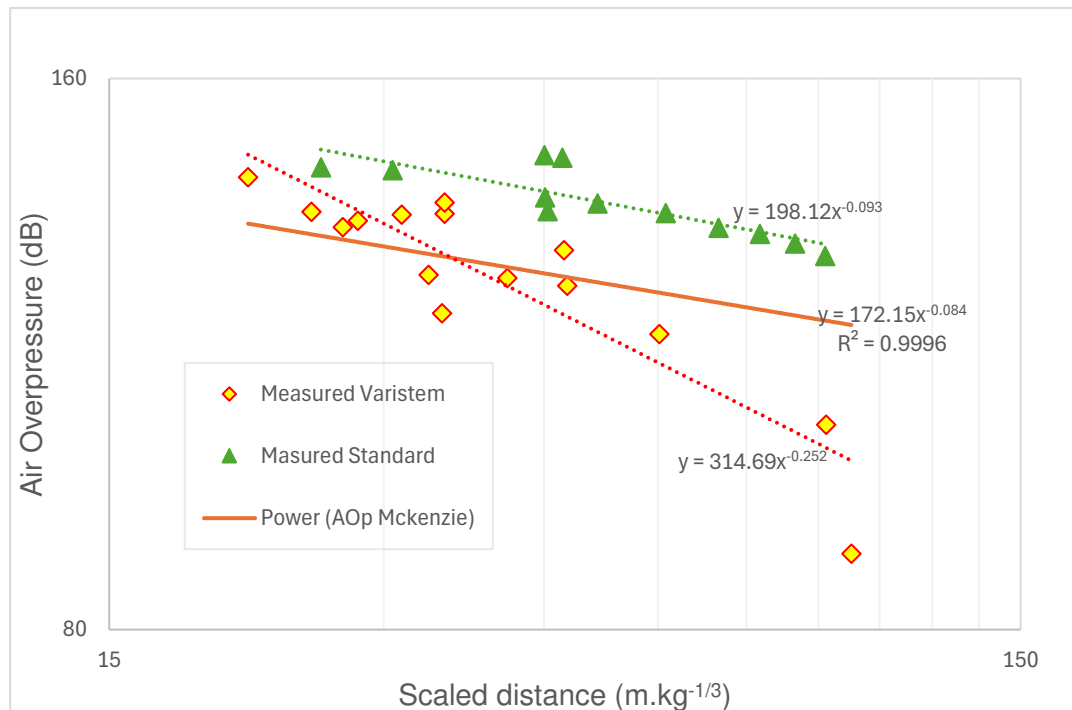


Figure 4.11: Mckenzie's predicted air overpressure levels at Station A

Table 4.6: Mckenzie's predictor model for the Varistem® blasts

	Station A: Varistem® blast				Station B: Varistem® blast			
Blast #	D_1 (m)	W_1 (kg)	d_s (m kg ^{-1/3})	AOp (dB)	D_1 (m)	W_1 (kg)	d_s (m kg ^{-1/3})	AOp (dB)
1	411	90	91.71	117.90	327	90	72.97	120.28
2	370	478.7	47.30	124.80	322	478.7	41.16	126.25
3	235	419.2	31.40	129.07	456	419.2	60.93	122.16
4	151	82	34.76	128.02	553	82	127.29	114.49
5	220	479.9	28.10	130.23	392	479.9	50.07	124.21
6	128	106	27.05	130.63	585	106	123.61	114.79
7	320	475.4	41.00	126.29	585	475.4	74.96	120.00
8	470	111	97.80	117.23	286	111	59.51	122.41
9	168	490.7	21.30	133.12	312	490.7	39.60	126.67
10	383	517	47.70	124.71	540	517	67.28	121.13
11	215	262	33.60	128.37	427	262	66.73	121.22
12	434	374.7	60.20	122.29	314	374.7	43.55	125.66
13	265	434.04	35.00	127.94	299	434.04	39.49	126.68
14	210	592.7	25.00	131.45	110	592.7	13.10	138.19
15	250	364.4	35.00	127.94	342	364.4	47.88	124.68

From Figure 4.11, the resultant trend power function for the Varistem® blasts was $y = 314.69 x^{-0.252}$. On the other hand, the power trend function for the standard blasts was $y = 198.12 x^{-0.093}$. Performance indices such as the R^2 and the RMSE were used to determine the accuracy and precision of the model at Station A as illustrated in Table 4.7.

Table 4.7: Performance indices for Mckenzie's model at Station A

	R^2	RMSE
Varistem® blast	0.9996	9.9196
Standard blast	0.9996	13.599

A similar experimental test was conducted for the data sets recorded at Station B. Table 4.8 provides an overview of the calculations carried out to get new scaled distances and air overpressure levels using Mckenzie's empirical model. The logarithmic graph plot of the cube-root scaled distance versus air overpressure is illustrated in Figure 4.12 below.

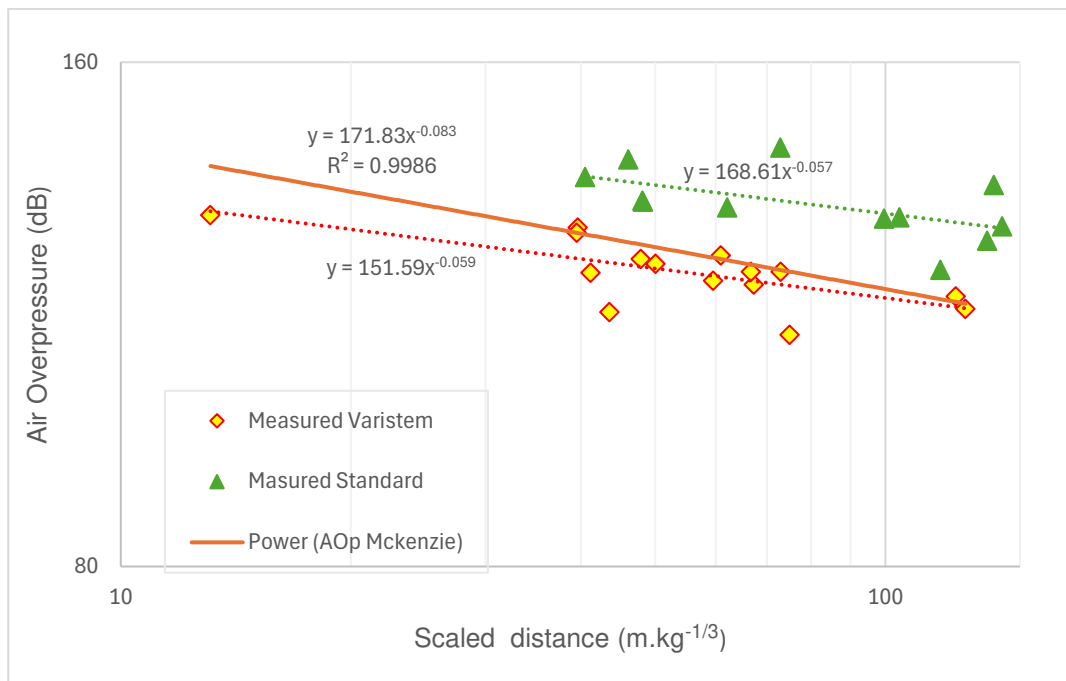


Figure 4.12: Mckenzie's predicted air overpressure at Station B

Table 4.8: Mckenzie's predictor model for the standard blasts

	Station A: Standard blast				Station B: Standard blast			
Blast #	D_1 (m)	W_1 (kg)	d_s (m kg ^{-1/3})	AOp (dB)	D_1 (m)	W_1 (kg)	d_s (m kg ^{-1/3})	AOp (dB)
1	325	366.8	45.40	125.23	345	366.8	48.20	124.61
2	341	65.0	84.80	118.72	293	65.0	72.90	120.30
3	360	61.0	91.50	117.93	465	61.0	118.10	115.26
4	258	75.0	61.20	122.12	585	75.0	138.70	113.59
5	352	319.3	51.50	123.92	315	319.3	46.10	125.07
6	320	70.0	77.60	119.64	430	70.0	104.30	116.56
7	305	309.2	45.10	125.30	420	309.2	62.10	121.96
8	186	386.5	25.60	131.23	295	386.5	40.50	126.42
9	209	100.0	45.03	125.32	660	100.0	142.20	113.33
10	220	368.6	30.70	129.31	345	368.6	48.10	124.62
11	215	95.0	47.12	124.84	620	95.0	135.90	113.80
12	330	105.0	69.90	120.73	470	105.0	99.60	117.04

The resultant trend power function from Figure 4.12 for the Varistem® blasts was $y = 151.59 x^{-0.059}$. On the other hand, the power trend function for the standard blasts was $y = 168.61 x^{-0.057}$. Performance indices such as the R^2 and the RMSE were used to determine the accuracy and precision of the model at Station B as illustrated in Table 4.9.

Table 4.9: Performance indices for Mckenzie's model at Station B

	R^2	RMSE
Varistem® blast	0.9986	5.2067
Standard blast	0.9986	13.3785

4.4 Comparing air blasts with and without stemming plugs

For comparison purposes, an analysis of variance (ANOVA) test was performed which focused on a comparative experiment between the Varistem® blast and the standard blast. This was done to establish whether the mean air blast level produced between the two data sets would be the same or different. As such, the ANOVA test used for this purpose was expressed formally as indicated in Equation (4.9):

$$\begin{cases} H_0: \mu_V = \mu_S \\ H_1: \mu_V \neq \mu_S \end{cases} \quad (4.9)$$

The statement $H_0: \mu_V = \mu_S$ in Equation (4.9) is the null hypothesis; it assumes that the average AOP produced by Varistem® blasting (μ_V) is the same as that produced by standard blasting (μ_S). On the other hand, the statement $H_1: \mu_V \neq \mu_S$ is the alternative hypothesis.

The following AOp data sets in Table 4.10 were used to compute the ANOVA test.

Table 4.10: Air overpressure levels at the two stations

Station A (AOp)		Station B (AOp)	
Varistem® blast (dB)	Standard blast (dB)	Varistem® blast (dB)	Standard blast (dB)
103.5	135.4	120.0	132.1
128.9	130.0	119.8	142.3
134.8	128.0	122.7	120.3
119.1	135.1	114.0	135.2
133.8	136.7	121.3	140.0
132.7	131.6	116.0	129.3
124.5	137.8	110.0	131.1
88.0	143.1	118.5	136.7
141.3	145.3	127.5	127.7
123.3	142.6	117.9	132.3
125.0	144.8	120.0	125.2
116.0	132.6	113.5	129.1
135.0		126.6	
135.3		129.7	
136.9		122.1	

Furthermore, while conducting this test, the significance level (α) was set at 0.05. The significance level was set at 0.05 for statistical considerations and also to create a balance between interpreting the null and alternative hypothesis. A 0.05 significance level facilitates result interpretation by indicating that, if the null hypothesis is correct, there is only a 5% chance of observing the data. After performing an ANOVA test on the air blast levels for the two blasts, the following results (Tables 4.11 and 4.12) were established.

Table 4.11: Statistical analysis of variances for air blasts at Station A

ANOVA: Single Factor Station A						
Groups	Count	Sum	Average	Variance		
Varistem®	15	1878.1	125.2067	200.7807		
Standard	12	1643	136.9167	34.87606		
Source of Variation	SS	df	MS	F	P-value	F crit
Between Groups	914.1607	1	914.1607	7.154029	0.012996	4.241699
Within Groups	3194.566	25	127.7826			
Total	4108.727	26				

From Table 4.11, the letter SS represents the Sum of Squares, df represents the degree of freedom, MS is the Mean Square, and F represents the F-Ratio. The Analysis of Variance (ANOVA) around the monitoring Station A generated a p-value at 95% confidence level of $p = 0.013$ which is lower than the threshold or critical p-value set at $p_{crit} = 0.05$.

Table 4.12: Statistical analysis of variance for air blasts at Station B

ANOVA: Single Factor Station B						
Groups	Count	Sum	Average	Variance		
Varistem®	15	1799.6	119.9733	29.15924		
Standard	12	1570.3	130.8583	20.45538		
Source of Variation	SS	df	MS	F	P-value	F crit
Between Groups	789.8882	1	789.8882	31.18447	8.2871E-06	4.241699
Within Groups	633.2385	25	25.32954			
Total	1423.127	26				

From the monitoring Station B, the ANOVA gave the following outcome: $p = 0.000$ (i.e., 0.000008) also lower than $p_{crit} = 0.05$.

4.5 Summary of findings

A test programme was carried out which involved 27 production blasts. Out of these production blasts, 15 incorporated the Varistem® stemming plugs while the remaining 12 were conducted using standard stemming consisting of aggregates only. Two stations were used to record and monitor the blasts, namely, Station A and Station B. Additionally, these stations were located approximately 100 to 700 m away from the blast blocks. A Nomis seismograph was positioned at each station where data was recorded simultaneously for each of the 27 blasts. Historical data representative of the standard blasts was made available for the purpose of this study. This data was recorded and archived prior to the quarry adopting the use of Varistem® stemming plugs.

As demonstrated in Figure 4.3, a comparative analysis of the results derived from Station A showed that 5 out of the 15 blasts for the Varistem® blasts were above the 134-dB threshold limit. Meanwhile 8 out of the 12 blasts for the standard blasts were above the regulatory limit. Furthermore, plotting the lines of best fit for both groups of blasts produced an R^2 of 0.8020 for the Varistem® blasts. This implies that only 80.20% of the air blast data was accounted for by the selected model. In contrast, the standard blasts at the same station produced an R^2 of 0.7021 which suggests that 70.21% of the air blast data was accounted for on the graph plot.

Similarly, the same test work was carried out for Station B. In this case all the 15 blasts carried out for the Varistem® were below the 134-dB air blast threshold limit as evidenced in Figure 4.6. With the standard blasts, 3 out of the 12 blasts were above limit at the same station. Additionally, the line of best fit for the Varistem® blasts produced an R^2 of 0.5070 at Station B. An R^2 value of 0.5070 implies that the line of best fit for the data set accounts for only 50.7% of the air overpressure data collected. On the other hand, the line of best fit for the standard blasts produced an R^2 of 0.7394. This value implies that only 73.94% can be accounted for of the air overpressure data collected at Station B.

Air overpressure was also modelled as a function of the scaled distance. Two prediction models were used for this purpose: the USBM predictor model and Mckenzie's predictor model. The USBM model was found to be the best predictor of air blast for this study with lower coefficient of determination (R^2) for both stations compared to McKenzie's model that recorded an R^2 of 0.9996 for Station A and 0.9986 for Station B. The RMSE derived from the USMB model at Station A was 6.067 for the Varistem® blasts and 3.085 for the standard blasts. Meanwhile the same model produced a RMSE of 3.663 for the Varistem® blasts and 4.842 for the standard blasts at Station B. Mckenzie's model on the other hand produced a RMSE of 9.9196 for the Varistem® and an RMSE of 13.599 for the standard blasts at Station A. Similarly, when looking at Station B, Mckenzie's model produced a RMSE of 5.206 for the Varistem® blasts and an RMSE of 13.379 for the standard blasts.

Finally, the analysis of variance (ANOVA) around the monitoring Station A generated a p-value at 95% confidence level of $p = 0.013$ which is lower than the threshold or critical p-value set at $p_{crit} = 0.05$. From the monitoring Station B, the ANOVA gave the following outcome: $p = 0.000$ (i.e., 0.000008) also lower than $p_{crit} = 0.05$.

Chapter 5 Understanding the effects of stemming plugs on the reduction of air blast

5.1 Introduction

This research study was aimed at determining the contribution of the Varistem® stemming plugs in reducing the blast induced air blast at a South African open pit quarry. More emphasis was placed on the effect of monitoring distance from two different stations away from the blast blocks. Other factors of interest included the explosive charge weight per delay, blast design parameters and geological properties of the rock mass. An analysis of variance (ANOVA) test was also conducted on the air blast measurements observed for the Varistem® and standard blasts. This was done to test and compare the hypotheses between the means of the air blast levels between the two types of blasts. Also, to establish if the data observed would be statistically significant. Lastly, two air blast empirical models were tested on the Varistem® and standard blasts. The observations presented in Chapter 4 are the subject of discussion in this section of the report. The discussion is carried out in line with the literature covered in Chapter 2. This is to help clarify the observations reported in Chapter 4. Remarks regarding feasibility are also discussed.

5.2 Effect of stemming plugs on air blast at Station A

Distance from the blast site to the monitoring station is one of the factors that has a direct influence on the level of air blast recorded in surface mines. The observations made from Station A as captured in Table 4.1 are interpreted in this section. The propagation of air overpressure over different monitoring distances per production blast was captured. As discussed in Chapter 2, the USBM regulations of air blast safe limits are widely followed in South Africa. As such, Quarry TM also operates under these regulations of keeping the air blast threshold limit at 134 dB.

The resultant air overpressure (AOp) levels from Station A for the Varistem® blasts varied between 88 and 141.3 dB. On the other hand, the air overpressure levels for the Standard blasts at the same station varied between 128 and 145.3 dB. The 15 Varistem® blasts had a sample mean of 125.21 dB while the 12 standard blasts had a sample mean of 136.92 dB. The difference between these two-sample means is therefore 9.35%. This variation between the two blasts also highlights the USBM air blast regulatory limits for human and structural response as discussed in Table 2.1. Air blast levels of up to 134 dB threshold are the recommended limit for human irritation (Siskind et al., 1980). Ideally some window breakage or structural damage may occur beyond this level of threshold.

A comparison analysis was conducted between the Varistem® and standard production blasts at this station. This involved plotting the recorded air blast levels captured for different monitoring distances. Air overpressure was plotted as a function of scaled distance as demonstrated in Figure 4.3 of Chapter 4. The line of best fit for the Varistem® data set was found to be: $y = 314.69 x^{-0.252}$. And the best fit line for the standard data set at the same station was found to be: $y = 198.12 x^{-0.093}$. A 134-dB boundary line was introduced on the graph plot to highlight the regulatory threshold limit of air blast as per the USBM and assist in interpreting the results.

As demonstrated in Figure 4.3, Station A recorded some blasts which lie below the 134-dB USBM limit with some few points slightly above. In essence, 5 out of 12 trials (33.33%) for the Varistem® blasts were above the 134-dB line. Meanwhile, out of the 12 trials for the Standard blasts, 8 were above the 134-dB line. This means about 67% of the blast conducted for the standard blasts were above the threshold limit and may have caused some irritation to humans or damage to nearby infrastructure as highlighted in Table 2.1. The 145.3-dB air blast level recorded for standard blast was the highest at this station. According to the USBM regulatory standards, recording such levels of air overpressure is unacceptable and may cause damage to structures nearby. On this specific blast, the escape of explosive gases caused a high magnitude of noise and air overpressure. This is also

supported by Saharan et al. (2017) who stated that “boreholes stemmed with conventional stemming uniformly allows escape of the borehole pressure as it keep on generating and thus poor utilization of explosive energy”.

In principle, during blasting the explosives transfer energy into the rock mass, and part of this energy is also released into the atmosphere, thus, causing air blast. About 13 of the 27 blasts (or 48.15%) carried out for this station had higher air blast levels (see Table 4.1 and Figure 4.3). The results derived from this station support the review covered in Chapter 2 about the fact that stemming plugs have the potential to optimise blast performance. The Varistem® stemming plugs were able to reduce the air blast in 10 blasts by deflecting the released energy into the rock mass and consequently, improving the rock fragmentation. Indeed, Saharan et al. (2017) and Yang et al. (2018) also showed that the incorporation of stemming plugs into the blast design does improve explosive energy utilisation. Yang et al. (2018) further reported that stemming plugs increased gas retention during blasting. At Station A, the recorded air blast levels for the Varistem® blasts showed an improvement in gas energy retention as highlighted by the 9.35% improvement discussed above. The highest value of air blast recorded for the Varistem® blasts at this station was 141.3 dB while the standard blasts was 145.3 dB.

Additionally, the air blast levels recorded at this station can be attributed to the existing geological discontinuities (see Figure 5.1) which had an impact on the outcome of some of the blasts. Some areas of the block to be blasted had geological joints, with some areas on the highwall showing a fractured face. This is also supported by the geographical map of the quarry illustrated in Figure 3.3 where a dolerite dyke is located next to the area that was blasted. When geological discontinuities are present, explosive gases intensely escape from them, causing large vibration magnitudes (Hajihassani et al., 2015). At Quarry TM, precautionary measures were put in place especially when drilling an area with geological discontinuities. To minimise the potential explosive energy that could be lost, angled holes were used on certain blast holes, and this was also incorporated in the blast design.



Figure 5.1: Geological discontinuities present within the rock mass – Field observation by the author at Quarry TM

In light of the above, a further analysis was made to make sense of the recorded air blast results through the use of an ANOVA test. This involved analysing the observed results to assess if there is any statistical significance between the two groups of data. As highlighted in Section 4.4, the statistical test was done around the null hypothesis ($H_0: \mu_V = \mu_S$) and the alternative hypothesis ($H_1: \mu_V \neq \mu_S$).

From Figure 4.11, the ANOVA test around monitoring Station A generated a p-value at 95% confidence level of $p = 0.013$ which is lower than the threshold or critical p-value set at $p_{crit} = 0.05$. A p-value below the critical (i.e., below α) signifies statistical significance in the observed data. Considering this, the null hypothesis can be rejected because of the substantial evidence against it. This further supports the evidence presented above that there is indeed a significant difference or effect present in the two groups of data. Furthermore, a bootstrap analysis was also performed since the best fit lines of the two groups of blasts in Figure 4.3 are not parallel. The

results from bootstrapping showed that there is variability in the data set of the two blast hence confirming that there is a difference in the blasts.

To test the validity of the best fit line in Figure 4.3, the confidence bands at 95% significance level were constructed for both blasts recorded at Station A. The purpose of these 95% confidence bands were to show the plausible range of values for the fitted line. The 95% confidence bands were calculated using the following formula (Verschuuren, 2014):

$$X = Y \pm t_{\alpha} SE \sqrt{\frac{1}{n} + \frac{(x-x_m)^2}{SS_{xx}}} \quad (5.1)$$

Where X : 95% confidence interval

Y : Predicted air overpressure value

t_{α} : Student's two tailed t-test at 95%

SE : Standard error

n : Sample number

x : Scaled distance values

x_m : Average of the scaled distance values

SS_{xx} : Sum of the squares of deviations of data points from their sample mean.

Using Equation (5.1) above, the Varistem® series of data points were plotted as illustrated in Figure 5.2 below. A detailed illustration of how these confidence bands were calculated is included as part of the Appendices (see Annexure C). The upper and lower bound lines denoted as “confidence bands” below loosely imply that there is a 95% probability that the true best-fit line for the data set lies within the confidence bands. The line of best-fit for these data points was established by fitting the data set to a power function.

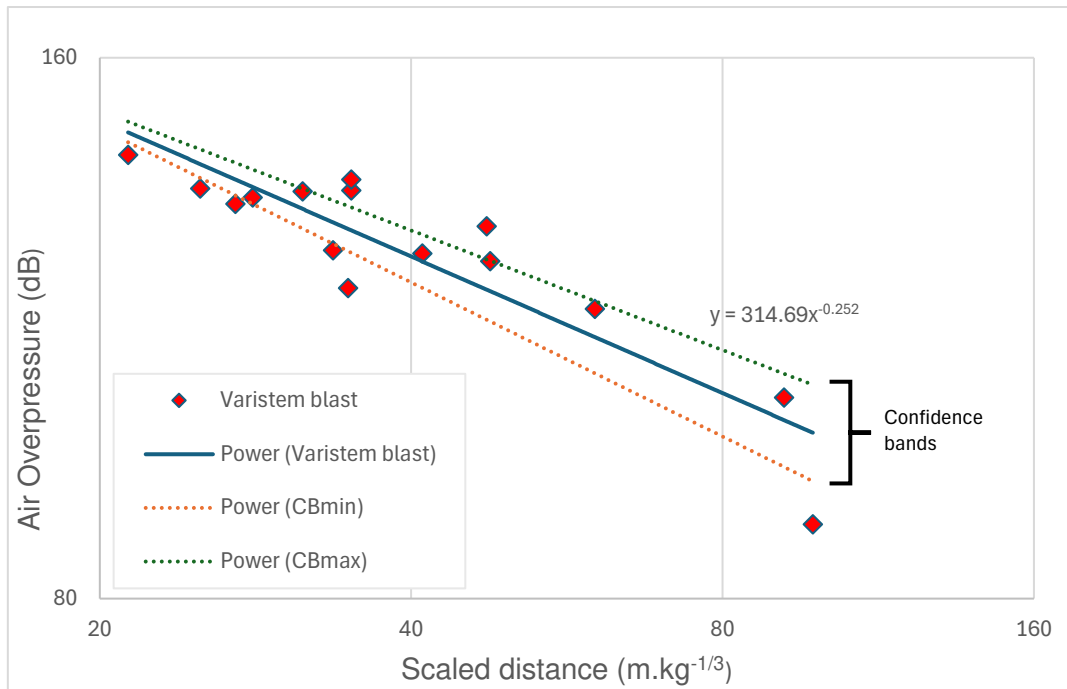


Figure 5.2: Confidence band at 95% significance level for the Varistem® blast at Station A

From Figure 5.2 above, the line of best fit for the Varistem® blasts ($y = 314.69 x^{-0.252}$) does indeed lie within the 95% confidence bands. There are also about nine data points which fall outside the confidence bands. It is worth noting that these data points are not necessarily all outliers or errors in the data. This is because the confidence interval represents the variability in estimating the mean response and not individual observations.

Similarly, 95% confidence bands were plotted for the standard blasts at this station as illustrated in Figure 5.3 below. The line of best fit for the standard blasts ($y = 198.12 x^{-0.093}$) was found to lie within the confidence bands.

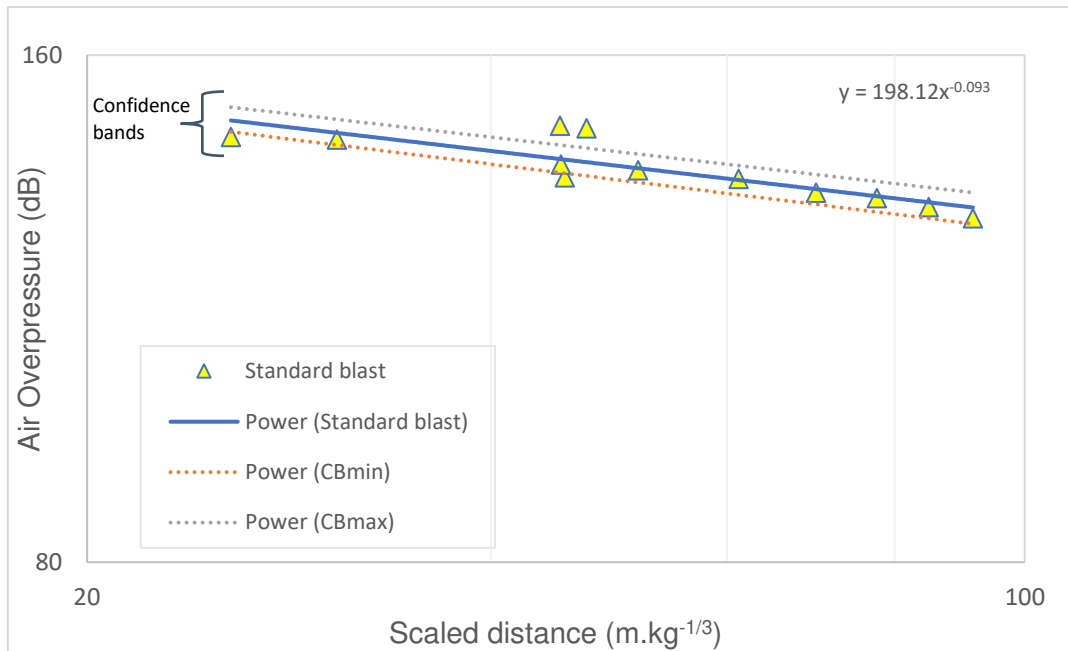


Figure 5.3: Confidence band at 95% significance level for the Standard blast at Station A

For a better comparison analysis between the two data sets, Figure 5.2 and Figure 5.3 were plotted on the same set of axes to produce Figure 5.4.

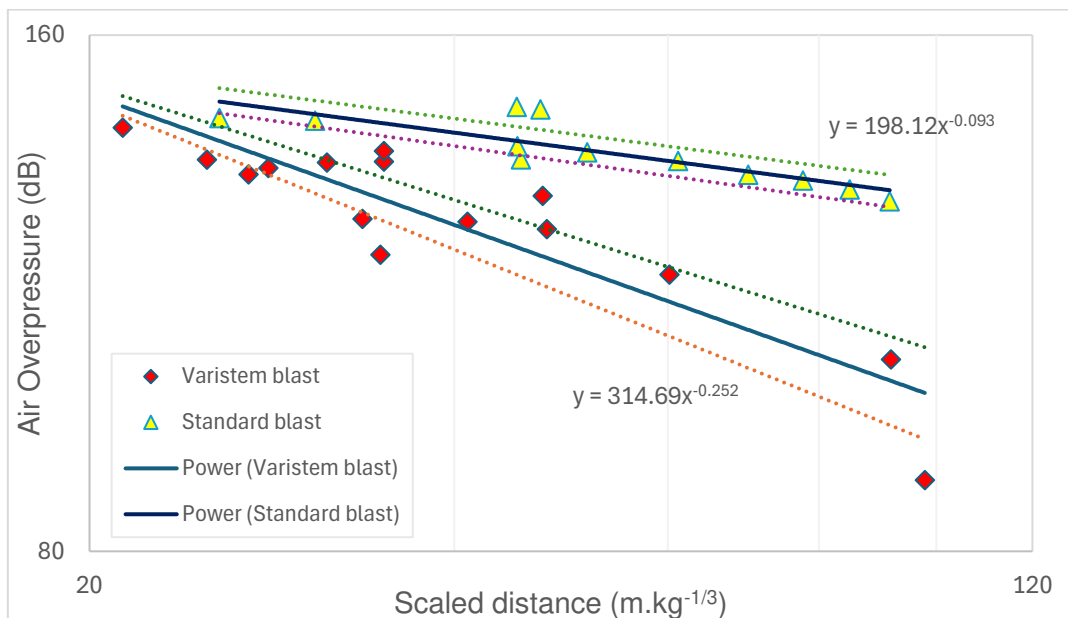


Figure 5.4: Confidence bands at 95% significance level for Station A

The 95% confidence bands plotted in Figure 5.4 above show that the line of best fit for the two blasts does lie within the confidence bands. However, when comparing the two sets of blasts, their lines of best fit are not parallel.

The same observation was noted about the 95% confidence bands for the two blasts. This suggests a slope variation between the two data sets which implies that the effect of the independent variable (Scaled distance) on the dependent variable (Air overpressure) is different for each dataset.

5.3 Effect of stemming plugs on air blast at Station B

Similarly, the observations made from the 27 blasts at Station B were also captured in Table 4.2. The propagation of air overpressure over different monitoring distances per blast was studied. The USBM air blast regulatory limits were also used to make conclusions for air overpressure levels at this station.

The resultant air overpressure (AOp) levels from Station B for the Varistem® blasts varied between 110 and 129.7 dB. With the standard blasts and for the same station, the AOp levels varied between 125.5 and 140 dB. The Varistem® blasts had a sample mean of 119.97 dB while the standard blasts had a sample mean of 130.86 dB. The difference between these two-sample means is therefore 9.08%.

A logarithmic scatter graph plot was also produced for the Varistem® and standard data set as evidenced in Figure 4.6 of Chapter 4. Since the data points are not linear, a power function was fitted into the data set to aid in interpreting the relationship between the dependant and independent variables. In this case, the dependent variable is the air overpressure, and the independent variable is the scaled distance.

After plotting the graph, the line of best fit for the Varistem® data set was found to be: $y = 151.59 x^{-0.059}$. And for comparison purposes, the best fit line for the standard data set at the same station was found to be: $y = 171.23 x^{-0.062}$.

A boundary line at 134 dB was also plotted to feature the USBM limits and aid in interpreting the results. As can be seen in Figure 4.6, all the Varistem® data points were below the 134-dB line which is acceptable according to the

USBM regulatory standards. Based on the discussion done in Chapter 2, AOp levels below 134 dB mean low levels of noise and irritation produced. Interestingly, 3 of the 12 blasts for the standard blasts were found to lie above the 134-dB line. This means 25% of the data points were above the 134-dB line for the standard blasts. According to the USBM guidelines, AOp levels above 134 dB may cause damage to nearby infrastructure (Siskind, 1980). Unlike Station A, most of the observed data for this Station B were within the acceptable USBM air blast limits. It is also worth noting that air overpressures at farther monitoring distances were not greater than those near the source and this is demonstrated in Table 4.2.

To establish if there is a difference between the recorded data of the Varistem® as well as the standard blasts, an ANOVA of the observed data was also done in a similar fashion as was done in Station A. From monitoring Station B, the ANOVA gave the following outcome: $p = 0.000$ (i.e., 0.000008) which is lower than $p_{crit} = 0.05$. As highlighted in Section 5.2, a p-value below the critical signifies statistical significance in the observed data. In light of this, the null hypothesis should be rejected because of the substantial evidence against it. This also supports the evidence presented above that there is a significant difference or effect present in the two groups of data.

Additionally, the confidence bands at 95% significance level were also established for the plotted Varistem® and standard blasts at this station. This was aimed at determining if there is any statistical significance between the two sets of blasts. The purpose of these 95% confidence bands was to show the plausible range of values for the best fit line of the data sets. For the Varistem® blasts, a series of data points were plotted as illustrated in Figure 5.5 below. The upper and lower bound lines denoted as “confidence bands” below demarcate the region within which there is a high likelihood of finding the true best-fit line for the population.

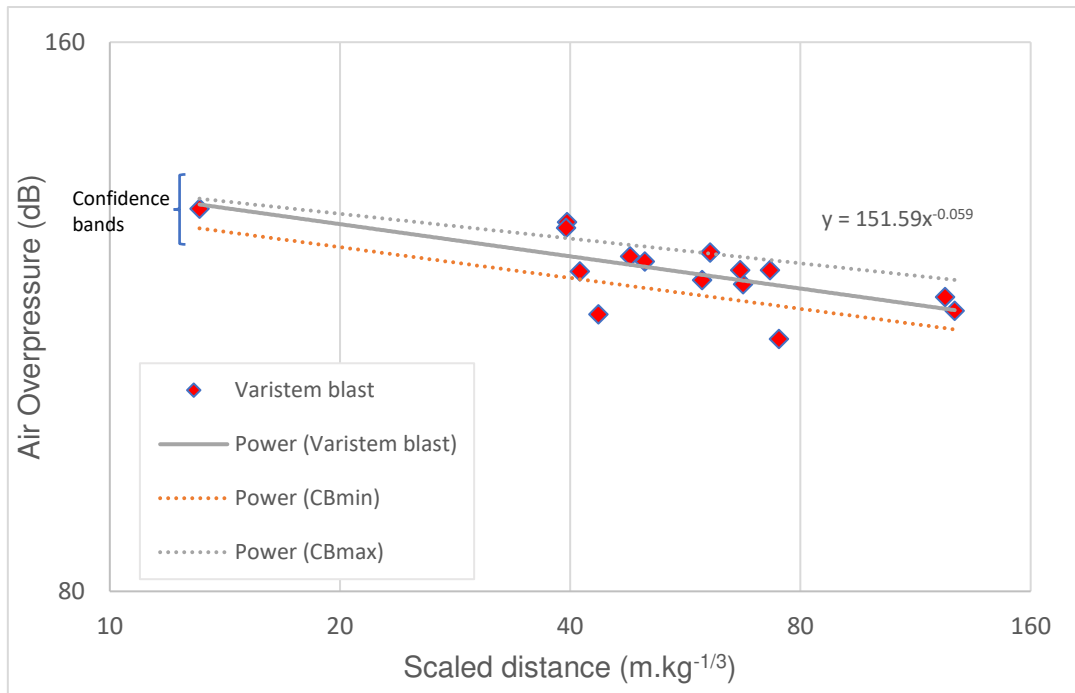


Figure 5.5: Confidence band at 95% significance level for the Varistem® blast at Station B

As illustrated in Figure 5.5 above, the line of best fit for the Varistem® blasts ($y = 151.59 x^{-0.059}$) does indeed lie within the 95% confidence band. The same 95% confidence bands were also constructed for the standard blasts as illustrated in Figure 5.6 below.

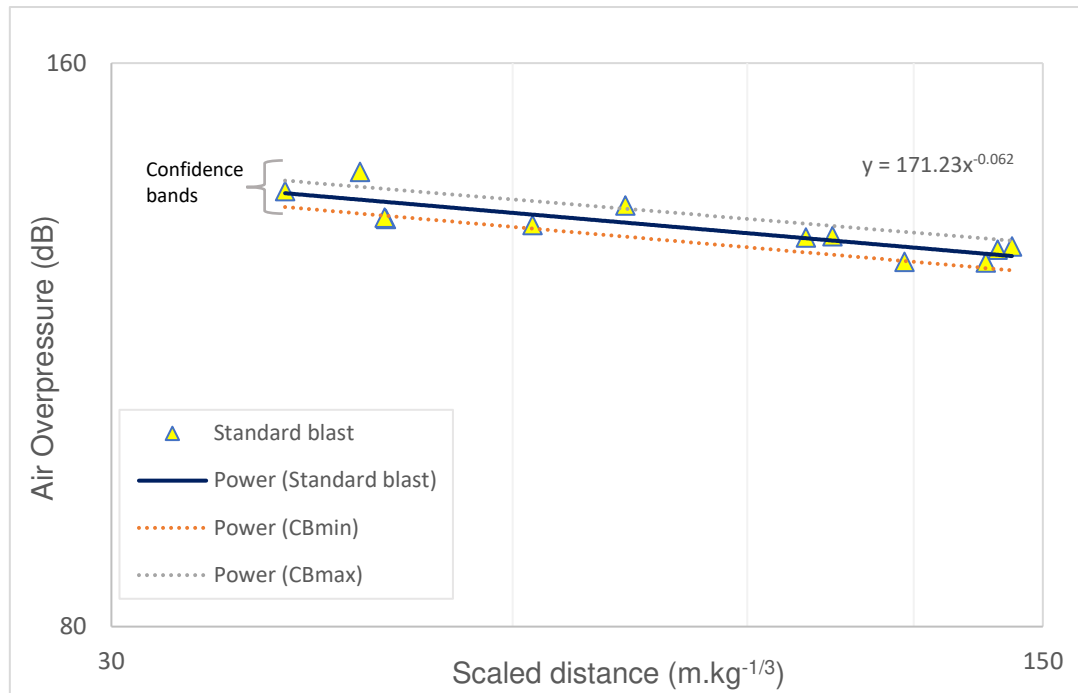


Figure 5.6: Confidence bands at 95% significance level for the standard blasts at Station B

A similar observation can be made for the line of best fit for the standard blast ($y = 171.23 x^{-0.062}$) which is within the constructed 95% confidence bands (see Figure 5.6). For a better comparison analysis between the two data sets, Figures 5.5 and 5.6 were plotted on the same set of axes to produce Figure 5.7.

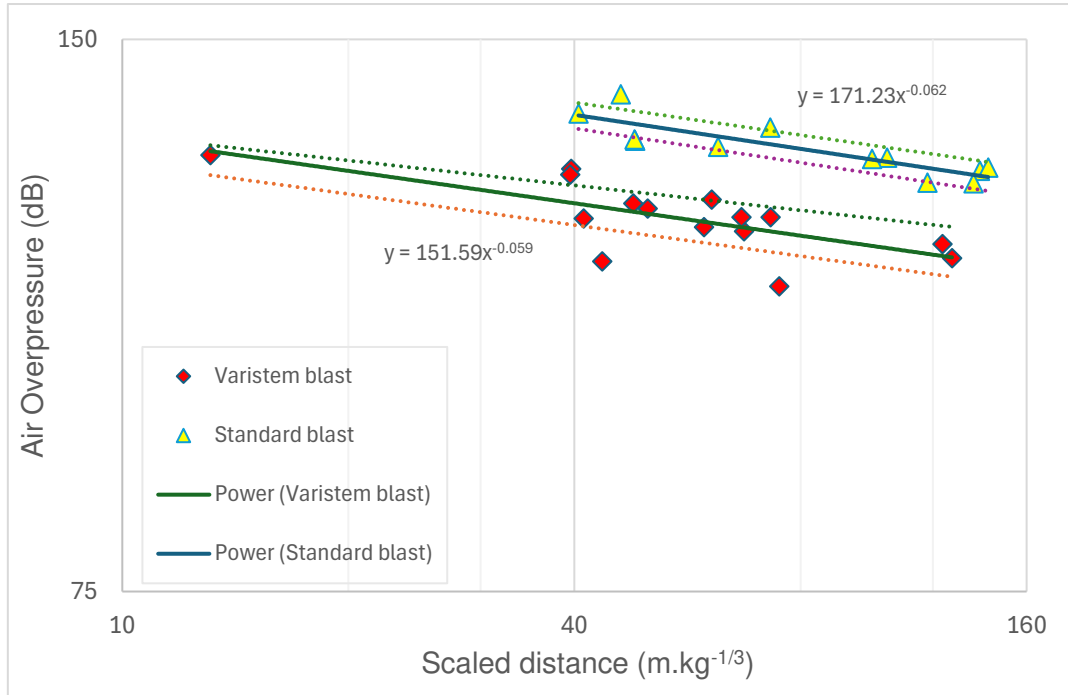


Figure 5.7: Confidence bands at 95% significance level for Station B

At monitoring Station B (as illustrated in Figure 5.7), the lines of best fit for the data sets seem parallel suggesting a similarity in slope. However, a further analysis shows that the slopes of the two data sets were slightly different. The Varistem® blasts had a slope of -0.059 while the standard blasts had a slope of -0.062. This shows a slope variability of 0.003.

Finally, the Student's t-test around Station B generated a p-value at 95% confidence level of $p = 0.00000619$ which is lower than the threshold or critical p-value set at $p_{crit} = 0.05$. This further supports the observations made at this station about the variability in the data sets.

5.4 Linking air blast reduction to blast energy confinement

The aim of calculating the scaled depth of burial (SDoB) in Table 4.3 was to measure the amount of energy confinement afforded by the Varistem® plugs for each blast. However, it should be noted that this calculation was not performed for the 12 standard blasts due to lack of sufficient blast parameter data to carry out the tests. Using the blast design parameters provided in Table 3.2, the calculated scaled depth of burial for all 15 blasts were found to

be in the range between 1.13 and 1.37 $\text{m.kg}^{-1/3}$. According to the earlier illustration of Figure 2.19, and the calculated SDoB values, the measure of energy containment for all 15 blasts falls within the controlled energy range (SDoB = 0.92 to 1.40 $\text{m.kg}^{-1/3}$). This controlled energy range means that the blasts were able to yield (Chiappetta, 2010):

- Good fragmentation
- Maximum volume of broken rock in the collar zone
- Acceptable ground vibration and air blast
- Good heave and muckpile mound.

Subsequently, when looking at the air blast levels recorded for the Varistem® trials and the discussions covered in the previous sections for the two stations, it is evident that most of the recorded AOp levels were within acceptable regulatory limits.

It should be noted that Quarry TM does consider the scaled depth of burial during planning of the blast design process to aid in mitigating potential environmental impacts. ERG Industrial (2023) also found that using the scaled depth of burial to optimize blast design parameters can help mining operations to obtain the desired production outcomes while reducing environmental impacts. Tobin (2013) also conducted a similar study to measure blast energy confinement while incorporating the Varistem® plugs into the blast design. He found that the plugs significantly increased explosive energy retention compared to cases where blast holes were normally stemmed as the SDoB values were within the “controlled energy” range. In essence, deeper burial depths are directly associated with higher SDoB values which result in controlled blast energy and minimal surface activity. Moreover, considering the SDoB during blast design can also aid in understanding the ratio of stemming to explosives and how it influences the measure of blast energy confinement for better blast outcomes.

5.5 Air overpressure as a function of scaled distance

In this section, the USBM modelling scheme discussed earlier in Section 4.3 is used in an attempt to better understand how AOp varies with scaled distances as a result of blasting.

First, let us discuss the results obtained when applying the air blast model at Station A. To successfully apply the model, the USBM predictor formula required the determination of site-specific constants (i.e., H and β) for Quarry TM. This was done by performing curve fitting on all the data sets recorded at the station and thus translating the USBM predictor equation into a power function as illustrated in Figures 4.7 and 4.8. The resultant site constants for the Varistem® blasts at monitoring Station A were found to be $H = 295.3$ and $\beta = 0.235$. On the other hand, the site constants for the standard blasts were $H = 196.6$ and $\beta = 0.091$.

In essence, the Varistem® blasts produced a USBM empirical formula of $AOp = 295.3 (d_s)^{-0.235}$. In comparison, the standard blasts produced an empirical formula of $AOp = 196.6 (d_s)^{-0.091}$. These two empirical equations were generated by means of curve fitting. As such, the variability of these empirical equations was deduced for Station A. This was done by looking at performance indices such as the coefficient of determination (R^2) and root mean squared error (RMSE) as given in Table 4.4. The curve fit for the Varistem® blasts produced an R^2 of 0.8649 and a RMSE of 6.0671. The standard blasts, on the other hand, produced an R^2 of 0.7636 with an RMSE of 3.0853. Ideally, an $R^2 = 1$ would mean that the fitted model can account for all AOp data collected at Quarry TM, i.e., 100%. However, imperfections and irregularities inherent to the testing conditions and the site produced R^2 values below 100%. And for the errors, RMSE of 6.0671 and 3.0353 indicate that there are level of deviations to be expected when using the USBM model produced as part of this study for future predictions of air blast at Quarry TM.

Additionally, as highlighted in Figures 4.7 and 4.8, a USBM predictor equation for quarry blasts was introduced on the graph plots for comparative purposes. This specific predictor equation, $AOp = 622 (d_s)^{-0.515}$, was

adopted from the literature presented in Chapter 2. The resultant RMSE for the Varistem® blasts was found to be 30.3720 when that for the standard blasts was 55.8233. The values of RMSE of 30.3720 and 55.8233 indicate that the USBM predictor model is not a better model fit on the data set at this station since it did not produce a good prediction of air blast. This can be attributed to the different blast design parameters involved in the generation of this site specific USMB predictor model. The geological setting of the rock being blasted could have also influenced the outcome of the results.

Similarly, the USBM predictor model was applied on the recorded data at Station B. The site constants for the Varistem® blasts derived from Station B were $H = 151.61$ and $\beta = 0.059$ as illustrated on the power function in Figure 4.9. On the other hand, the standard blasts produced the following site constants; $H = 168.31$ and $\beta = 0.056$ as illustrated in Figure 4.10.

The resultant USBM predictor equations for Station B were $AOp = 151.61 (d_s)^{-0.059}$ for the Varistem® blasts and $AOp = 168.31 (d_s)^{-0.056}$ for the standard blasts. Here as well, the curve fitting of the USBM model to the Varistem® blast data produced an R^2 of 0.8070 and a RMSE of 3.663068. The standard blasts produced an R^2 of 0.6303 with a RMSE of 4.841641 as illustrated in Table 4.5.

According to Turney (2022), a coefficient of determination (R^2) of between 0 and 1 means a model partially predicts an outcome. However, an R^2 of 1 means the model perfectly predicts the outcome. This is supported by a study by Alaba et al. (2023) where it was stated that “a model is considered a good fit if its coefficient of determination is equal to one and a Root Mean Squared Error equal to zero”. In essence, the USBM predictor model produced a good R^2 at both monitoring stations. However, in terms of RMSE values, one would say that the USBM model performed better suggesting the possibility of better predictions farther from the production blast. However, additional test work is needed to confirm this assertion.

Furthermore, a USBM predictor equation for quarry blasts was introduced in Figures 4.9 and 4.10. For Station B, this predictor equation was found to be

$AOp = 622 (d_s)^{-0.515}$. It should be also noted that the resultant RMSE for the Varistem® blasts was 43.74055 while that of the standard blasts was 65.82015. These RMSE values indicate that the selected USBM predictor model is not a better model fit on the data set at this station in view of the high variability expected in the prediction of air blast. Similar to Station A, this outcome can be attributed to the different blast design parameters involved in the generation of this site specific USMB predictor model. The geological setting of the rock being blasted could have also influenced the outcome of the results. Further research is required to elucidate this.

Alaba et al. (2023) also conducted a similar study where the USBM predictor model was applied to predict AOp levels for their study. The site constants for their study according to the USBM predictor were $H = 141.48$ and $\beta = 0.0568$ respectively. The coefficient of determination of the model was found to be $R^2 = 0.9913$ and the RMSE was 0.2729. Furthermore, their study also found that the USBM predictor model was the best performing model when compared to other predictor models which had a slight deviation according to the performance indices.

Kuzu et al. (2009) also adopted the USBM predictor model on their study to predict air overpressure in the absence of monitoring. The resultant empirical predictor equations were $AOp = 261.54 (d_s)^{-0.706}$ for the competent zone blasts and $AOp = 1833.8 (d_s)^{-0.981}$ for blasts conducted in the weak zone. The errors levels were less than 7% when compared with the recorded air overpressure levels.

The abovementioned studies by Kuzu et al. (2009) and Alaba et al. (2023) also highlight the effect of site-specific factors and their performance on each mine or study area.

According to Khandelwal and Singh (2005), the generation of blast-induced air overpressure is directly influenced by the explosive charge weight per delay. This is evident from Table 4.1 (see Chapter 4) where the air overpressure generated shows to grow with an increase in explosive charge weight. Furthermore, the monitoring distance from the blast also influenced

air blast as depicted in Table 4.2. According to Faramarzi et al. (2014), air blast level does indeed decrease with distance away from the blast site.

According to Rehman et al. (2021), stemming blowouts during blast hole blasting result in excessive vibration and loss of gas confinement. In this study, blast-hole stemming blowouts were observed mostly for the standard blast. Additionally, in some other cases where observed air blast levels are higher, this can be attributed to water seepage within the blocks. There was a serious instance of water seepage present within the blocks to be blasted at the quarry, and loose material was eroded by this water. Water seepage can also affect how air blasts are generated since it can change the physical characteristics of the rock, thereby increasing environmental and safety concerns (Jang et al., 2018).

5.6 Testing the contribution of stemming plugs to air blast

As highlighted in Section 4.4, a statistical ANOVA test was performed for both stations. This focused on comparing the Varistem® blasts against the standard blasts. The purpose of the statistical analysis was to determine whether the mean air blast levels produced between the two groups of blasts would be the same or different for all 27 blasts. The significance level (α) was set at the commonly used 0.05 for the statistical test.

For monitoring Station A, the mean air blast levels for the Varistem® blasts and the standard blasts were found to be 125.21 and 136.92 respectively. And for Station B, the mean air blast levels were 119.97 for the Varistem® blasts and 130.86 for the standard blasts. The ANOVA around monitoring Station A generated a p-value at 95% confidence level of $p = 0.013$ which is lower than the threshold or critical p-value $p_{crit} = 0.05$. Similarly, Station B gave a p-value of 0.000008 at 95% confidence also lower than $p_{crit} = 0.05$.

In essence, a p-value of less than 0.05 is regarded as statistically significant in practice, meaning that it provides strong evidence opposing the null hypothesis. This suggests that the null hypothesis has a lower than 5%

chance of being true, hence supporting the idea that the observed results of the two data sets are different. As such, the null hypothesis was rejected, and the alternative hypothesis accepted based on the strength of evidence provided by the data analysis. From these observations, the ANOVA confirms that the stemming plugs contribute to reducing air blast at a 95% confidence level. Simply put, this means that the Varistem® plugs are playing a major role in controlling air blast.

5.7 Summary of findings

There is a notable difference between the air blast levels produced by the Varistem® blasts and the standard blasts for the two stations. Incorporating the Varistem® stemming plugs into the blast design seems to produce better blast outcome. This is evident in Figures 4.3 and 4.6 for the two stations respectively where the Varistem® blasts produced data points which were closer to or less than the 134-dB USBM regulatory limit. Generally, most of the air overpressure data for the Varistem® blasts were below the USBM limits. The USBM model was deemed to be a good predictor for desktop studies and might assist the quarry at forecasting air blast levels if adopted.

Finally, the outcome of the hypothesis test (ANOVA) was that the difference between Varistem® and standard blasts is statistically significant for both stations considered. This simply means that assumption of null hypothesis, i.e., similarity between the two sets of blast trials, may not be supported by empirical evidence. In other words, the observations made from this chapter show that the two groups of blasts are statistically different at 95% confidence level. One is therefore in a position to say that the Varistem® plugs are indeed contributing towards reducing air blast.

Chapter 6 Conclusion and recommendations

6.1 Introduction

The main objective of this study was to assess the application of Varistem® stemming plugs on blast induced air blast in surface mines. This was done in comparison to a standard blast stemming method. Varistem® stemming plugs were incorporated into the blast design to improve blast performance and thereby reduce air blast generation. The size of plugs used for this study were 102 mm. A total of 27 blasts were organised and carried-out for this study: 15 included Varistem® plugs and 12 used standard aggregate stemming only. These blasts were monitored in a near field at two locations termed Station A and Station B in this study. The monitoring distances varied between 100 to 700 m away from the blasts. At each station, a mobile Nomis blasting seismograph station was set up to monitor and record air blast levels during each blast. The effect of blast parameters such as the distance from the blast to the monitoring station and the explosive charge weight were studied and used as input parameters to calculate for the scaled distances. Air blast safety limits at the quarry were guided by the USBM regulatory standards. The amount of blast energy confinement offered by the Varistem® plugs were also studied by calculating the scaled depth of burial for each blast. Two air blast prediction models were also tested to find a model which would best predict the air blast levels at Quarry TM in the absence of monitoring.

6.2 Varistem® stemming plugs on air blast reduction

The Varistem® stemming plugs were found to have reduced air blast sample mean by 9.35% at Station A when compared with the standard blasts. However, the Varistem® plugs reduced air blast by 9.08% around Station B. A further analysis of the results captured at Station A showed that 5 out of the 15 blasts tested using the Varistem® plugs were above the regulatory air

blast limit of 134 dB as set by the United States Bureau of Mines (USBM). This means 33% of the recorded Varistem® blasts were above limit. When compared with the standard blasts at the same station, it was found that 67% of the recorded air blast levels for the standard blasts were above limit. In addition to this, the air blast levels recorded at Station B showed that all the Varistem® data points were below 134 dB. This means, low levels of noise and irritation were produced by the Varistem® blasts at this station. On the other hand, 25% of the recorded standard blasts were found to lie above the 134-dB threshold. According to USBM guidelines, air overpressure levels above 134 dB may cause damage to nearby infrastructures. Therefore, a notable improvement in using the Varistem® plugs was evident at Station B where all the recorded blasts were within acceptable regulatory limits. Furthermore, this study highlighted the fact that air blast decreases with an increase in monitoring distance. It was determined that the air overpressure recorded at Station B, which was the farthest away, was not greater than that measured near the source, i.e., around Station B.

In terms of energy containment, calculations showed the corresponding scaled depths of burial ranged between 1.13 to 1.37 $\text{m.kg}^{-1/3}$ for all 15 Varistem® blasts. This range of calculated values confirmed that Varistem® blasts produced controlled energy as it fell between 0.92 to 1.40 $\text{m.kg}^{-1/3}$. This controlled energy range means that the blasts were able to yield good fragmentation, high rock fracturing in collar zone, adequate air blast and ground vibration, as well as excellent heave and muck pile mound.

The AOp levels predicted for the Varistem® blast at Station A using the USBM model produced an R^2 of 0.8649 and a RMSE of 6.067144. The standard blasts, on the other hand, produced an R^2 of 0.7636 with an RMSE of 3.085334. And at Station B, the predicted AOp levels for the Varistem® blasts produced an R^2 of 0.8070 and a RMSE of 3.663068. As for the standard blasts, R^2 and RMSE were found to be 0.6303 and 4.841641 respectively.

In terms of the Mckenzie's model, the following was obtained at Station A for the Varistem® blasts: $R^2 = 0.9996$ and RMSE = 9.9196. In comparison, the standard blasts produced an R^2 of 0.9996 and an RMSE of 13.599. When looking at the predicted air overpressure levels at Station B, Mckenzie's model produced an R^2 of 0.9986 and an RMSE of 5.2067 for the Varistem® blasts. With the standard blasts, the model was able to produce an R^2 of 0.9986 and an RMSE of 13.3785.

In essence, the results observed from this study shows that the USBM model is a better model fit at Quarry TM than Mckenzie's model. The study also further confirmed that the stemming plugs are contributing to reducing air blast at a 95% confidence level. In simple terms, this means that the Varistem® plugs are playing a major role in controlling air blast at Quarry TM.

6.3 Recommendations for future work

The current study has addressed the potential use of the Varistem® plug as a stemming accessory to aid in blast performance improvement. Considering this, further areas of research work can be done which would provide key information to the engineering body of knowledge. These include the below amongst others:

- It is recommended that an experimental study be conducted where both sets of blasts are carried out concurrently instead of relying on historical data. This will provide a clear comparison study since the tests will be carried out under the same conditions.
- The study also recommends that the USBM predictor should further scrutinise to include the effects of the geological setting of the site so that the refined model is used for prediction of air blast at Quarry TM.
- It would finally be beneficial to carry advanced research work on other predictor models that were not considered in this study.

References

Alaba, O.C., Opafunso, Z.O., Nyanney, E., 2023. Prediction of airblast levels at Anglogold Iduapriem mine using empirical models. *Noise and Vibration Worldwide*, no. 54, no. 1, pp. 24 – 30

Anders, G., Borges, I., 2011. Topological analysis of the molecular charge density and impact sensitivity models of energetic molecules. *Journal of Physical Chemistry A*, vol. 115, no. 32, pp. 9055 – 9068

Balamadeswaran, P., Mishra, A.K., Sen, P., Ramesh, S., 2018. Investigations into the influence of decking on rock fragmentation and ground vibrations by blasting in shallow benches of limestone quarries – A case study. *Journal of Mines, Metals and Fuels*, pp. 39 – 47

Bansah, K.J., Arko-Gyimah, K., Kansake, B.A., Dumakor-Dupey, N.K., 2016. Mitigating blast vibration impact. *UMat Biennial International Mining and Mineral Conference*, vol. 4, pp. 30 – 36

Better Blasting, 2021. Measuring tapes – Better blasting. [online] Available at: <https://betterblasting.ca/products/measuring-tapes/> [Accessed on 01 November 2024]

Bilim, N., Çelik, A., Kekeç, B., 2020. Assessment of the effect of blasthole design parameters on total cost in quarries. *Arabian Journal of Geosciences*, vol. 13, no. 21, p. 1168

Bruce, P.J., 2017. Improved stemming plugs. Australian Patent, AU2016905045A0, Nov. 20, 2017

Bullard, J.E., Wiggs, G.F.S., Nash, D.J., 2000. Experimental study of wind directional variability in the vicinity of a model valley. *Geomorphology*, vol. 35, no. 1 – 2, pp. 127 – 143

Cevizci, H., 2012. A newly developed plaster stemming method for blasting. Journal of the Southern African Institute of Mining and Metallurgy, vol. 112, no. 12, pp. 1071 – 1078

Cevizci, H., 2013. A new stemming application for blasting: A case study. REM-International Engineering Journal, vol. 66, no. 4, pp. 513 – 519

Cevizci, H., 2014. Fragmentation, cost and environmental effects of plaster stemming method for blasting at a basalt quarry. Archives of Mining Sciences, vol. 59, no. 3, pp. 835 – 846

Cevizci, H., 2019. Comparison of the efficiency of plaster stemming and drill cuttings stemming by numerical simulation. Journal of the Southern African Institute of Mining and Metallurgy, vol. 119, no. 5, pp. 465 – 470

Chiappetta, R.F., 2010. Combining electronic detonators with stem charges and air decks. Blasting Analysis International, Inc., Allentown, Pennsylvania, U.S.A., pp. 1 – 79

Choudhary, B.S., Agrawal, A. and Arora, R., 2021. Stemming material and Inter-row delay timing effect on blast results in limestone mines. Indian Academy of Sciences, *Sādhana*, vol. 46, no. 1, pp. 1-12

Chung, S.H., Mustoe, G.G.W., 2002. Effects of particle shape and size distribution on stemming performance in blasting. In Discrete Element Methods: Numerical Modelling of Discontinua, American Society of Civil Engineers, pp. 288 – 293

Docrat, M., 2023. Personal communication. Quarry TM, South Africa

ERG Industrial, 2021. Varistem® trial blast: Afrisam Rooikraal Quarry. Brakpan, Gauteng

ERG Industrial, 2023. Varistem – Blasting hole plugs. [online] Available at: <https://ergindustrial.com/varistem/> [Accessed 6 June 2024]

ERG Industrial, 2023. Scaled depth of burial explained. [online] Available at: <https://ergindustrial.com/scaled-depth-of-burial-explained/> [Accessed 01 July 2024]

Faramarzi, F., Ebrahimi Farsangi, M.A., Mansouri, H., 2014. Simultaneous investigation of blast induced ground vibration and airblast effects on safety level of structures and human in surface blasting. *International Journal of Mining Science and Technology*, vol. 24, no. 5, pp. 663 – 669

Fei, J., Wu, Ruiling, W., Xuemei, W., Tao, Z., 2020. Emulsion explosive and production process thereof. Chinese Patent, CN102173967B, Sep. 19, 2019

Fişne, A., Kuzu, C., Hüdaverdi, T., 2010. Prediction of environmental impacts of quarry blasting operation using fuzzy logic. *Environmental Monitoring and Assessment*, vol. 174, no. 1 – 4, pp. 461 – 470

Fomina, N., Polyanskiy, M., 2019. Grain size distribution of aggregates of crushed concrete. In *E3S Web of Conferences*, vol. 97, p. 02018

Ghosh, S., Behera, C., Mishra, M.K., 2024. Prediction of blast-induced ground vibration using multivariate statistical analysis in the opencast chromite mines of the Indian State of Odisha. *Sadhana*, vol. 49, no. 2, pp. 1 – 14

Gomes-Sebastiao, G.L., De Graaf, W.W., 2017. An investigation into the fragmentation of blasted rock at Gomes Sand. *Journal of the Southern African Institute of Mining and Metallurgy*, vol. 117, no. 4, pp. 321 – 328

Goncalves, C.G., Tose, S.J., 2009. Shaft sinking with electronic detonators at the Gautrain Rapid Rail project. In: *Shaft Sinking and Mining Contractors Conference*. The Southern African Institute of Mining and Metallurgy, pp. 1 – 10

Gou, Y., Shi, X., Zhou, J., Qiu, X., Chen, X., Huo, X., 2020. Attenuation assessment of blast-induced vibrations derived from an underground mine.

International Journal of Rock Mechanics and Mining Sciences, vol. 127, p. 104220

Griffiths, M.J., Oates, J.A.H., Lord, P., 1978. The propagation of sound from quarry blasting. *Journal of Sound and Vibration*, vol. 60, no. 3, pp. 359 – 370

Hajihassani, M., Armaghani, D.J., Sohaei, H., Mohamad, E.T., Marto, A., 2014. Prediction of airblast-overpressure induced by blasting using a hybrid artificial neural network and particle swarm optimization. *Applied Acoustics*, vol. 80, pp. 57 – 67

Hannah, L., 2007. Wind and temperature effects on sound propagation. *New Zealand Acoustics*, vol. 20, no. 2, pp. 22 – 29

Hidayat, S., 2021. Environmental impacts of open pit mining blasting: Particular discussions on some specific issues. *Journal of Mining and Environmental Technology*, vol. 1, no. 1, pp. 1 – 11

Himanshu, V.K., Mishra, A.K., Roy, M.P., Singh, P.K., 2023. Rock-explosive interaction during underground blasting. In *Blasting Technology for Underground Hard Rock Mining*, pp. 25 – 48, Springer Nature Singapore

He, M., Hu, Y., Chen, J., Zhang, J., Li, H., Cai, C., 2022. Numerical simulation study on parameter optimization of time sequential controlled blasting. *Shock and Vibration*, pp. 1 – 12

Hosseini, M., Khandelwal, M., Lotfi, R., Eslahi, M., 2023. Sensitivity analysis on blast design parameters to improve bench blasting outcomes using the Taguchi method. *Geomechanics and Geophysics for Geo-Energy and Geo-Resources*, vol. 9, no. 1, p. 9

Hustrulid, W., 1999. *Blasting principles for open pit mining – General design concepts*. vol. 1, Balkema, Rotterdam

Huynh, M.P., Laefer, D.F., McGuill, J., White, A., 2017. Temperature-related performance factors for chemical demolition agents. *International Journal of Masonry Research and Innovation*, vol. 2, no. 2/3, pp. 220 – 240

International Society of Explosives Engineers, 1998. *Blasters' handbook*. 17th Edition, International Society of Explosives Engineers, Cleveland, Ohio, p. 626

Jaroonpattanapong, P., Indarid, O., Van Hoa, P., 2018. Application of wavefront reinforcement model for reduction blast-induced ground vibration. *Songklanakarin Journal of Science and Technology*, vol. 40, no. 2. pp. 424 – 429

Jaroonpattanapong, P., Tachom, K., 2021. Monitoring and control airblast overpressures in an open pit coal mine. *Physics and Chemistry of the Earth, Parts A/B/C*, vol. 121, pp.1 – 8

Jhanwar, J.C., 2011. Theory and practice of air-deck blasting in mines and surface excavations: A review. *Geotechnical and Geological Engineering*, vol. 29, no. 5, pp. 651 – 663

Kabwe, E., Wang, Y., 2016. Airblast and ground vibration monitoring at Chimiwungo Pit. *Geomaterials*, vol. 6, no. 1, pp. 28 – 38

Kabwe, E., 2017. Improving collar zone fragmentation by top air-deck blasting technique. *Geotechnical and Geological Engineering*, vol. 35, no. 1, pp. 157 – 167

Khandelwal, M., Kankar, P.K., 2009. Prediction of blast-induced air overpressure using support vector machine. *Arabian Journal of Geosciences*, vol. 4, no. 3 – 4, pp. 427 – 433

Khandelwal, M., Singh, T.N., 2005. Prediction of blast induced air overpressure in opencast mine. *Noise and Vibration Worldwide*, vol. 36, no. 2, pp. 7 – 16

Khemlani, S., Trafton, J.G., 2014. Percentile analysis for goodness-of-fit comparisons of models to data. Proceedings of the Annual Meeting of the Cognitive Science Society, vol. 36, no. 36, pp. 737 – 742

Kojovic, T., 2005. Influence of aggregate stemming in blasting on the SAG mill performance. Minerals Engineering, vol. 18, no. 15, pp. 1398 – 1404

Konya, C.J., Konya, A., 2018. Effect of hole stemming practices on energy efficiency of comminution. Energy Efficiency in the Minerals Industry: Best Practices and Research Directions, pp. 31 – 53

Konya, A., Konya, C.J., 2018. Blasting practices to control quarry floors and correct toes. [online] Agg-net. Available at: <https://www.agg-net.com/resources/articles/drilling-blasting/blasting-practices-to-control-quarry-floors-and-correct-toes> [Accessed on 19 August 2023]

Konya, A., Konya, C.J., 2020. Blast performance based on violence. [online] Pit and Quarry. Available at: <https://www.pitandquarry.com/blast-performance-based-on-violence/> [Accessed on 19 August 2023]

Kuzu, C., Fisne, A., Ercelebi, S.G., 2009. Operational and geological parameters in the assessing blast induced airblast-overpressure in quarries. Applied Acoustics, vol. 70, no. 3, pp. 404 – 411

Legesse, A.N., Saha, A.K. and Carpanen, R.P., 2017. Characterisation of wind speed series and power in Durban. *Journal of Energy in Southern Africa*, vol. 28, no.3, pp.66-78.

Lopes, G.S., Vinueza, G., Trzaskos, B., Ribeiro, A.F., Araujo, R.G., 2022. Correlating blast vibrations and geomechanical properties to determine damage profiles and improve wall conditions in open pit mining. *Anais Da Academia Brasileira De Ciencias*, vol. 94, no. 4, p. e20211080

Marchenko, L.N., 1982. Raising the efficiency of a blast in rock crushing. Soviet Mining Science, vol. 18, no. 5, pp. 395 – 399

Marín, J.A., Rodríguez, R., Díaz, M.B., Antón, S., 2022. Empirical attenuation law for air blast waves due to the detonation of explosives outdoors. *Applied Sciences*, vol. 12, no. 18, p. 9139

Marto, A., Hajihassani, M., Armaghani, D.A., Mohamad, E.T., Makhtar, A.M., 2014. A novel approach for blast-induced flyrock prediction based on imperialist competitive algorithm and artificial neural network. *The Scientific World Journal*, pp. 1 – 11

Mckenzie, C., 1990. Quarry blast monitoring: Technical and environmental perspective. *Quarry Manage*, vol. 17, pp. 23 – 29

Mckenzie, J., Fowkes, N., Mckensie, J., Carvalho, C., Thomson, S., Mason, D., Hutchinson, A., Stacey, R., n.d. Predicting and mitigating the effects of air blasts in mines. Study Group Participants Industry Representatives. [online] Available at: <https://www.wits.ac.za/media/migration/files/cs-38933-fix/migrated-pdf/pdfs-2/Predicting.pdf> [Accessed on 22 July 2024]

Mel'nikov, N.V., Marchenko, L.N., Zharikov, I.F., Seinov, N.P., 1979. A method of enhanced rock breaking by blasting. *Soviet Mining Science*, vol. 15, no. 6, pp. 565 – 572

Miller, J.T., Brown, R.B., 1999. Blasting stemming plug. [online] Available at: <https://patentimages.storage.googleapis.com/d6/cc/1a/1212def4c7c945/US5936187.pdf> [Accessed on 26 March 2024]

Mishra, R., Mishra, A.K., Choudhary, B.S., 2023. High-speed motion analysis-based machine learning models for prediction and simulation of flyrock in surface mines. *Applied Sciences*, vol. 13, no. 17, p. 9906

Mishra, A.K., Rout, M., Singh, D.R., Jana, S.P., 2017. Influence of gassing agent and density on detonation velocity of bulk emulsion explosives. *Geotechnical and Geological Engineering*, vol. 36, no. 1, pp. 89 – 94

Mpofu, M., Ngobese, S., Maphalala, B., Roberts, D., Khan, S., 2021. The influence of stemming practice on ground vibration and air blast. *Journal of*

the Southern African Institute of Mining and Metallurgy, vol. 121, no. 1, pp. 1 – 10

Monjezi, M., Amiri, H., Mousavi, M.N.S., Hamidi, J.K., Khandelwal, M., 2022. Comparison and application of top and bottom air decks to improve blasting operations. AIMS Geosciences, vol. 9, no. 1, pp. 16 – 33

Neale, A.M., 2010. Blast optimization at Kriel Colliery. Journal of the Southern African Institute of Mining and Metallurgy, vol. 110, no. 4, pp. 161 – 168

Nicholls, A., 2014. Confidence limits, error bars and method comparison in molecular modeling. Part 1: The calculation of confidence intervals. Journal of Computer-Aided Molecular Design, vol. 28, no. 9, pp. 887 – 918

Oates, T.E., Spiteri, W., 2021. Stemming and best practice in the mining industry: A literature review. Journal of the Southern African Institute of Mining and Metallurgy, vol. 121, no. 8, pp. 1 – 11

O'Brien, S.F., Yi, Q.L., 2016. How do I interpret a confidence interval? Transfusion, [online] vol. 56, no. 7, pp. 1680 – 1683

Orica., n.d. Blasting principles. [online] Available at: <https://www.orica.com/products-services/resources/blasting-principles> [Accessed on 13 November 2023]

Ozer, U., Karadogan, A., Ozyurt, M.C., Sertabipoglu, Z., Sahinoglu, U.K., 2020. Modelling of blasting-induced air overpressure wave propagation under atmospheric conditions by using ANN model. Arabian Journal of Geosciences, vol. 13, no. 16, pp. 1 – 11.

Patidar, P., 2017. Role of stemming in open cast mine. [Online] Available at: <https://www.slideshare.net/pankajpatidar15/role-of-stemming-in-open-cast-mine> [Accessed on 15 July 2024]

Persson, P.-A., Holmberg, R., Lee, J., 1993. Rock blasting and explosives engineering. CRC Press, Boca Raton, Florida, USA

Preskitt, S.V., Cornelius, L.R., 1979. Seismic triggered seismograph. Journal of the Acoustical Society of America, vol. 69, no. 5, p. 1536

Pyra, J., Kłaczyński, M., 2019. Vibroacoustic measurements and analysis of blasting works. Journal of Vibroengineering, vol. 21, no. 2, pp. 526 – 537

Raines, E., Doup, B., 2023. An alternative methodology addressing United Nations classification type for self-reactive substances. Process Safety Progress, vol. 42, no. 1, pp. 12 – 20

Ratcliff, J., Sheehan, E., Carte, K., 2011. Predictability of airblast at surface coal mines in West Virginia. Technical Report, West Virginia Department of Environmental Protection, Office of Explosives and Blasting, USA

Reed, J.W., 1972. Airblast overpressure decay at long ranges. Journal of Geophysical Research, vol. 77, no. 9, pp. 1623 – 1629

Rehman, A.U., Emad, M.Z., Khan, M.U., 2021. Improving the environmental and economic aspects of blasting in surface mining by using stemming plugs. Journal of the Southern African Institute of Mining and Metallurgy, vol. 121, no. 7, pp. 369 – 377

Richards, A.B., 2013. Predictive modelling of airblast overpressure. Mining Technology, vol. 122, no. 4, pp. 215–220.

Rodríguez, R., Toraño, J., Menéndez, M., 2007. Prediction of the airblast wave effects near a tunnel advanced by drilling and blasting. Tunnelling and Underground Space Technology, vol. 22, no. 3, pp. 241 – 251

Roy, S., Adhikari, G.R., Renaldy, T.A., Singh, T.N., 2011. Assessment of atmospheric and meteorological parameters for control of blasting dust at an Indian large surface coal mine. Research Journal of Environmental and Earth Sciences, vol. 3, no. 3, pp. 234-248.

Saharan, M.R., Sazid, M., Singh, T.N., 2017. Explosive energy utilization enhancement with air-decking and stemming plug, 'SPARSH'. *Procedia Engineering*, vol. 191, pp. 1211–1217.

Sapra, R.L., 2014. Using R^2 with caution. *Current Medicine Research and Practice*, vol. 4, no. 3, pp. 130 – 134

Sazid, M., 2014. Investigating the role of effective stemming in engineering blasting operations for open-pit mines. Doctoral Dissertation, Indian Institute of Technology Bombay

Segarra, P., Domingo, J.F., López, L.M., Sanchidrián, J.A., Ortega, M.F., 2010. Prediction of near field overpressure from quarry blasting. *Applied Acoustics*, vol. 71, no. 12, pp. 1169 – 1176

Şengün, B., Gül, Y., 2023. Evaluation of ground vibration and air blast measurements induced by blasting in a quarry mine. *Journal of Scientific Reports-A*: no. 053, pp. 131 – 146

Sharma, S.K., Rai, P., 2015. Investigation of crushed aggregate as stemming material in bench blasting: A case study. *Geotechnical and Geological Engineering*, vol. 33, no. 6, pp. 1449 – 1463

Shoko, M., 2021. Varistem stemming plugs winning the day for mines in SA. *Modern Mining*, [online on 01 December 2024] vol. 17, no. 12, pp. 22 – 24. Available at: https://www.crown.co.za/images/magazines/modern-mining/2021/Modern_Mining_December_2021.pdf [Accessed on 06 October 2024].

Siamaki, A., 2022. Advanced analytics for drilling and blasting. In *Advanced Analytics in Mining Engineering*. [online] Springer, Cham, pp. 323 – 343

Silva, J., Worsey, T., Lusk, B., 2019. Practical assessment of rock damage due to blasting. *International Journal of Mining Science and Technology*, vol. 29, no. 3, pp. 379 – 385

Singh, P.K., Sirveiya, A.K., Babu, K.N., Roy, M.P., Singh, C.V., 2006. Evolution of effective charge weight per delay for prediction of ground vibrations generated from blasting in a limestone mine. *International Journal of Mining, Reclamation and Environment*, vol. 20, no. 1, pp. 4 – 19

Singh, P.K., Klemenz, M., Niemaan-Delius, C., 2005. Air overpressure. [Online] Available at: <https://www.agg-net.com/resources/articles/drilling-blasting/air-overpressure> [Accessed 04 October 2023].

Singh, M.M., Singh, R.B., Gupta, R.N., 1991. Blast design to improve fragmentation in a mismatched combination of drill diameter and depth in bedded rock. *Mining Science and Technology*, vol. 12, no. 2, pp. 179 – 186

Siskind, D.E., Stachura, V.J., Stagg, M.S., Kopp, J.W., 1980. Structure response and damage produced by airblast from surface mining. In *Bureau of Mines Report of Investigations 8485*, United States Bureau of Mines Washington DC, pp. 64 – 74

Szendrei, T., Tose, S., 2023. Flyrock in surface mining. Part II – Causes, sources, and mechanisms of rock projection. *Journal of the Southern African Institute of Mining and Metallurgy*, vol. 123, no. 12, pp. 557 – 564

Taylor, L.W., 1997. An R^2 criterion based on optimal predictors. *Econometric Reviews*, vol. 16, no. 1, pp. 109 – 118

Tobin, G., 2013. The importance of energy containment to the blast outcome and justification for use of stemming plugs in over burden removal. *ORESOME Products*, pp. 1 – 13

Tran, Q.H., Nguyen, H., Bui, X.N., Drebenstedt, C., Arnoldovich, B.V., Atrushkevish, V., Nguyen, V.D., 2021. Evaluating the effect of meteorological conditions on blast-induced air over-pressure in open pit coal mines. In *Proceedings of the International Conference on Innovations for Sustainable and Responsible Mining, ISRM 2020*, vol. 1, pp. 170 – 186. Springer International Publishing

Turney, S., 2022. Coefficient of determination (R^2) | Calculation & interpretation. [online] Scribbr. Available at: <https://www.scribbr.com/statistics/coefficient-of-determination/> [Accessed on 02 November 2024]

Varistem, 2023. Explore how Varistem® works. [online] Available at: <https://varistem.com/how-varistem-works/?srsltid=AfmBOopAe2cc-kMWgBCwjXDluaM1-JggKSa9 tx6Laco7B k5rhNln3v> [Accessed on 02 November 2024]

Verschuuren, G., 2014. Excel 2013 for scientists. Excel for Professional series, Revised & Expanded 3rd Edition, Holy Macro! Books, Ohio, USA

Vladimirovich, V.J., Evich, V.K.J., Fadeevich, M.A., 2014. Safety emulsion explosive composition for blasthole charges. Russian Patent, RU2526994C1, Aug. 27, 2014

Yang, D., Zhao, Y., Ning, Z., Lv, Z., Luo, H., 2018. Application and development of an environmentally friendly blast hole plug for underground coal mines. Shock and Vibration, vol. 2018, no. 1, pp. 1 – 12

Zhang, X.J., Wang, X.G., Yu, Y.L., 2018. The application of deck charge technology in Hua Neng open pit mine. E3S Web of Conferences, vol. 38, no. 2, p. 03031

Zheng, H.C., Song, C.Y., Hu, L., Xiao, G., Li, M., Zhang, X.J., 2010. Simulation of air shock waves induced by large-scale roof caving in huge mined-out area. Chinese Journal of Engineering. vol. 32, no. 3, pp. 277 – 281

Appendices

Annexure A

The links below contain the blast reports for all 27 blasts at Station A and Station B. These blast reports were generated and printed from the Nomis seismograph machines:

[Varistem Blasts \(1\)](#)

[Standard Blasts \(1\)](#)

Annexure B: USBM Model calculated data for Station A and Station B

Station A: Varistem (USBM Model)					Station A: Standard blast (USBM Model)				
Scaled distance	Measured AOp	Curve fit AOP	Error^2	USBM Model AOP	Scaled distance	Measured AOp	Curve fit AOP	Error^2	USBM Model AOP
97.71	103.50	102.30	1.436	60.69	45.40	135.40	138.70	10.889	87.18
47.30	128.90	119.49	88.491	85.36	84.80	130.00	130.99	0.996	63.19
31.40	134.80	131.55	10.574	105.41	91.50	128.00	130.09	4.370	60.77
34.76	119.10	128.45	87.385	100.03	61.20	135.10	134.96	0.019	74.75
28.10	133.80	135.02	1.488	111.61	51.50	136.70	137.11	0.168	81.70
27.05	132.70	136.23	12.472	113.82	77.60	131.60	132.07	0.216	66.15
40.00	124.50	123.57	0.869	91.88	45.10	137.80	138.78	0.968	87.48
97.80	88.00	100.77	163.079	58.72	25.60	143.10	146.16	9.362	117.10
21.30	141.30	144.09	7.770	128.73	45.03	145.30	138.80	42.201	87.55
47.70	123.30	119.26	16.344	84.99	30.70	142.60	143.75	1.327	106.64
33.60	125.00	129.47	20.024	101.79	47.12	144.80	138.23	43.177	85.52
60.20	116.00	112.92	9.485	75.39	69.90	132.60	133.33	0.538	69.80
35.00	135.00	128.24	45.686	99.68			SUM	114,231	
25.00	135.30	138.77	12.068	118.54			n	12	
35.00	136.90	128.24	74.981	99.68					
		SUM	552.153						
		n	15						

Station B: Varistem (USBM Model)					Station B: Standard blast (USBM Model)				
Scaled distance	Measured AOp	Curve fit AOP	Error^2	USBM Model AOP	Scaled distance	Measured AOp	Curve fit AOP	Error^2	USBM Model AOP
72.97	120.00	117.93	4.276	68.28	48.20	132.10	135.48	11.431	84.53
41.16	119.80	121.95	4.634	91.69	72.90	142.30	132.38	98.433	68.31
60.93	122.70	119.18	12.363	74.92	118.10	120.30	128.85	73.116	53.28
127.29	114.00	114.15	0.023	51.27	138.70	135.20	127.70	56.309	49.05
50.07	121.30	120.56	0.545	82.89	46.10	140.00	135.82	17.479	86.49
123.61	116.00	114.35	2.728	52.05	104.30	129.30	129.75	0.203	56.80
74.96	110.00	117.75	60.009	67.34	62.10	131.10	133.57	6.113	74.19
59.51	118.50	119.35	0.720	75.84	40.50	136.70	136.81	0.012	92.45
39.60	127.50	122.23	27.785	93.54	142.20	127.70	127.52	0.033	48.42
67.28	117.90	118.49	0.353	71.19	48.10	132.30	135.50	10.218	84.62
66.73	120.00	118.55	2.099	71.49	135.90	125.20	127.84	6.980	49.57
43.55	113.50	121.55	64.808	89.07	99.60	129.10	130.09	0.972	58.17
39.49	126.60	122.25	18.933	93.67			SUM	281.297	
13.10	129.70	130.41	0.500	165.34			n	12	
47.88	122.10	120.88	1.494	84.82					
		SUM	201.271						
		n	15						

Annexure C: 95% Confidence band calculations at both stations

Station A: Varistem blast			Confidence	
Scaled distance	AOp(dB)	Predicted Y	min	max
21,3	141,3	138,14874	133,9561	142,3414
25	135,3	136,01999	132,1612	139,8788
47,7	123,3	122,95977	119,9691	125,9504
97,8	88	94,135247	86,39001	101,8805
41	124,5	126,81455	123,8459	129,7832
60,2	116	115,76802	112,106	119,4301
35	135	130,26659	127,0985	133,4346
91,71	103,5	97,639067	90,63418	104,644
28,1	133,8	134,23643	130,6296	137,8433
35	136,9	130,26659	127,0985	133,4346
47,3	128,9	123,18991	120,208	126,1718
33,6	125	131,07206	127,831	134,3131
31,4	134,8	132,33781	128,9646	135,711
34,76	119,1	130,40467	127,2248	133,5846
27,05	132,7	134,84054	131,1515	138,5295

slope	-0,57534	150,4035	intercept	n	15
SEslope	0,061397	3,014783	SE interc	Xm	43,79467
RSQ	0,871046	5,280443	SEy	SSxx	7396,772
F	87,81129	13	d.f	t95	2,160369
SSreg	2448,449	362,4801	SSres	SE	5,280443

Station A: Standard Blast		Confidence		
Scaled distance	AOp(dB)	Predicted Y	min	max
45,4	135,4	139,61296	137,4174	141,8085
84,8	130	129,85554	126,4961	133,215
91,5	128	128,19628	124,2897	132,1029
61,2	135,1	135,70008	133,7148	137,6854
51,5	136,7	138,10229	136,1198	140,0848
77,6	131,6	131,63862	128,8198	134,4575
45,1	137,8	139,68725	137,4777	141,8968
25,6	143,1	144,51644	140,983	148,0498
45,03	145,3	139,70459	137,4917	141,9175
30,7	142,6	143,25342	140,1209	146,386
47,12	144,8	139,187	137,0658	141,3082
69,9	132,6	133,54553	131,2127	135,8784

slope	-0,24765	150,8563	intercept	n	12
SEslope	0,043306	2,586607	SE interc	Xm	56,2875
RSQ	0,765821	2,997329	SEy	SSxx	4790,373
F	32,7023	10	d.f	t95	2,228139
Ssreg	293,7969	89,83981	Ssres	SE	2,997329

Station B: Varistem Blast			Confidence	
Scaled distance	AOP	Predicted Y	min	max
72,97	120	118,693841	116,1509	121,2368
41,16	119,8	122,362329	119,4509	125,2738
60,93	122,7	120,082354	117,7025	122,4622
127,29	114	112,429387	106,6186	118,2402
50,07	121,3	121,334783	118,7709	123,8986
123,61	116	112,853783	107,3138	118,3938
74,96	110	118,464344	115,86	121,0687
59,51	118,5	120,246115	117,8598	122,6325
39,6	127,5	122,542236	119,5561	125,5284
67,28	117,9	119,35004	116,9314	121,7687
66,73	120	119,413469	117,0025	121,8244
43,55	113,5	122,086702	119,2825	124,8909
39,49	126,6	122,554922	119,5634	125,5465
13,1	129,7	125,598349	120,9848	130,2119
47,88	122,1	121,587345	118,9521	124,2226

slope	-0,11533	127,1091	intercept	n	15
SEslope	0,037515	2,56915	Seinterc.	Xm	61,87533
RSQ	0,420936	4,264261	SEy	SSxx	12920,32
F	9,45002	13	d.f	t95	2,160369
SSregr	171,8384	236,3909	Ssres	SE	4,264261

Station B: Standard Blast			Confidence	
Scaled distance	AOp (dB)	Predicted Y	min	max
48,2	132,1	134,721157	132,3674	137,0749
72,9	134,3	132,327386	130,5814	134,0734
118,1	125,3	127,94688	125,8776	130,0162
138,7	127,2	125,950455	123,2432	128,6577
46,1	140	134,924676	132,5049	137,3444
104,3	129,3	129,284291	127,5205	131,0481
62,1	131,1	133,374055	131,4087	135,3394
40,5	136,7	135,467394	132,8647	138,0701
142,2	127,7	125,611257	122,7825	128,44
48,1	132,3	134,730849	132,374	137,0877
135,9	125,2	126,221814	123,6096	128,834
99,6	129,1	129,739786	128,0452	131,4343

Slope	-0,09691	139,3924	Intercept	n	12
Seslope	0,019217	1,841984	SEinterc	Xm	88,05833
RSQ	0,717771	2,520002	Sey	SSxx	17195,49
F	25,43222	10	d.f	t95	2,228139
Ssregr	161,5051	63,50411	Ssres	SE	2,520002